



## **University of Huddersfield Repository**

Abdulshahed, Ali

The Application of ANN and ANFIS Prediction Models for Thermal Error Compensation on CNC Machine Tools

### **Original Citation**

Abdulshahed, Ali (2015) The Application of ANN and ANFIS Prediction Models for Thermal Error Compensation on CNC Machine Tools. Doctoral thesis, University of Huddersfield.

This version is available at <http://eprints.hud.ac.uk/27946/>

The University Repository is a digital collection of the research output of the University, available on Open Access. Copyright and Moral Rights for the items on this site are retained by the individual author and/or other copyright owners. Users may access full items free of charge; copies of full text items generally can be reproduced, displayed or performed and given to third parties in any format or medium for personal research or study, educational or not-for-profit purposes without prior permission or charge, provided:

- The authors, title and full bibliographic details is credited in any copy;
- A hyperlink and/or URL is included for the original metadata page; and
- The content is not changed in any way.

For more information, including our policy and submission procedure, please contact the Repository Team at: [E.mailbox@hud.ac.uk](mailto:E.mailbox@hud.ac.uk).

<http://eprints.hud.ac.uk/>

THE UNIVERSITY OF HUDDERSFIELD

# **The Application of ANN and ANFIS Prediction Models for Thermal Error Compensation on CNC Machine Tools**

by

ALI MOHAMED ABDULSHAHED

A thesis submitted in partial fulfilment for the  
degree of Doctor of Philosophy

in the

School of Computing and Engineering  
Centre for Precision Technologies

November 2015

## **Copyright Statement**

- The author of this thesis (including any appendices and/or schedules to this thesis) owns any copyright in it (the “Copyright”) and s/he has given The University of Huddersfield the right to use such copyright for any administrative, promotional, educational and/or teaching purposes.
- Copies of this thesis, either in full or in extracts, may be made only in accordance with the regulations of the University Library. Details of these regulations may be obtained from the Librarian. This page must form part of any such copies made.
- The ownership of any patents, designs, trademarks and any and all other intellectual property rights except for the Copyright (the “Intellectual Property Rights”) and any reproductions of copyright works, for example graphs and tables (“Reproductions”), which may be described in this thesis, may not be owned by the author and may be owned by third parties. Such Intellectual Property Rights and Reproductions cannot and must not be made available for use without the prior written permission of the owner(s) of the relevant Intellectual Property Rights and/or Reproductions.

## Abstract

Thermal errors can have significant effects on Computer Numerical Control (CNC) machine tool accuracy. The errors come from thermal deformations of the machine elements caused by heat sources within the machine structure or from ambient temperature change. The effect of temperature can be reduced by error avoidance or numerical compensation. The performance of a thermal error compensation system essentially depends upon the accuracy and robustness of the thermal error model and its input measurements. This thesis first reviews different methods of designing thermal error models, before concentrating on employing Artificial Intelligence (AI) methods to design different thermal prediction models. In this research work the Adaptive Neuro-Fuzzy Inference System (ANFIS) is used as the backbone for thermal error modelling.

The choice of inputs to the thermal model is a non-trivial decision which is ultimately a compromise between the ability to obtain data that sufficiently correlates with the thermal distortion and the cost of implementation of the necessary feedback sensors. In this thesis, temperature measurement was supplemented by direct distortion measurement at accessible locations. The location of temperature measurement must also provide a representative measurement of the change in temperature that will affect the machine structure. The number of sensors and their locations are not always intuitive and the time required to identify the optimal locations is often prohibitive, resulting in compromise and poor results. In this thesis, a new intelligent system for reducing thermal errors of machine tools using data obtained from thermography data is introduced. Different groups of key temperature points on a machine can be identified from thermal images using a novel schema based on a Grey system theory and Fuzzy C-Means (FCM) clustering method. This novel method simplifies the modelling process, enhances the accuracy of the system and reduces the overall number of inputs to the model, since otherwise a much larger number of thermal sensors would be required to cover the entire structure.

An Adaptive Neuro-Fuzzy Inference System with Fuzzy C-Means clustering (ANFIS-FCM) is then employed to design the thermal prediction model. In order to optimise the approach, a parametric study is carried out by changing the number of inputs and number of Membership Functions (MFs) to the ANFIS-FCM model, and comparing the relative robustness of the designs. The proposed approach has been validated on three different machine tools under different operation conditions. Thus the proposed system has been shown to be robust to different internal heat sources, ambient changes and is easily extensible to other CNC machine tools.

Finally, the proposed method is shown to compare favourably against alternative approaches such as an Artificial Neural Network (ANN) model and different Grey models.

## **Acknowledgements**

First of all, I would like to express my sincere and great thanks to my excellent supervisor, Dr Andrew Peter Longstaff, and Dr Simon Fletcher for their expert guidance, continuous support and constructive advice throughout the whole period of this thesis.

I would like to thank all of my colleagues and friends in the Centre for Precision Technologies at the University of Huddersfield.

I would like to thank my sponsor, the ministry of higher education in Libya for their financial support throughout the whole period of my Ph.D studies in the UK.

Last, but not least, I am grateful to my family for their continual support and encouragement throughout my life; to my mother, for her understanding, to my father, for his enthusiasm, to my brothers and sisters, for long-distance motivation. Finally, I would like to thank my wife for her support, encouragement and understanding.

# Contents

ABSTRACT .....	III
ACKNOWLEDGEMENTS .....	IV
CONTENTS .....	V
LIST OF FIGURES.....	VIII
LIST OF TABLES.....	XI
ABBREVIATIONS.....	XII
<b>CHAPTER 1: INTRODUCTION .....</b>	<b>14</b>
1.1 INTRODUCTION AND OVERVIEW .....	14
1.2 TECHNIQUES FOR INCREASING MACHINE TOOL ACCURACY .....	16
1.2.1 <i>Elimination or Avoidance</i> .....	17
1.2.2 <i>Reduction of Generated Heat</i> .....	19
1.2.3 <i>Compensation Strategies</i> .....	21
1.3 AIMS .....	23
1.4 MOTIVATION .....	23
1.5 OBJECTIVES .....	23
1.6 THESIS STRUCTURE .....	24
<b>CHAPTER 2: THERMAL-ERROR MODELLING TECHNIQUES .....</b>	<b>26</b>
2.1 THERMAL MODELLING METHODS.....	26
2.1.1 <i>Principle-Based Models</i> .....	28
2.1.2 <i>Data-Driven Models</i> .....	30
2.1.2.1 Statistical Models.....	30
2.1.2.2 Artificial Intelligence (AI) models .....	31
2.1.3 <i>Fuzzy Logic Models</i> .....	33
2.2 TEMPERATURE SENSOR PLACEMENT .....	35
2.3 HYSTERESIS IN THERMAL ERROR MODELLING.....	38
2.4 FUSION MEASUREMENTS.....	39
2.5 A SUMMARY OF CHALLENGES .....	40
2.6 SUMMARY .....	42
<b>CHAPTER 3: ARTIFICIAL INTELLIGENCE TECHNIQUES AND METHODS .....</b>	<b>43</b>
3.1 INTRODUCTION .....	43
3.2 FUZZY LOGIC AND FUZZY SYSTEMS.....	44
3.3 ADAPTIVE NEURO-FUZZY INFERENCE SYSTEM (ANFIS).....	46
3.3.1 <i>ANFIS Architecture</i> .....	46

3.3.2	<i>Extraction of the Initial Fuzzy Model</i> .....	48
3.3.2.1	Fuzzy C-Means (FCM) Clustering.....	49
3.4	GREY MODELS.....	51
3.4.1	<i>Accumulation Generation Operation (AGO)</i> .....	51
3.5	OPTIMISATION METHODS.....	53
3.5.1	<i>The Particle Swarm Optimisation (PSO)</i> .....	53
3.6	GMC (1, N) AND ITS LEARNING ALGORITHM.....	54
3.7	VARIABLES SELECTION USING GREY MODELS.....	56
3.7.1	<i>Grey Model GM (0, N)</i> .....	57
3.7.2	<i>The GM (1, N) Model</i> .....	58
3.7.3	<i>Grey Relational Analysis (GRA) Method</i> .....	60
3.8	MODEL VALIDATION.....	61
3.8.1	<i>Direct Validation</i> .....	61
3.8.2	<i>Cross Validation</i> .....	62
3.9	SUMMARY.....	62
<b>CHAPTER 4:</b>	<b>THERMAL CHARACTERISATION OF MACHINE TOOLS</b> .....	<b>64</b>
4.1	INTRODUCTION.....	64
4.2	MEASUREMENTS OF THERMAL DEFORMATION OF MACHINE TOOLS.....	64
4.2.1	<i>Measurement of Temperature</i> .....	64
4.2.1.1	Thermal Imaging Camera.....	65
4.2.1.2	Discrete Temperature Sensors.....	67
4.2.2	<i>Measurement of Displacement</i> .....	68
4.2.2.1	Non-Contact Displacement Transducers (NCDTs).....	68
4.2.2.2	Laser Triangulation Sensor (LTS).....	69
4.2.2.3	Fiber Bragg Grating (FBG) Sensors.....	69
4.3	TEST MACHINES.....	70
4.3.1	<i>Machine A - Vertical Milling Centre (VMC)</i> .....	71
4.3.2	<i>Machine B - Vertical Milling Centre (VMC)</i> .....	71
4.3.3	<i>Machine C – A 5-axis Gantry Milling Machine</i> .....	72
4.4	KEY THERMAL MEASUREMENT POINTS.....	73
4.4.1	<i>Summary of the Proposed System</i> .....	80
4.5	ROBUSTNESS OF GREY MODELS.....	82
4.5.1	<i>Setup of Measurement System</i> .....	82
4.5.2	<i>Thermal Key Point Identification Using GRA Model</i> .....	84
4.6	EXAMPLE OF THE FUSION MEASUREMENT ON MACHINE C.....	88
4.6.1	<i>Hysteresis Effect</i> .....	90
4.7	SUMMARY.....	92
<b>CHAPTER 5:</b>	<b>ARTIFICIAL INTELLIGENCE MODEL DEVELOPMENT</b> .....	<b>94</b>

5.1	INTRODUCTION .....	94
5.2	GENERATING ANFIS ARCHITECTURE .....	94
5.3	ROBUSTNESS OF THE MODEL TO MACHINING PARAMETERS.....	101
5.3.1	<i>ANFIS Models Design</i> .....	104
5.3.2	<i>Results and Discussion</i> .....	106
5.3.2.1	Same Spindle Speed under Different Operation Conditions .....	106
5.3.2.2	Different Spindle Speed under Different Operation Conditions .....	109
5.4	FUSION OF TEMPERATURE AND DISTORTION MEASUREMENT.....	111
5.4.1	<i>Results and Discussion</i> .....	115
5.4.1.1	Case 1: Z-axis Heating Test.....	115
5.4.1.2	Case 2: C-axis Heating Test .....	116
5.4.1.3	Case 3: Combined Axis (Helical) Test .....	117
5.5	SUMMARY .....	119
<b>CHAPTER 6:</b>	<b>MODEL VALIDATION AND COMPARISON.....</b>	<b>121</b>
6.1	INTRODUCTION .....	121
6.2	MODELLING OF ETVE .....	121
6.2.1	<i>Grey Model</i> .....	123
6.2.2	<i>ANFIS Model</i> .....	125
6.2.2.1	Different Ambient Conditions .....	128
6.3	ROBUSTNESS OF THE ANFIS MODEL.....	133
6.3.1	<i>ANN Model Development</i> .....	136
6.3.2	<i>Grey Model Development</i> .....	137
6.3.3	<i>Results and Discussion</i> .....	138
6.4	SUMMARY .....	145
<b>CHAPTER 7:</b>	<b>SUMMARY AND CONCLUSIONS.....</b>	<b>147</b>
7.1	THESIS SUMMARY AND CONTRIBUTIONS .....	147
7.2	FUTURE WORK .....	149
7.3	PUBLISHED PAPERS.....	150
7.3.1	<i>Refereed Journal Papers</i> .....	150
7.3.2	<i>Refereed Conference Papers</i> .....	150
<b>REFERENCES.....</b>		<b>152</b>
<b>APPENDIX A:</b>	<b>GNNMCI (1, N) ARCHITECTURE .....</b>	<b>160</b>
<b>A.1</b>	<b>GNNMCI (1, N) LEARNING ALGORITHM .....</b>	<b>162</b>

# List of Figures

FIGURE 3-1: BLOCK DIAGRAM OF THE PROPOSED SYSTEM.....	44
FIGURE 3-2: BASIC STRUCTURE OF ANFIS.....	47
FIGURE 3-3: THE ORIGINAL DATA VS AGO CONVERTED DATA.....	53
FIGURE 3-4: SCHEMATIC DIAGRAM OF PSO-BASED GREY MODEL.....	56
FIGURE 4-1: A GENERAL OVERVIEW OF A TYPICAL THERMOGRAPHIC EXPERIMENTAL SETUP.....	66
FIGURE 4-2: PRINCIPLE OF EDDY CURRENT SENSOR [111]. .....	68
FIGURE 4-3: LASER TRIANGULATION PRINCIPLE.....	69
FIGURE 4-4: A GENERAL OVERVIEW OF MACHINE A. ....	71
FIGURE 4-5: LOCATION OF THERMAL SENSORS ON THE MACHINE B.....	72
FIGURE 4-6: A GENERAL OVERVIEW OF THE 5-AXIS MILLING MACHINE AND LOCATION OF THE (FBG). ....	73
FIGURE 4-7: MEASUREMENT OF THE THERMAL EFFECT USING A TEST BAR AND NCDTs.....	74
FIGURE 4-8: A GENERAL OVERVIEW OF THE EXPERIMENTAL SETUP. ....	74
FIGURE 4-9: THERMAL RESPONSE OF THE SPINDLE.....	75
FIGURE 4-10: THERMAL IMAGES CAPTURED DURING THE EXPERIMENT WITH 525 SELECTED SPOTS.....	76
FIGURE 4-11: THERMAL DATA EXTRACTED FROM IMAGES USING MATLAB. ....	76
FIGURE 4-12: SURFACE OF INFLUENCE RANKING OF TEMPERATURE DATA USING GM (0, N). ....	77
FIGURE 4-13: THERMAL IMAGE CAPTURED DURING THE EXPERIMENTAL WITH 10 SELECTED POINTS.....	78
FIGURE 4-14: THERMAL DATA EXTRACTED FROM IMAGES WITH 10 SELECTED POINTS.....	78
FIGURE 4-15: INFLUENCE RANKING OF TEN TEMPERATURE SPOTS USING GM (0, N). ....	79
FIGURE 4-16: AN EXAMPLE OF CLUSTERING PROCEDURE FOR FOUR CLUSTERS. ....	80
FIGURE 4-17: BLOCK DIAGRAM OF THE PROPOSED SYSTEM.....	81
FIGURE 4-18: LOCATION OF THERMAL POINTS AND DISPLACEMENT SENSORS ON THE MACHINE. ....	83
FIGURE 4-19: THERMAL RESPONSE OF THE SPINDLE.....	84
FIGURE 4-20: SIMILARITY RANKING OF TEMPERATURE POINTS USING GRA MODEL. ....	86
FIGURE 4-21: INFLUENCE RANKING OF TEMPERATURE DATA USING GRA MODEL.....	88
FIGURE 4-22: STRATEGY OF TEMPERATURE SENSOR PLACEMENT ON RAM STRUCTURE.....	89
FIGURE 4-23: PROCEDURES FOR MEASURING THE THERMAL ERRORS. ....	90
FIGURE 4-24: DATA FUSION (TEMPERATURE AND STRAIN).....	91
FIGURE 4-25: HYSTERESIS PLOT FROM DIFFERENT SENSORS. ....	92
FIGURE 5-1: THE CHARACTERISTICS OF THE ANFIS MODELS DURING TESTING STAGE.....	96
FIGURE 5-2: RESIDUAL VALUES FOR ALL EIGHT MODELS. ....	97
FIGURE 5-3: THE STRUCTURE OF ASSOCIATED NETWORK MODEL.....	98

FIGURE 5-4: THERMAL DATA EXTRACTED FROM FOUR POINTS. ....	98
FIGURE 5-5: MEMBERSHIP FUNCTIONS OBTAINED THROUGH FCM.....	99
FIGURE 5-6: THERMAL DATA EXTRACTED FROM IMAGES FROM SELECTED POINTS. ....	100
FIGURE 5-7: ANFIS-FCM MODEL OUTPUT VS THE ACTUAL THERMAL RESPONSE. ....	100
FIGURE 5-8: ABSOLUTE TEMPERATURE OF THE SELECTED SENSOR IN DIFFERENT TESTS. ....	102
FIGURE 5-9: MAGNITUDE OF TEMPERATURE CHANGES IN DIFFERENT TESTS. ....	102
FIGURE 5-10: THERMAL RESPONSE OF THE SPINDLE (SPINDLE SPEED 8000 RPM).....	103
FIGURE 5-11: (A) ANFIS-GRID MODEL OUTPUT VS THE ACTUAL THERMAL RESPONSE. (B) ANFIS-FCM MODEL OUTPUT VS THE ACTUAL THERMAL RESPONSE. (TWO HOURS, TEST I).....	108
FIGURE 5-12: (A) ANFIS-GRID MODEL OUTPUT VS THE ACTUAL THERMAL RESPONSE. (B) ANFIS-FCM MODEL OUTPUT VS THE ACTUAL THERMAL RESPONSE. (FIVE HOURS, TEST II).....	108
FIGURE 5-13: (A) ANFIS-GRID MODEL OUTPUT VS THE ACTUAL THERMAL RESPONSE. (B) ANFIS-FCM MODEL VS THE ACTUAL THERMAL RESPONSE. (FIVE HOURS, TEST III). ....	109
FIGURE 5-14: (A) ANFIS-GRID MODEL OUTPUT VS THE ACTUAL THERMAL RESPONSE. (B) ANFIS-FCM MODEL OUTPUT VS THE ACTUAL THERMAL RESPONSE. (FIVE HOURS, TEST V). ....	110
FIGURE 5-15: (A) ANFIS-GRID MODEL OUTPUT VS THE ACTUAL THERMAL RESPONSE. (B) ANFIS-FCM MODEL OUTPUT VS THE ACTUAL THERMAL RESPONSE. (FIVE HOURS, TEST VI). ....	110
FIGURE 5-16: ANFIS MODEL OUTPUT VS THE ACTUAL THERMAL RESPONSE (ONLY TEMPERATURE).....	112
FIGURE 5-17: ANFIS MODEL OUTPUT VS THE ACTUAL THERMAL RESPONSE (TEMPERATURE AND STRAIN). ....	112
FIGURE 5-18: (A) TEMPERATURE AND STRAIN AS MODEL INPUTS. (B) GNNMCI (1, 6) MODEL OUTPUT VS THE ACTUAL THERMAL RESPONSE.....	115
FIGURE 5-19: (A) TEMPERATURE AND STRAIN AS MODEL INPUTS. (B) GNNMCI (1, 6) MODEL OUTPUT VS THE ACTUAL THERMAL RESPONSE.....	116
FIGURE 5-20: (A) TEMPERATURE AND STRAIN AS MODEL INPUTS. (B) GNNMCI (1, 6) MODEL OUTPUT VS THE ACTUAL THERMAL RESPONSE.....	117
FIGURE 5-21: (A) TEMPERATURE AND STRAIN AS MODEL INPUTS. (B) GNNMCI (1, 6) MODEL OUTPUT VS THE ACTUAL THERMAL RESPONSE.....	118
FIGURE 6-1: A GENERAL OVERVIEW OF THE EXPERIMENTAL SETUP. ....	122
FIGURE 6-2: TEMPERATURE MEASUREMENTS AND MACHINE MOVEMENT DUE TO ENVIRONMENT. ....	123
FIGURE 6-3: SIMULATION RESULTS FOR 80 MINUTES. ....	124
FIGURE 6-4: CORRELATION BETWEEN THE MEASURED AND SIMULATED Z-AXIS DISPLACEMENT USING GNNMCI MODEL. ....	125
FIGURE 6-5: CORRELATION BETWEEN THE MEASURED AND SIMULATED Y-AXIS DISPLACEMENT USING GNNMCI MODEL. ....	125
FIGURE 6-6: MEMBERSHIP FUNCTIONS OBTAINED THROUGH ANFIS AND FCM CLUSTERING. ....	127

FIGURE 6-7: CORRELATION BETWEEN THE MEASURED AND SIMULATED Z-AXIS DISPLACEMENT USING THE ANFIS MODEL. ....	128
FIGURE 6-8: THREE-DAY SUMMER TEST (BEFORE OPTIMISATION). ....	129
FIGURE 6-9: THREE-DAY SUMMER TEST (AFTER OPTIMISATION). ....	129
FIGURE 6-10: TEMPERATURE MEASUREMENTS DUE TO ENVIRONMENTAL CHANGES. ....	130
FIGURE 6-11: MACHINE MOVEMENT DUE TO ENVIRONMENTAL CHANGES. ....	130
FIGURE 6-12: MACHINE MOVEMENT AND TEMPERATURE CHANGES. ....	131
FIGURE 6-13: CORRELATION BETWEEN THE MEASURED AND SIMULATED Y-AXIS DISPLACEMENT USING ANFIS MODEL. ....	131
FIGURE 6-14: CORRELATION BETWEEN THE MEASURED AND SIMULATED Z-AXIS DISPLACEMENT USING ANFIS MODEL. ....	132
FIGURE 6-15: FIVE-DAY WINTER TEST.....	133
FIGURE 6-16: A GENERAL OVERVIEW OF THE EXPERIMENTAL SETUP. ....	134
FIGURE 6-17: RUNNING THE SPINDLE AT DIFFERENT SPEEDS. ....	135
FIGURE 6-18: THE MACHINE MOVEMENT (TEST-I).....	136
FIGURE 6-19: TEMPERATURE MEASUREMENTS AND MACHINE MOVEMENT IN Z-DIRECTION (TEST-II). ....	136
FIGURE 6-20: THE STRUCTURE OF ASSOCIATED NETWORK MODEL. ....	137
FIGURE 6-21: ANFIS MODEL OUTPUT VS THE ACTUAL THERMAL RESPONSE. ....	140
FIGURE 6-22: ANN MODEL OUTPUT VS THE ACTUAL THERMAL RESPONSE. ....	140
FIGURE 6-23: GREY MODEL WITH PSO OUTPUT VS THE ACTUAL THERMAL RESPONSE. ....	141
FIGURE 6-24: STANDARD GREY MODEL OUTPUT VS THE ACTUAL THERMAL RESPONSE. ....	141
FIGURE 6-25: ANFIS MODEL OUTPUT VS THE ACTUAL THERMAL RESPONSE IN Y-DIRECTION. ....	142
FIGURE 6-26: ANFIS MODEL OUTPUT VS THE ACTUAL THERMAL RESPONSE. ....	143
FIGURE 6-27: IMPROVED ANFIS MODEL OUTPUT VS THE ACTUAL THERMAL RESPONSE. ....	144
FIGURE A-1: THE MAPPING STRUCTURE OF GNNMCI (1, 6). ....	161
FIGURE A-2: FLOWCHART FOR PSO IMPLEMENTATION. ....	164

## List of Tables

TABLE 4-1: THERMAL IMAGING CAMERA SPECIFICATION. ....	65
TABLE 4-2: THERMAL IMAGING CAMERA PARAMETERS. ....	66
TABLE 4-3: THE CLUSTER RESULTS. ....	79
TABLE 4-4: THE LOCATION OF THE THERMAL MEASUREMENT POINTS. ....	83
TABLE 4-5: THE CLUSTERING RESULT. ....	86
TABLE 4-6: SELECTED TEMPERATURE SENSORS. ....	87
TABLE 5-1: PERFORMANCE OF ANFIS-FCM MODELS WITH VARIOUS NUMBERS OF MFs. ....	95
TABLE 5-2: THE CHARACTERISTICS OF THE ANFIS-FCM MODELS. ....	96
TABLE 5-3: THE VARIOUS HEATING AND COOLING TESTS ....	103
TABLE 5-4: THE CLUSTERING RESULT. ....	104
TABLE 5-5: PERFORMANCE OF ANFIS-FCM MODELS WITH VARIOUS NUMBERS OF $N_c$ ....	106
TABLE 5-6: LINGUISTIC RULES ....	106
TABLE 5-7: PERFORMANCE CALCULATION OF THE USED MODELS ....	107
TABLE 5-8: PERFORMANCE CALCULATION OF THE USED MODELS ....	109
TABLE 5-9: THE TRAINING DATA FROM FIRST 5 READINGS. ....	114
TABLE 5-10: THE MODELLING VALUES OF THERMAL ERRORS BASED ON GNNMCI (1, 6) MODEL. ....	114
TABLE 6-1: THE LOCATION OF THE TEMPERATURE SENSORS. ....	135
TABLE 6-2: PSO-BASED GREY MODEL PARAMETERS ....	138
TABLE 6-3: LS-BASED GREY MODEL PARAMETERS ....	138
TABLE 6-4: PERFORMANCE CALCULATION OF THE USED MODELS. ....	139

## Abbreviations

AGO	ACCUMULATED GENERATING OPERATION
AI	ARTIFICIAL INTELLIGENCE
ANFIS	ADAPTIVE NEURO-FUZZY INFERENCE SYSTEM
ANN	ARTIFICIAL NEURAL NETWORK
BP	BACK-PROPAGATION
CMM	COORDINATE MEASURING MACHINE
CNC	COMPUTER NUMERICAL CONTROL
CPT	CENTRE FOR PRECISION TECHNOLOGIES
EPSRC	ENGINEERING AND PHYSICAL SCIENCES RESEARCH COUNCIL
ETVE	ENVIRONMENTAL TEMPERATURE VARIATION ERROR
FBG	FIBER BRAGG GRATING
FCM	FUZZY C-MEANS
FDEM	FINITE DIFFERENCE ELEMENT METHOD
FEA	FINITE ELEMENT ANALYSIS
FEM	FINITE ELEMENT METHOD
FIS	FUZZY INFERENCE SYSTEM
FL	FUZZY LOGIC
FLS	FUZZY LOGIC SYSTEM
GA	GENETIC ALGORITHM
G-FISs	GENETICALLY EVOLVED FUZZY INFERENCE SYSTEMS
GM	GREY MODEL
GMC	GREY PREDICTION MODEL WITH CONVOLUTION INTEGRAL
GNNMCI	GREY NEURAL NETWORK MODEL WITH CONVOLUTION INTEGRAL
GRA	GREY RELATIONAL ANALYSIS
GUI	GRAPHICAL USER INTERFACE
HARCO	HIERARCHICAL AND ADAPTIVE SMART COMPONENTS
HGA	HIERARCHY-GENETIC-ALGORITHM
IAGO	INVERSE OPERATION OF ACCUMULATED GENERATING OPERATION
LCM	LUMPED CAPACITANCE METHOD
LS	LEAST SQUARES
LTS	LASER TRIANGULATION SENSOR
MF	MEMBERSHIP FUNCTION
MRA	MULTIPLE REGRESSION ANALYSIS
NCDTs	NON-CONTACT DISPLACEMENT TRANSDUCERS

NSE	NASH-SUTCLIFFE EFFICIENCY COEFFICIENT
PSO	PARTICLE SWARM OPTIMISATION
RBFNs	RADIAL BASIS FUNCTION NETWORKS
RMSE	ROOT MEAN SQUARE ERROR
T-S	TAKAGI-SUGENO
VMC	VERTICAL MILLING MACHINE

## Chapter 1: Introduction

### 1.1 Introduction and Overview

Manufacturing industry demands a continual improvement in the positioning accuracy of machine tools. Increasingly, changes in the business requirements of manufacturing industries are driving machining systems to be more accurate and more productive. To produce high quality parts to high accuracy and to close tolerances, the CNC machine tools must have greater accuracy than the tolerances of the manufactured parts. The ability to produce parts accurately has many advantages such as improved performance of the finished product, reduced waste, reduced rework, more predictable production schedules, etc.

Machine tools with three axes have been used to fabricate a large variety of products with relatively simple geometry to a satisfactory accuracy. However, thermal errors are still one of the main factors affecting the machine accuracy. They are caused by exogenous and endogenous heat sources and result in non-uniform expansion and deformations of the structural elements. The interaction of the differing heat sources, asymmetry of the structure, differing expansion coefficients and time constants of disparate materials, etc. result in complex mechanical behaviour that are difficult to predict deterministically. Thermal errors have been reported to contribute approximately 70% of the total positioning error of the CNC machine tool [1], although this differs from machine-to-machine. In addition, higher accuracies are being required on large machine tools because of the increasing demand for high-value, large parts, such as impeller blades, engine blocks, aerofoil, etc. The accuracy of a gantry-type 5-axis machine tool has historically not been as good as that of three-axis machine tools, because the numbers of errors increase inevitably by increasing the size and the number of machine's axes. Finding an efficient modelling solution for such machines is particularly timely.

Serious attention has been paid to the influence of temperature changes on the accuracy of the CNC machine tools [2-5]. Thermal errors arise from changes in the size and shape of the structural elements of the machine tool, and of the workpiece, due to varying temperature gradients on the machine and workpiece during the machining process. Thermal fluctuations of the machine tool structure are caused by changes in environmental temperature and heat sources that exist within the structure of the machine tool itself. The internal heat sources

include, drive motors, gear trains and other transmission devices. However, heat sources around a machine tool can be split into two categories [6]: heat sources internal to the machine and heat sources external to the machine.

Internal heat sources consider all heat sources that are directly connected to the machine tool structure. They directly conduct the heat into the machine structure and cause deformations and thermal response. Understanding the effect of each of these sources has been the focus of various publications [6-8]. The research has shown that spindle system and its bearings are considered to be one of the main sources of heat generation and resulting deformations. Without error avoidance methods, such as a cooling jacket, the heat generated by the spindle system will cause temperature gradients in the machine elements. This thesis makes extensive use of thermal imaging for rapid assessment of the internal heat sources of the machine tool. To illustrate the use of thermal imaging for this purpose, examples of internal heating test will be seen through this thesis.

There are other important internal heat sources such as the cutting process itself, which warms up the tool, tool-holder, clamping device, and workpiece. Although, there is extensive research which addresses the friction modelling of the machining process [9], the thermal aspects of the machining process have not been investigated adequately [2, 10]. The table and other components can also be heated up indirectly by hot chips (swarf) from the cutting process. This heat source can be reduced by using cutting fluid (coolant). However, such a process can create additional negative heat sources so must be used only with sufficient consideration.

External heat sources are attributed to the environment in which the machine is located, such as neighbouring machines, opening/closing of machine shop doors, variation of the environmental temperature during the day and night cycle and differing behaviour between seasons. It's not a trivial problem to keep the machine thermal environment in homogeneous and stable condition, due to the complexity of the surrounding working environment and the total budget consideration. Even the small heat sources, such as lighting, and electrical cabinet of the machine, could cause significant change in the machine structure. The complex thermal behaviour of a machine is created by interaction between these different heat sources. Ambient effects are arguably one of the most important, but most neglected in thermal error compensation systems [3]. An integrated model can be used in machine tool error

compensation, taking into account the different heat sources [2]. An example of such a model for a CNC machine tool is given by White et al. [7].

Thermal errors are variables that can vary with time. They change the relative tool-to-workpiece position and orientation, and can be either dependent or independent of axis position, depending on their source. Position dependent thermal errors are functions of both temperature and axis positions [11]. Some of them may change quickly (heat generated by spindle); others may change slowly (ambient temperature change). Some of the thermal errors may combine, and some may cancel each other out with respect to the geometry of the machine. Thermal errors change according to the operation being carried out by the machine, heat sources related to moving axes and fluid flow that may produce thermal errors that stem from the machining operation's history. This complexity of the problem of thermal errors has led to the development of a wide range of approaches and strategies to reduce their effects. There are three primary approaches to mitigate these thermal errors which will be addressed in the next section.

## **1.2 Techniques for Increasing Machine Tool Accuracy**

High value manufacturing requires machine tools that can produce consistently high accuracy parts. Deformations due to the changes in the temperature of the machine tool structure create relative displacement between the tool tip and the workpiece during the machining process, which affects the dimensional accuracy of manufactured parts. Thermal errors are yet more complex since they represent a response to the interaction between environmental changes and internally generated heat. There are three primary approaches to mitigate these thermal errors which can be categorised as: elimination or avoidance, reduction of generated heat, and compensation strategies. Elimination or avoidance strategies try to eliminate any change in dimensions due to temperature changes. They are best implemented during the design stage of the machine tool. Some examples of these strategies are use of symmetry in machine design, choice of materials and use of direct closed-loop feedback. Reduction of generated heat strategies tends to directly cool the heat sources, for instance, through on machine cooling systems. However, the end-user must also be responsible for improved environmental temperature control, or good operating practices such as spindle warm up. Compensation approaches tend to compensate numerically or electronically for any change in the size and the shape of the machine structure due to temperature gradients. They can be implemented

during any stage of the machine tool design and development. Many compensation techniques have been explored to reduce thermal errors in a direct or indirect way. More detail will be presented in the next subsections.

### 1.2.1 Elimination or Avoidance

Thermal errors can be reduced by amending a machine tool's structure using advanced design and manufacture procedures, such as structural symmetry and separation of heat sources, etc. These strategies are best implemented during the design stage of the machine tool; retrofit solutions are unlikely to be feasible. The efficient numerical model of the machine tool is today an essential part of the design and improvement of CNC machine tools. It is possible to design the machine tool structure and its assemblies with regard to their material and geometry in order to ensure the lowest sensitivity to changes in temperature. However, this is not always practical due to cost and the compromise it might cause on, for instance, accessibility for part-loading location of tool changer, overall footprint, etc. The numerical modelling of machine tool should include the mutual interactions between the heat sources in a way most faithfully identifying all the naturally occurring phenomena [12]. Finite Element Analysis (FEA) is a very helpful tool especially during the design phase of a new machine. It has been used to gain accurate knowledge of the influence of different factors on the thermal behaviour of machine tools [2, 13]. This allows the arrangement of machine structure, elements, and heat sources to be decided. The final design usually is determined by optimisation in terms of size, capital, and running costs. The following list describes some design changes that have helped significantly to reduce thermal errors:

- The geometry of the machine is critical in the deformation behaviour [14]. Thermally symmetric design of a machine structure leads to lower temperature gradients as well as reduced distortions [15]. For example, machine element such as rams and columns have in most cases a square section to achieve a symmetrical design and balanced thermal behaviour. Mayr et al. [16] proposed different design modifications for a prototype lathe and made comparisons by simulation study. The simulation example illustrates that the thermal error of the prototype can be reduced to about 15% of the original error by design modifications. Furthermore, the light-weight structure with thin walls is recommended (for smaller heat capacity) to reduce the thermal deformation [17]. Nevertheless, it is very important for the machine tool designer to understand to what extent the light-weight structure can be practically implemented.

- Utilising materials that have a low thermal expansion coefficient and high specific heat capacity such as cast iron, fibre-reinforced plastics and polymer concrete [1, 14]. In the machine tool sector, the most commonly used material is cast iron due to its stability, easy casting, and economy in machining. Nevertheless, polymer concrete has received increasing attention since it can be used in manufacturing bases requiring material properties such as good thermal stability. Haddad and Kobaisi [18] investigated the application of polymer concrete compositions on the thermal expansion of the base and how it affected the level of precision of the machine tool. ANSYS software was employed in visualizing the influence of different compositions of aggregates on the thermal expansion. According to their results, the optimum composition of the area that they investigated is basalt, sand and fly ash, respectively, which has the least coefficient of thermal expansion and acceptable flexural strength. Recently, some companies apply innovative silicon carbide ceramics for their new CMM machines, which gives around 50% lower thermal expansion, and 20% less weight than standard ceramics [19].
- Ballscrews are often used in machine tools with a rotary encoder feedback on the end of the screw. Thermal deformation of the ballscrew shaft can be a serious source of positioning error. During the normal function of ballscrew system, heat generating from the friction of balls movement on the thread produces a significant thermal growth of the screw. Using linear scales or laser scales provide direct feedback removing the ballscrew from the positioning loop. However, fitting such scales to many machines may be mechanically difficult and costly [20]. Additionally, convenient locations for the scales might be non-ideal from a thermal point of view, so cannot be considered a complete solution to the problem. Another common technique used to reduce the effect of ballscrew expansion is application of pre-tension to the ballscrew. This technique suffers from a number of drawbacks such as potentially incurring vibration, ballscrew buckling and bearing failure problems [21].
- Isolation of spindle driving system: Motor spindles are equipped with high-power motors, which generate a significant amount of lost heat [22]. To prevent transferring the heat produced in a spindle motor to a main spindle, the spindle is coupled with a high-speed drive motor by using a diaphragm-type coupling. As a result, the spindle system can be isolated from the heat generated in spindle motor through the diaphragm-type coupling [17].

- The efficiency of the spindle bearings is especially important for the spindle system performance. Improved bearing systems, where the change from plain to angular contact bearings with high contact angles has resulted in increased speeds and stiffness whilst achieving lower heat generation. Recently, ceramic bearings have also been used to reduce the friction and hence the excessive generation of heat in the bearings [22].
- Painting and coating materials: For the structural body component, the painting material and its emissivity have significant effects on the thermal boundary condition of the machine tool [17]. As similar topic is concerned with the coating technology for some parts of the machine structure such as cutting tools [4]. For instance, enamel is an excellent coating material to increase the heat dissipation from the surface of the machine, although it has certain difficulties in practical use [17].
- Use of slant type bed structure: a large amount of the heat generated by the machining process is transferred to the chips (swarf). In order to achieve high machining accuracy, immediate removal of chips from the machining work space is an important issue. An inclined guide way is an effective means to prevent a pile of swarf on the bed. The latest designs of turning centres have slanted bed structures [17]. In such bed structures, the chips are quickly removed from the machining work space by a conveyer, and thus the heat dissipation to the machine elements can be avoided. Furthermore, the cutting fluid can also help to alleviate this problem of localised heating though care should be taken since it can conversely cause a cooling (negative heating) effect.

### 1.2.2 Reduction of Generated Heat

Controlling workshop temperature is always a good practice for reducing thermal error because normal daily environment temperature fluctuation is one of the main heat disturbances in an ordinary machine shop. Much research has been focused on how to control the heat sources and achieve temperature equilibrium faster in order to avoid the negative effects of excessive heat during the machining process. A more effective method for controlling the heat can be realised by reinforcing an effective flow of temperature-controlled media around the heat sources. More specific techniques and their applications are listed below:

- Environment temperature change is also a major cause of machine tool structural temperature variation [23]. Longstaff et al. [3] presented several Environmental Temperature Variation Error (ETVE) tests conducted on a wide range of machine tools and discussed the implications for produced parts. It has been reported that external temperature variation are attributed to the environment in which the machine is located, such as neighbouring machines, opening/closing of machine shop doors, variation of the environmental temperature during the day and night cycle and differing behaviour between seasons. Temperature controlled environments and modification of the machine shop floor are possible and can effectively reduce thermal errors on a number of machines at once, but may be difficult and costly to achieve.
- Some machine tool designers apply coolant down system to the ballscrew. Xu et al. [24] tried to control the heat sources of the ballscrew system and achieve temperature equilibrium quickly. They carried out a heat source control method called “centre hole air cooling” on a high precision ballscrew drive system. A thermal behaviour model using the Finite Element Method (FEM) and a Lumped Capacitance Method (LCM) were used to estimate the effectiveness of the air cooling system. Thermal error was reduced by 66.8% at 500 rpm, and 65.9% at 1000 rpm. According to their results, the most important finding is that air-cooling brings temperature equilibrium faster to the ballscrew system.
- Forced oil cooling of machine tool components: Several specific designs incorporate oil cooling jackets equipped with a temperature sensor around the spindle bearings. The oil is circulated continuously through these jackets and passed through a refrigeration unit. This method is a simple way for reducing bearing temperature and is widely applied to the cooling of high-speed spindle systems supported by rolling bearings [23].
- Air circulation controlled at a constant temperature: Air temperature control systems provide an alternative means for reducing the thermal error of machine tools when other effective means are not practical. However, such air cooling system is not as effective as a liquid cooling system to remove heat due to lower heat capacity of the medium [17, 25]. Several designs tried to improve the cooling performance of air and make it a practical alternative to cool machine tool components for new and existing machines. Donmez et al. [25] proposed a method of cooling by using commercially available silicon tubing with small slits and forcing a compressed air through them based on Coanda-effect cooling. An average of 30% improvement in spindle response was observed. According to their

results, the power requirement for their method is about 0.6 kW. In comparison, an air fan producing high velocity air flow around the machine would require about 40 kW power.

Jiang and Min [26] investigated a thermal design method for a vertical machining centre headstock using a dual forced cooling system, including a forced air cooling subsystem and a forced water cooling one. The air cooling subsystem was used to cool the driven motor, while the water cooling subsystem is used to remove the heat generated by the spindle bearing. The integrated thermal model of the headstock system was developed by aid of the FEM. Their results indicate that the thermal behaviour of the headstock can be improved by 77% using their proposed method.

Numerous attempts have made to introduce special design and manufacture procedures, such as the above-mentioned strategies. These strategies can reduce the effect of structural temperature change, but at the same time increase the cost of its manufacture and can compromise other design targets such as size and speed. A more advantageous way of improving machine tool accuracy is through the use of an error compensation system.

### **1.2.3 Compensation Strategies**

Compensation is a process where the thermal error present at a particular time and position is corrected by adjusting the position of a machine's axes by an amount equal to the error at that position [23]. Error compensations can be more attractive than making physical changes to the machine structure. Firstly, error compensation is often less expensive than the design effort, manufacturing and running costs involved in error avoidance. Secondly, error compensation is more adaptable in that it can accommodate changes in error sources, which sometimes cannot be accommodated by structural change techniques [6].

Many compensation techniques have been explored to reduce thermal errors in a direct or indirect way. Direct compensation is simple yet efficient philosophy, making use of directly measured displacements between a tool and a workpiece, often using probing. However, direct measurement compensation has a number of disadvantages. For instance, it is likely that some of the most significant thermal problems are caused by rapid thermal changes. Tracking and correcting these rapid movements would require frequent measurements. When a tool-mounted probe is used, each measurement requires a break in machining, therefore introducing undesirable time delays. In addition, probing measurements can be prone to errors caused by swarf or coolant on the surface of the workpiece [6]. This can be overcome by repeated measurements or other means, but incurs further cost in terms of hardware or

production time. Realistically, direct thermal compensation is most applicable to fixed tooling, such as lathes [2], where a dedicated sensor can be conveniently located.

In indirect compensation the thermal error is calculated from measurements of some other parameters, most commonly temperature [23, 27-29]. The indirect compensation concept is to build a compensation model by continuously monitoring the temperature changes at selected points, using different type of sensors (temperature and/or strain). A relationship is then found between these sensors and the deformation of the machine. A comprehensive survey of compensation techniques was given in 2009 by Li et al. [30] and in 2015 by Li et al. [31].

Rather than attempting to eliminate thermal errors, this research work provides a systematic methodology for predicting thermal errors, thus improving the accuracy of CNC machine tools by allowing accurate compensation movements. The Artificial Intelligence (AI) modelling will be used as a generic tool to develop a thermal prediction model which can be readily transferred to other CNC machine tools. An efficient strategy of selecting significant model inputs and their locations has been introduced.

During the manufacturing processes, the temperature/strain signals are collected in real time and the errors are estimated with the artificial intelligence model. The calculated compensation values will be used to modify the axis positions to maintain the end of the tool at the datum position.

This thesis proposes a thermal error modelling method based on the Adaptive Neuro-Fuzzy Inference System (ANFIS) in order to establish the relationship between the thermal errors and the temperature changes. The proposed methodology has the ability to provide a simple, transparent and robust thermal error compensation system. It has the advantages of fuzzy logic theory and the learning ability of the Artificial Neural Networks (ANNs) in a single system. A thermal imaging camera was used to record temperature distributions across the machine structure during the experiments. The thermal images were saved as a matrix of temperatures with a specific spatial resolution of one pixel, each of which can be considered as a possible temperature measurement point. Methods of optimising sensor location, using automatic clustering of thermography data, have also been proposed. This allows efficient modelling of new machines.

The proposed approach has been validated on three different machine tools under different operation conditions. Thus the proposed system has been shown to be robust to different internal heat sources, ambient changes and is easily extensible to other CNC machine tools.

### 1.3 Aims

- To produce intelligent techniques for robust modelling of machining errors caused by the thermal distortion of CNC machine tools.
- To make these techniques readily applicable to any common CNC machine with minimal effort.

### 1.4 Motivation

This research was motivated by the high accuracy requirements of the manufacturing industry. Increasingly, changes in the business requirements of manufacturing industries are driving machining systems to be more accurate and more productive. As a consequence, the research approach taken in this thesis addresses an intelligent compensation strategy which can be implemented in a timely and cost effective manner on existing CNC machine tools with different configurations. A compensation strategy which effectively improves the accuracy of a machine tool would significantly reduce waste and rework, and lead to more predictable production schedules, etc.

### 1.5 Objectives

The objectives of this research work are:

- To undertake an in-depth literature review to ascertain the past, current and future requirements of CNC machine tools, particularly in terms of their thermal error compensation.
- To develop a systematic methodology to define a precise selection of thermal sensors and their positions in order to ensure the prediction accuracy and robustness of compensation models.
- Provide a thorough and complete description of the data-driven modelling.
- To derive a novel thermal prediction model for a CNC machine tool, using the Artificial Intelligence (AI) tools such as Adaptive Neuro-Fuzzy Inference System (ANFIS), Artificial Neural Networks (ANNs), Particle Swarm Optimisation (PSO) and Grey system theory.

- To investigate and evaluate the performance of the thermal error compensation models for CNC machine tools and their requirements.
- To develop a general thermal prediction model, that can be readily transferred to other machine tools in a timely and cost effective manner.
- Provide a generalised, cost-effective approach to thermal error compensation that can be implemented on a wide range of machine tools with different configurations, the following considerations should be taken into account:
  - Accurate, reliable and robust;
  - Capable of being implemented on a wide range of CNC machine tool configurations;
  - Quick to apply, without excessive downtime.
- Validation using disparate cycles on multiple machines.

## 1.6 Thesis Structure

The previous sections of this chapter have presented a background of thermal error sources, and an overview of primary approaches to mitigate these thermal errors of CNC machine tools. A breakdown of the work presented in the body of this thesis is as follows.

Chapter 2 presents a review of literature relating to the modelling of thermal errors and current developments in the field of thermal error compensation of CNC machine tools. Subjects include the principle-based models, empirical-based models, and thermal key point identification approaches. Studies relating to application of AI techniques to various machining processes are also reviewed. The chapter is also concluded with a discussion of the challenges of the current models.

This is followed in Chapter 3 by a thorough description of the current state of artificial intelligence systems, including details of ANFIS model and extraction of the initial fuzzy model. Particular focus is also given to the Grey system theory for both modelling and selection of the most relevant thermal variables. The chapter is concluded with a discussion of the model validation procedure.

Chapter 4 outlines the experimental considerations taken into account when collecting the data to build the compensation models of the CNC machine tool. Details will also be provided on the equipment setup used during the various experimental tests. This is followed

by a systematic methodology to a precise selection of thermal sensors and their positions in order to ensure the prediction accuracy and robustness of compensation models. The effect of using different physical quantities (temperature and strain) will also be explored. The effect of hysteresis will also be investigated in this chapter.

In Chapter 5 the proposed model will be developed for the purpose of verification of the techniques that will be developed in subsequent chapters.

In Chapter 6 a new concept will be added to ANFIS modelling for prediction of ETVE. Also, four models will be developed for the purpose of validation of the proposed approach which will be designed to predict the thermal error of a number of machines in different operation conditions. The first model will be the proposed ANFIS model. The second model that will be developed is an ANN model. The third and fourth models that will be developed are two Grey models.

The deep understanding of literature review and main findings from Chapter 2 to Chapter 6 are brought together and summarised in Chapter 7, followed by an explicit statement of the conclusions drawn from this thesis.

## Chapter 2: Thermal-Error Modelling Techniques

This chapter provides the literature review of machine tool error compensation techniques relevant to this thesis. It starts by providing an overview of different modelling approaches that have been used for thermal error compensation. Next, a comprehensive review of the areas of machine tool error modelling and compensation is conducted. This followed by discussion of the application of AI techniques to various machining processes. The gaps in the literature are identified and the objectives of this work are highlighted based on the key findings from previous research and response to the limitations of existing techniques. The chapter ends with separate sections containing the challenges and summary of the literature review.

### 2.1 Thermal Modelling Methods

Error compensation has become a cost-effective way to improve the accuracy of machine tools, in which error modelling play a fundamental role [6]. Robust modelling is one of the greatest challenges in the field of the machine tools thermal error compensation [32]. Generally, different types of modelling approaches are used for thermal error compensation. The first one is known as the principle-based models (white-box models). In principle-based method; the system models are derived based on heat transfer mechanisms (i.e., conduction, convection, and radiation) [17, 33]. Here, the relationships between thermal errors and heat generated are described by a system of non-linear differential equations [30]. The solution to such differential equations can be obtained by analytical methods as well as numerical methods. Therefore, principle-based models are further divided into analytical models and numerical models. It is worth mentioning that the principle-based model is interpretable but not necessarily sufficiently accurate because, there are always uncertain factors affecting the system. An accurate principle-based model can hardly ever be obtained because of the interaction between multiple moving parts with multiple ill-defined heat inputs. The second type is known as data-driven models (empirical-based models) [34, 35]. The relationships between the system inputs and outputs are not based on physical representations, as for principle-based models, but are deduced through suitable experimental tests. This is done by making use of the principle “cause and effect” where the temperature variable is the cause and the thermal error is the effect. The experimental data are divided into two different sets, one used at the training/calibrating stage and one used for the model testing. It is worth

mentioning that in data-driven models, the interpretation of the model is often difficult. In the third type, known as the grey-box models [36], the basic structure of the model is formed by using the principle-based method and the model parameters are calibrated by using the parameter estimation algorithms on the measured data of the system. This means that the starting point is a model structure based on physical representations. Because so much engineering knowledge and experimental work comes in terms of verbal rules, a sound engineering approach is to attempt to integrate such linguistic information (words) into the modelling process. A convenient and common way of doing this is to use Fuzzy Logic (FL) concepts in order to cast the verbal knowledge into a conventional mathematical representation (a model structure), which subsequently can be fine-tuned using expert knowledge and/or experimental data [37], for more detail about Fuzzy Logic Systems (FLS), the reader is referred to section 3.2.

A fuzzy model is a computation framework based on the concepts of fuzzy sets, fuzzy “if-then” rules, and fuzzy reasoning. In real world problems, if the designer has information such as human experience described by linguistic rules “if-then” rules, the mechanistic modelling approach is less important and the application of rule-based approaches like FL models is more appropriate. Fuzzy modelling allows us to deal with the complex system by building a linguistic model which could become interpretable by human beings [38]. The flexibility of a fuzzy model allows us to extract rules that describe the behaviour of a system. In other words, fuzzy modelling takes advantage of engineering knowledge and experimental work that might not be easy to be directly applied in other modelling methods. A common practice is to use such knowledge for structure identification (determination of the relevant inputs, type and number of the Membership Functions (MFs) and number of the rules, and so on). These parameters can then easily be calibrated and fine-tuned by experimental data with the use of various learning techniques such as a neural network (known as neuro-fuzzy models). Models based on this method are partially linguistic statements and partially empirical. Different from black-box models, neuro-fuzzy models require both the knowledge of the process system (represented by linguistic rules) and empirical data. The rule base of these neuro-fuzzy models is initialised by expert knowledge or clustering techniques, and the model parameters are calibrated via similar methods that are used for the data-driven models. As the neuro-fuzzy model can initialise and learn linguistic rules, the modelling framework can be considered as a direct transfer of knowledge [33]. This is the powerful advantage of adaptive fuzzy systems in comparison with principle-based and other data-driven models.

This chapter will present a comprehensive review of the thermal error modelling techniques. It will not attempt to provide a broad survey of the field of fuzzy modelling. For such a survey, the reader is referred to the next chapter. Current challenges in the thermal error models, reported in the literature, are also discussed. This is followed by a summary of the literature review presented in this chapter.

### 2.1.1 Principle-Based Models

Principle-based models, also called white-box models, describe in space differential equations to simulate the system behaviour. These models are usually interpretable and based on theoretical relationships. Numerical methods such as the Finite Element Analysis (FEA) [39] and Finite Difference Element Method (FDEM) [2, 40] are powerful tools in simulating the practical heat transfer, where analytical solutions to temperature fields and thermal responses are discarded due to the complexity of machine tool elements. With the development of computer technology, FEA has proved to be a powerful tool to predict the thermal error of machine tools. FEA is now being more frequently applied to simulate the thermal error [8, 39, 41].

Mian et al. [8] developed an offline technique using FEA to simulate the effects of the major internal heat sources of a small Vertical Milling Centre (VMC) and the effects of ambient temperature pockets that build up during the machine operation. Their work has shown that consideration of air pockets is needed to improve the FEA model accuracy. The simulation results closely matched the experimental results and revealed a maximum error range of 70  $\mu\text{m}$  reduced to less than 10  $\mu\text{m}$ .

Creighton et al. [42] carried out analytical approaches by FEA model to study the temperature distribution characteristics of a spindle, motor and its housing. The results from the characterisation tests were used to develop a simple exponential model of the axial thermal error related to the spindle speed and running time. It was reported that the model was successful in reducing spindle growth by up to 80% under random spindle speed. However, the thermal error of a machine tool is a mutual coupling of many complex factors that are affected by many variables; therefore, their model cannot compensate the cyclic variation due to the ambient temperature changes. It is extremely difficult to predict the thermal error from a simple exponential equation.

Mian et al. [39] proposed an offline environmental thermal error modelling approach based on a finite element analysis model that reduces the machine downtime usually needed for the environmental temperature variation error test from a fortnight to 12.5 h. Their modelling approach was tested and validated on a production machine tool over a one-year period and found to be very robust.

Postlethwaite et al. [6] made a distinction between the temperature model and distortion model of a thermally affecting CNC machine, and used a thermal imaging camera for rapid assessment of a machine tool thermal behaviour and off-line development of the compensation models. Their proposed technique can calculate the temperature distribution and distortion when the machine is subjected to widely varying operating conditions.

White et al. [7] outlined a combination of geometric and thermal error compensation systems with a flexible structure that is “general purpose” in its application to any machine tool. The proposed system can use any number of temperature sensor inputs. MATLAB model can be programmed in such a way that it estimates its thermal movement using data from a single test on the machine. The program then applies error compensation to a number of outputs, which are used by the machine controller to obtain a compensation value. The compensation model can either be integrated into an open architecture CNC machine controller, or into a stand-alone computer which accepts a large range of feedback signals. The compensation model can reduce both dependent and independent thermal errors. It has been applied to different types of machine tools, and has been proven to reduce thermal errors between the tool and the workpiece by more than six times when applying a cooling and quick heating test for calibration.

Freeman et al. [20] established a system which minimises the number of temperature sensors used as inputs to a thermal model of the ballscrew. The authors used their model to predict on-line the thermal errors of the ballscrew. If the position measurements of the nut are available from the encoder, it is possible to determine the speed of the screw. Assuming knowledge of heat transfer characteristics and the friction, and using the measured temperatures of the nut and bearings, the heat generated in the nut, bearings and screw can be calculated. The thermal model constitutes a one-dimensional finite analysis of the screw. The output of their proposed model is a temperature distribution along the screw and an estimate of the thermal errors of the screw.

However, building a numerical model can be a great challenge due to problems of establishing the boundary conditions and accurately obtaining the characteristics of heat transfer. Because the FEA models are built based on assumptions and empirical formula, which inevitably have inaccuracies, the FEA model must be modified by experimental tests. It is also noted that most validation only represents a similar input-output condition to the modelling process. It is therefore difficult to estimate robustness of the model to changing parameters.

The following paragraphs will give a discussion of different kinds of data-driven models most of which aim to predict the thermal error of machine tools.

### **2.1.2 Data-Driven Models**

The data-driven models are behavioural models that are based on historical data to predict the performance of a given system, in this case the distortion of the machine. Contrary to the numerical models, they are not based on explicit physical equation definitions but on experimental database which is capable of reflecting the relationship between inputs and outputs. Data-driven techniques for thermal error modelling can be divided into two categories: statistical techniques such as regression methods, linear polynomial models, etc., and artificial intelligence techniques such as Artificial Neural Networks (ANNs), fuzzy systems, etc.

#### **2.1.2.1 Statistical Models**

Linear regression is the simplest method to correlate measured temperatures with resulting displacement. A Least Squares (LS) approach is used to obtain the coefficients that determine the relationship between inputs and output without using any physical equation. Although this method can provide reasonable results for a given machine test regime, the thermal displacement usually changes with variation in the machining process and the environment, which introduces an error into the model [43]. The linear regression model is also time-consuming and labour intensive to design.

Hardwick [44] established a Multiple Regression Analysis (MRA) model of a vertical machining centre and a horizontal machining centre. The author highlighted the complexity of the interrelation between the different heat sources and the different mechanisms of response. Test results showed that the thermal error could be reduced to less than 7  $\mu\text{m}$ , representing an improvement in accuracy of almost 7 times.

Chen et al. [45] used an MRA model for thermal error compensation of a horizontal machining centre. With their experimental results, the thermal error was reduced from 196 to 8  $\mu\text{m}$ . Yan et al. [46] also used the MRA model to form an error synthesis model, which merges both the thermal and geometric errors of a lathe. With their experimental results, the error could be reduced from 60 to 14  $\mu\text{m}$ .

Grey model is another statistical approach that has been used for thermal error compensation system [47]. Grey system theory is a method introduced by Deng in early 1980s [48] with the intention to study the Grey systems by using mathematical methods with poor information and small datasets. In Grey system theory, GM (h, N) denotes a Grey model, where h is the order of difference equation and N is the number of variables. The GM (h, N) model can be used to describe the relationship between the influencing sequence factors and the major sequence factor of a system. Furthermore, weights of each factor represent their importance to the major sequence factor of the system. Its most significant advantage is that it needs only a small amount of experimental data for accurate prediction, and the requirement for the data distribution is also low [49]. For more detail about Grey models, the reader is referred to section 3.4.

Wang et al. [47] proposed a systematic methodology for the thermal error compensation of a machine tool. The thermal distortion was modelled using a Grey model based on Grey system theory to predict the thermal errors with only 30 minutes of measured data. Unfortunately, their model was lacking in the ability of self-learning, self-adaption, self-organisation, and taking feedback correction into consideration. Therefore, their model obtained under one particular operating condition is still not robust under other operation conditions.

In order to overcome the drawbacks of statistical models, more attention has subsequently been given to the artificial intelligence techniques such as artificial neural networks.

### **2.1.2.2 Artificial Intelligence (AI) models**

Artificial neural network as a form of AI is a data-driven approach. It is designed in a way that mimics the behaviour of biological neural network. A typical artificial neural network has an input layer, one or more hidden layers, and an output layer [50]. The neurons in the hidden layer, which are connected to the neurons in the input and output layers by adaptable weights, enable the ANN to compute complex associations between the input and output variables [51]. The inputs of each neuron in the hidden and output layers are summed and the

resulting summation is processed by an activation function [51]. Training the model is the process of determining the adjustable weights and it is similar to the process of determining the coefficients of a regression model by least squares approach. The weights are initially selected randomly and an optimisation algorithm is then used to find the weights that minimise the differences between the model-calculated and the experimental outputs [52]. Across the whole modelling procedure, no physical equation is used.

To find the relationship between inputs and outputs of a complex thermal behaviour, ANN techniques have drawn more attention rather than statistical models, and produce results without requiring a detailed mechanistic description of the phenomena that is governing the system. There are different ANN architectures to building thermal models, Back-Propagation (BP) artificial neural network modelling has proved to be a suitable nonlinear modelling method [50, 53].

One of the major advantages of ANNs is efficient handling of highly non-linear relationships in data. In recent years, it has been shown that thermal errors can be successfully predicted by artificial neural networks [50, 54, 55].

Chen et al. [56] proposed an ANN model structured with 15 nodes in the input layer, 15 nodes in the hidden layer, and six nodes in the output layer in order to drive a thermal error compensation of the spindle and lead-screws of a vertical machining centre. The ANN model was trained with 540 training data pairs and tested with a new cutting condition, which was not included within the training pairs. Test results showed that the thermal errors could be reduced from 40 to 5  $\mu\text{m}$  after applying the compensation model, but no justification for the number of nodes or length of training data was provided, so the scalability of the method cannot be assessed. Moreover, the compensation system must be flexible to extension to other physical inputs, meaning that alternative variables can be deployed with minimal effort.

Wang [57] used a neural network trained by a Hierarchy-Genetic-Algorithm (HGA) in order to map the temperature variation against the thermal distortion of the machine tool. Experimental results indicated that the thermal error compensation model could reduce the thermal error to less than 10  $\mu\text{m}$  under real cutting conditions.

Zhu et al. [58] presented a clustering approach based on correlation coefficient to pick out three optimal temperature variables. The output-hidden feedback Elman neural network is adopted to establish a model for the prediction of thermal errors on a CNC machine tool. The verification experiment shows that the combination of clustering and neural network model is

a good way for thermal error compensation. However, a small number of temperature sensors may lead to poor prediction accuracy under different operation conditions.

ANN models may be successfully applied in thermal error compensation systems and can capture effectively the non-linear relationships existing between variables in nonlinear systems such as thermal modelling. However, ANN models are considered as black-box models, because the mathematical relations in these models are unknown to the designer and have no physical meaning. Moreover, it is worth pointing out that these models need proper training to work effectively, and that their performance is limited by their design parameters. Therefore, using ANN involves a moderately tedious trial and error effort for obtaining the network structure, especially involving the hidden layer neurons, number of hidden layers, transfer function, training algorithm and learning rate parameter.

The purpose of this section was to give an overview about thermal modelling and to show the important role of data-driven models in this field of thermal error compensation. It was shown that ANN models are general black-box modelling tools, which have many attractive features: they are constructed without any physical laws but only a set of input-output data for training procedure. The training data has to cover the whole expected range of the operation conditions. However, the process of obtaining such data can take several hours for internal heating tests and several days or more for the environmental test [3].

An important implication obtained from the above mentioned models is that they have been proven for a single error source but not a whole (complete) machine structure. Furthermore, most of them have used only one approach, which usually cannot result in satisfactory thermal model. Combining different AI techniques, however can join the advantages of the different methods, can utilise different representations of knowledge, and can help to understand the result obtained. The latter is especially important in ANN modelling, because ANN models cannot give explanation of the system, and without explanation, the lack of physical meaning may reduce the acceptance of the ANN models even if their result are in good agreement with the experimental data.

### **2.1.3 Fuzzy Logic Models**

Fuzzy applications in machining process have become the focus of significant attention during the last two decades, and that is why much relevant research has been conducted. Fuzzy system theory has a wide range of applications in the machining process field and new directions are constantly given in machining process research.

Lee et al. [59] used a thermal error model with two temperature variables using fuzzy logic modelling. However, the membership functions typically have to be manually adjusted by trial and error. The fuzzy model performs like a white-box, meaning that the model designers can explicitly understand how the model achieved its goal. However, such models that are based only on expert knowledge may suffer from a loss of accuracy due to engineering assumptions [60]. Conversely, ANNs can learn from the data provided without preconceptions and assumptions. However, they perform as a “black-box,” which means that there is no information regarding the method by which the goal is achieved and so the achieved optimal solution can exhibit unrealistic physical characteristics that do not extrapolate to other situations. Furthermore, the final model is not easily understandable by domain experts for interpretation purposes [61].

In order to overcome the drawbacks of traditional artificial intelligence techniques such as ANNs and fuzzy logic, more attention has been focussed on hybrid models. For instance, applying the ANN technique to optimise the parameters of a fuzzy model allows the model to learn from a given set of training samples. At the same time, the solution is mapped out into a Fuzzy Inference System (FIS) that can be evaluated by the model designer as to produce a realistic representation of the physical system. The Adaptive Neuro-Fuzzy Inference System (ANFIS) is such a neuro-fuzzy technique. It combines fuzzy logic and neural network techniques in a single system.

Wang [62] also proposed a thermal model merging Grey system model GM (1, m) and an ANFIS. A hybrid learning method, which is a combination of both steepest descent and least squares estimator methods, was used in the learning algorithms. Experimental results indicated that the thermal error compensation model could reduce the thermal error to less than 10  $\mu\text{m}$  under real cutting conditions. The author used six inputs with three fuzzy sets per input, producing a complete rule set of 729 ( $3^6$ ) rules in order to build an ANFIS model. Clearly, Wang’s model is practically limited to low dimensional modelling.

Eskandari et al. [63] presented a method to compensate for positional, geometric, and thermally induced errors of three-axis CNC milling machine using an offline technique. Thermal errors were modelled by three empirical methods: MRA, ANN, and ANFIS. To build their models, the experimental data was collected every 10 minutes while the machine was running for 120 minutes. The experimental data was divided into training and checking sets. Their results found that ANFIS was a more accurate modelling method in comparison

with ANN and MRA. Their test results on a free form shape show average improvement of 41% of the uncompensated errors. However, the ANFIS model in this study is also limited to low dimensional modelling.

Construction of the ANFIS model using a data-driven approach usually requires division of the input/output data into rule patches. This can be achieved by using a number of methods such as grid partitioning or the subtractive clustering method [64]. However, one limitation of standard ANFIS is that the number of rules rises rapidly as the number of inputs increases (number of input sensors). For instance, if the number of input variables is  $n$ , and  $M$  is the partitioned fuzzy subset for each input variable, then the number of possible fuzzy rules is  $M^n$ . As the number of variables rises, so the number of fuzzy rules increases exponentially, increasing the load on the computer processor and increasing memory requirements. Thus, a reliable and reproducible procedure to be applied in a practical manner in ordinary workshop conditions was not proposed. It is important to note that an effective partition of the input space can decrease the number of rules and thus increase the speed in both learning and application phases. A fuzzy rule generation technique that integrates ANFIS with Fuzzy C-Means (FCM) clustering is applied in order to minimise the number of fuzzy rules. The FCM is used to systematically create the fuzzy MFs and fuzzy rule base for ANFIS. For more detail about this system, the reader is referred to section 3.3.

An accurate, robust thermal error prediction model is the most significant part of any thermal compensation system. In recent years, it has been shown that thermal errors can be predicted by empirical modelling techniques such as multiple regression analysis [45], types of artificial neural networks [56], fuzzy logic [59], an adaptive neuro-fuzzy inference system [50, 62], Grey system theory [47] and a combination of several different modelling methods [53, 57].

A common omission in the published research is discussion or scientific rigour regarding the selection of the number and location of thermal sensors. The following section explores the effect of the number and locations of sensors on the thermal model output.

## 2.2 Temperature Sensor Placement

Appropriate selection of input variables is an important task in modelling. In fact, not all input variables are equally important; some may have no significant effect on the system being modelled. Scholars have shown that a precise selection of thermal sensors and their

position is needed to ensure the prediction accuracy and robustness of compensation models, better interpretation, and lower measurement costs [32, 46]. The model designers often want to know which sources have a dominant effect and which exert less influence on thermal response of the machine tool. Poor location and a small number of thermal sensors will lead to poor prediction accuracy. However, a large number of thermal sensors may have a negative influence on a model's robustness because each thermal sensor may bring noise to the model as well as bringing useful information. Furthermore, issues relating to sensor reliability are commercially sensitive; the fewer sensors installed the fewer potential failures. Choosing the right sensor location can hugely affect the outcome of compensation models. Engineering judgment, correlation coefficient and stepwise regression have been used to select the temperature sensor placement for thermal error compensation models [30, 31].

The first method is engineering judgment, which is based on an individual's engineering experience about thermal displacement, machine heat sources and thermal behavior in order to design the models [31]. It is useful to remove totally uncorrelated sensors and to choose preliminary sensors for further study. For example, the axial movement of the ballscrew and the spindle physically depend on the bearing temperatures of the ballscrew and the spindle, respectively; thus, the bearing temperatures are considered as a possible variable in the models. However, many other error components, such as spindle displacement and squareness errors, have different relationships with temperature behavior on columns or spindle housings. It is unreliable to use a small number of temperature sensors without precise knowledge of thermal behavior in machine elements. It is clearly impossible to select the optimal thermal sensor location on the whole machine only using the engineering judgment.

The second method is a correlation analysis, which uses the correlation coefficients between the thermal displacements and the temperature sensors to select highly correlated temperatures sensors as compensation model inputs [13, 65, 66]. Since all the selected sensors are strongly correlated with the thermal displacement, however, the relationships between them were overlooked. The partial correlation between the thermal displacement and the sensors or the correlation between the sensors has to be identified; otherwise the technique is only suitable for designing a model with a single sensor which would impact the accuracy of the final model.

The third method is a standard stepwise regression [67], which is used to find the best thermal compensation model using the available temperature sensors. Stepwise regression is achieved by including the most strongly correlated sensors and then adding or subtracting one sensor at a time based on statistically significant criteria, thus evaluating the contribution of the added or withdrawn sensor. In each epoch of the stepwise regression procedure, only one sensor is added to or subtracted from the compensation model. The result of combining two or more sensors at a time is not considered. Since the temperature sensors on a machine element are interrelated, the merging of two or more sensors is significant during the modelling procedure. The stepwise regression could end in a model with insignificant sensors.

Moreover, there are further sensor selection methods, such as the sensor placement scheme based on thermal modal analysis [11, 31]. This method has a similar drawback to that of finite element analysis. Yan et al. [46] also proposed an MRA model combining two methods, namely the direct criterion method and indirect grouping method; both methods are based on synthetic Grey correlation. Using this method, the number of temperature sensors was reduced from sixteen to four and the residual range was reduced by 69%. Han et al. [68] proposed a correlation coefficient analysis and fuzzy c-means clustering for selecting temperature sensors both in their regression thermal error model and ANN model [69]; the number of thermal sensors was reduced from thirty-two to five. However, more efforts are still needed in order to prove that the selected sensors are indeed correct and important to the final model.

Sometimes, sensor selection is used in an automated manner in a black-box approach. However, this is not always the optimal approach. In order to develop accurate models, it is necessary to understand that sensor selection methods work under certain assumptions. Nevertheless, when used appropriately, they can give useful knowledge on what sensors seem important, what sensors seem unimportant and what sensors are of intermediate importance. With such knowledge combined with a comprehensive understanding of the data, an accurate approach for sensor selection can be achieved. Therefore, the above-mentioned methods suffer from the following drawbacks: a large amount of data is needed in order to select proper sensors; and the available data must satisfy a typical distribution such as normal (or Gaussian) distribution [70]. Therefore, a systematic approach is still needed to minimise the number of temperature sensors and select their locations so that the downtime and resources can be reduced while robustness is increased. It is notable that most publications deal only

with the reduction in sensors, but not the means by which the original set were determined. As a result the system is only shown for situations where the possible solutions are a subset of all potential locations, which requires non-trivial preconditioning of the problem. This is a situation where some aspects of the machine spatial temperature gradients might already have been missed and is typical when a machine model is being adapted, rather than evaluated from a new perspective.

This thesis makes extensive use of thermal imaging camera for rapid assessment of machine structure thermal behaviour and development of the compensation models. A thermal imaging camera will be used to record temperature distributions across the machine structure. Each pixel can be considered as a possible temperature measurement point. This is a good practice where many aspects of the machine spatial temperature gradients might already have been covered.

In this proposed approach, the Grey models and fuzzy c-means clustering are used to determine the major sensors influencing thermal errors of a number of CNC machine tools, which is capable of simplifying the system prediction model. Then ANFIS is used to build a number of thermal prediction models based on selected sensors. This combined methodology can help to improve robustness of the proposed model, and reduce the effect of sensor uncertainty.

### **2.3 Hysteresis in Thermal Error Modelling**

The hysteresis effect is defined as a system that has memory, where the effects of the current input to the system are experienced with a certain delay in time [71]. Due to varying thermal time constant, thermal effects on CNC machine tools have the characteristic of memorising the previous thermal status. Therefore, the errors in a machine tool are not only dependent on the current thermal status measured at the surface, but also influenced by the previous conditions of the machine. The hysteresis behaviour will introduce error in each cycle, which in a worst case scenario can be seen in large machine tools with bigger volumes, longer strokes and heavier cutting loads [43]. This hysteresis phenomenon makes the static/instantaneous modelling approach less robust. The characterisation of structural material which exhibits thermal hysteresis needs a special consideration. This is more evident when the rate of temperature change is low as compared with the speed of response of thermal displacement and also where surface-mounted sensors do not reflect the slower-

changing internal temperature. Therefore, most of the above-mentioned methods require a large amount of measured data during heating/cooling cycles. Methods that require a calibrated model to predict thermal errors are expected to be confounded by the very large variety of working conditions that exist in a machine tool. Furthermore, attention is often drawn to the prohibitive downtime required to conduct the experiments in an ordinary machine shop [3].

## 2.4 Fusion Measurements

Accurate and reliable measurements of key variables of the machine tool are very important. The information from these variables will be used for model training/calibration, therefore they should contain the most relevant feedback information. In most of the thermal error models of machine tools, temperature sensors are used as inputs to estimate thermal deformation [47, 57, 63]. However, spindle speed, axis feedrate, machining time and other parameters of the machine can also be taken into consideration because they are responsible for major heat sources [72]. In some cases [36, 73] no direct temperature measurement is taken and only the spindle speed and feedrate are used as inputs. However, this strategy is limited, because the model obtained under one particular operation condition is not robust under other operation conditions. Therefore, error reduction needs greater understanding of the machine tool properties and error sources. This results in the need for a machine tool structural monitoring system.

Fibre Bragg Grating (FBG) sensors are used for strain measurement purposes [74]. They have several advantages over other sensors in terms of sensitivity and quality [74] and could be embedded in a future, commercialised system. In literature, the common applications of FBG are damage detection, structure health monitoring and strain measurement in harsh environments [75, 76]. FBG can be employed to observe the change in the strain of the structure with respect to variation in temperature to provide a new response of the system. By using these sensors, the modelling process can become simpler, more robust and more efficient since the number of thermal sensors can be reduced and the effects of thermal hysteresis minimised.

Huang et al. [77] used FBG to investigate the effect of temperature variations of a heavy-duty machine tool on the shop floor. The variations of ambient temperature were measured by the FBG sensors and the spindle thermal shift errors were monitored by laser displacement

sensors simultaneously. Experimental results indicate that the spindle thermal errors have a similar change trend following the ambient temperature. Based on acquired data by FBG sensors and thermal error, the authors suggested that a thermal error compensation model could be built by using several modelling techniques such as multiple linear regressions, neural network, and other system identification methods; however, no implementation has been done in this regard.

This section has highlighted that many thermal error models of machine tools used temperature sensors as inputs to estimate thermal deformations. The development of a compensation system using other parameters of the machine is discussed and investigated in this research work.

### 2.5 A Summary of Challenges

Research aimed at improving the accuracy of machine tools has been very prolific over the last two decades. From the literature, every thermal compensation model is faced with a series of challenges. These challenges mainly concern the accuracy and the robustness of the thermal compensation model. In modelling thermal errors of machine tools, the issues that need to be considered are described as follows:

- Prediction accuracy: the main reason for implementing thermal error compensation is to reduce or minimise the thermal error. Prediction accuracy is therefore a key parameter when evaluating a system. Recently, artificial intelligence methods are becoming more popular and particularly amenable to modelling complex systems, because they have demonstrated superior predictive ability compared to traditional methods. For more detail about AI methods, the reader is referred to section [2.1.2](#).
- Robustness: the thermal error model must work properly in different operating conditions and with different machine tool configurations. A system that would not produce reliable results would never be deployed; CNC machine tools rely on repeatability.
- Simplicity: in the past, the model had to be kept as simple as possible. For instance, although the ANN models are more accurate than the regression models, the calibration of the regression models coefficients is simpler (least squares approach), see section [2.1.2.2](#). However, the use of mathematical software tool such as that existing in MATLAB facilitates the calibration of the model coefficients by using

optimisation/training tools. Nevertheless, there is still a strong argument for simplicity, where possible, to avoid over-constraining the system and introducing instability.

- **Model inputs:** from the literature, some research uses only machine parameters (spindle speed, axis feedrate and run-time) as input. This requires no additional hardware, but such systems cannot cope with change in performance. On the other hand, other authors used only temperature sensors as input variables to the developed models (see section 2.2). This philosophy has some merit, since it ensures that the model is driven by changes in temperature profile irrespective of the heat source. However, fusion of other sensor types and machine control values can also be taken into consideration, because they are responsible for major heat sources. One such value is the spindle speed, although other significant factors can also be considered (see section 2.4). For this reason, the inclusion of the primary parameters is non-trivial when looking for long-term accuracy from the model and it can be more robust only to include the derived values that directly affect accuracy.
- **Availability of data:** to obtain an accurate thermal prediction model, long term temperature data is required. However, the size of the input-output dataset is very crucial when the generation of data is a costly affair (machine downtime). For instance, the process of obtaining such data can take several hours for internal heating tests and for many days or more for the environmental tests (see sections 2.1.2.1, 2.1.2.2). One way to overcome this problem, the model designer needs to borrow a valid white-box model to supplement the experimental data.
- **Flexibility:** ideally the compensation system must be flexible to extension to other physical inputs, meaning that alternative variables can be deployed with minimal effort. This makes the system easier to deploy and adapt, increasing its usefulness across multiple systems (see section 2.4).
- **Sensor location:** It is notable that most publications related to “optimising sensor placement” deal only with the reduction in sensors, but not the means by which the original set were determined. This is a situation where some aspects of the machine spatial temperature gradients might already have been missed. The selection must be optimal to satisfy accuracy and robustness, but not imposed under commercial constraints. For more detail about sensor locations, the reader is referred to section 2.2.

- Structure of the AI models: from the literature, the ANN is considered one of the most appropriate models for thermal error compensation. However, using neural network involves a moderately tedious trial and error effort for obtaining the network structure, especially involving the hidden layer neurons, number of hidden layers, transfer function, training algorithm and learning rate parameter. Furthermore, the final model is not easily understandable by domain experts for interpretation purposes. A robust system requires their design to be more efficient (see section [2.1.3](#)).

## 2.6 Summary

Accurate modelling of machine tools is becoming ever more important because of current industrial demands for higher productivity at increasing quality levels. Thermal error modelling is still an innovative and developing area of CNC machine tool accuracy. There are still uncertainties and room for improvement. In summary, from this undertaken literature review, it appears that, despite a large amount of previous research undertaken in the thermal error compensation area, there is a number of issues that still remain to be addressed (see section [2.5](#)).

The main aim of this research work is to produce intelligent techniques for modelling machine tool errors caused by the thermal distortion of CNC machine tools. The goal of this investigation is to make the intelligent compensation system readily applicable to any common CNC machine with minimal effort.

## Chapter 3: Artificial Intelligence Techniques and Methods

### 3.1 Introduction

An artificial intelligence system is a system that can make decisions which would be considered intelligent if made by a human being. Artificial Intelligence (AI) is becoming more popular and particularly amenable to modelling complex systems, because it has demonstrated superior predictive ability compared to traditional methods.

In this chapter, the aim has been to present a description and analysis of the AI systems that will be used throughout this research work. This chapter first gives a short introduction to fuzzy logic and fuzzy systems, and then concentrates on methods for obtaining fuzzy models from data. These approaches are commonly referred to as neuro-fuzzy techniques since they exploit a link between fuzzy systems and neural networks. Within this chapter, only one architecture of neuro-fuzzy techniques is considered, the so called an adaptive neuro-fuzzy inference system. This is followed by an introduction to Grey models and their usage for thermal variables selection. Finally, a summary gives some guidelines for the reader to check the prediction quality of the resulting model and to assess the parameter accuracy.

The whole block diagram of the proposed system is shown in [Figure 3-1](#) where spots 1 to N represent the virtual temperature sensor data, and the thermal response. To obtain robust models, all the influence weighting of thermal sensors is clustered into groups using FCM. Then, one sensor from each cluster is selected to represent the temperature sensors of the same category according to its influence coefficient with the thermal response. Therefore, the ANFIS models can be built easily to predict the thermal response.

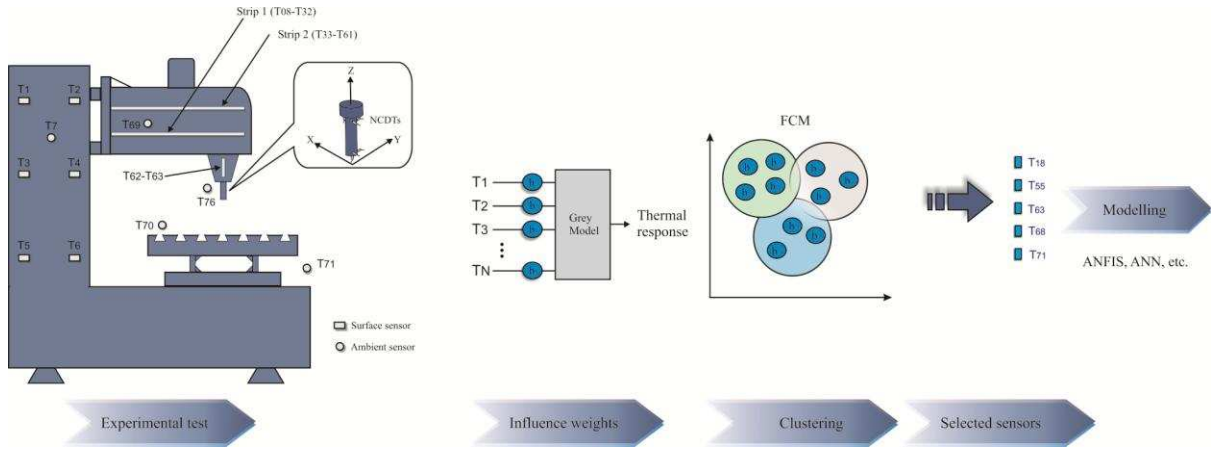


Figure 3-1: Block diagram of the proposed system.

### 3.2 Fuzzy Logic and Fuzzy Systems

The concept of Fuzzy Logic (FL) was pioneered by Zadeh [78, 79] and was introduced not as a control methodology, but as a way of processing data by allowing partial set membership rather than a crisp set membership or non-membership. In fuzzy logic, the membership function is a curve that defines how each point in the input space is mapped to a degree of membership between 0 and 1. Classical logic needs a deep understanding of a system's exact physical equations and precise crisp values. Fuzzy logic demonstrates an alternative way of thinking, which allows complex modelling using a higher level of abstraction created particularly from human knowledge and experience. Fuzzy logic allows formulating this knowledge in a subjective way which is mapped into exact crisp ranges. In classic set theory, elements either completely belong to a set or are completely excluded from it. The process of expressing the mapping from inputs to an output using fuzzy logic is named the Fuzzy Inference System (FIS) [80].

The particular structure of the fuzzy model, can be classified into: (i) Fuzzy linguistic model (Mamdani model) [81, 82] (ii) Fuzzy relational model [83] (iii) Takagi-Sugeno (T-S) fuzzy model [84]. A main distinction can be made between the Mamdani model, which has fuzzy propositions in both antecedents and consequents of the rules, and the T-S model, where the consequent is a crisp function of the input variables, rather than a fuzzy proposition [85]. Fuzzy relational models can be regarded as a generalisation of Mamdani model, allowing one particular antecedent proposition to be associated with several different consequent propositions via a fuzzy relation [33].

In the literature, it can be clearly seen that the Mamdani model structure demonstrates several advantages. It provides a natural framework to include expert human knowledge in the form of linguistic fuzzy “if-then” rules. This knowledge can be easily gathered with rules that describe the relation between system input-output [85]. Moreover, Mamdani model provides a flexible means to formulate knowledge, while at the same time it remains interpretable, as long as a proper design is developed. However, although Mamdani model possesses several advantages, it also comes with some weaknesses. One of the main drawbacks is the lack of accuracy when modelling some high-dimensional, complex systems. This is due to the limitation of human cognitive ability of codifying these complex systems. Therefore, during the last few years much of the research developed in fuzzy logic modelling focused on increasing the accuracy as much as possible, giving little attention to the interpretability of the resultant model. Hence, the T-S fuzzy models played a pivotal role in the contemporary research. These models are relatively easy to identify, and their structure can be readily calibrated.

Therefore, the two main objectives to be addressed in the fuzzy model are interpretability, and accuracy. General speaking, the ideal model would be to satisfy both criteria (interpretability and accuracy) to a high degree, but since they are contradictory issues of the conflicting aims for complex systems, it is generally impossible [83]. Consequently, researchers usually focus on obtaining the best trade-off between interpretability and accuracy, depending on the nature of the problem to be solved.

Although the measures of accuracy are well-known by using different statistical indices (e.g., root mean square error, and correlation coefficient), interpretability measures are difficult to state since interpretability depends on a number of factors; mainly the model structure, the number of inputs, the number of rules, the number of Membership Functions (MFs), etc. Furthermore, due to the subjectivity of the concept, the choice of proper interpretability measures is still an open problem [38].

As discussed above, fuzzy logic is a useful modelling technique for assessing ambiguous complex physical processes such as thermal dynamics and thus may be applicable for modelling thermal errors in machine tools which are affected by different heat sources. However, its applicability needs further evaluation with experimental data. Several hybrid methods have been introduced in the artificial intelligence field including a neuro-fuzzy

technique. Within this thesis only one architecture of neuro-fuzzy techniques is considered, the so called an adaptive neuro-fuzzy inference system.

### 3.3 Adaptive Neuro-Fuzzy Inference System (ANFIS)

The Adaptive Neuro-Fuzzy Inference System (ANFIS) was introduced by Jang [80, 86]. According to Jang, ANFIS is a neural network that is functionally the same as a Takagi-Sugeno type inference model. ANFIS has become an attractive, powerful modelling technique, combining well established learning laws of ANNs and the linguistic transparency of fuzzy logic theory within the framework of adaptive networks. Fuzzy inference systems are one of the most well-known applications of fuzzy logic theory. In the fuzzy inference systems, the membership functions typically have to be manually adjusted by trial and error. The FIS model performs like a white-box, meaning that the model designers can discover how the model achieved its goal. On the other hand, artificial neural networks can learn, but perform like a black-box regarding how the goal is achieved. Applying the ANN technique to develop the parameters of a fuzzy model allows us to learn from a given set of training data, just like an ANN. At the same time, the solution mapped out into the fuzzy model can be explained in linguistic terms as a collection of “if-then” rules.

#### 3.3.1 ANFIS Architecture

The architecture of ANFIS is shown in [Figure 3-2](#). Five layers are used to construct this model. Each layer contains several nodes described by the node function. Adaptive nodes, denoted by squares, represent the parameter sets that are adjustable in these nodes. Conversely, fixed nodes, denoted by circles, represent the parameter sets that are fixed in the model. A simple example ANFIS architecture, which uses two variables ( $T_1$  and  $T_2$ ) as inputs and one output ( $F$ : Thermal response), will be described in this section in order to explain the concept of the ANFIS structure.

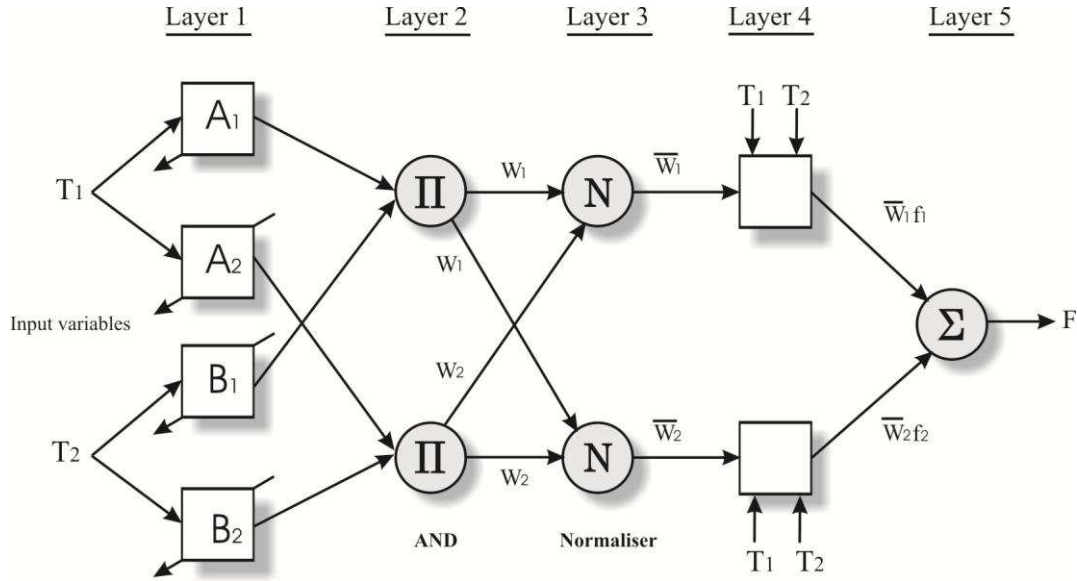


Figure 3-2: Basic structure of ANFIS.

**Layer 1:** The first layer is the fuzzy layer that converts the inputs into a fuzzy set by means of Membership Functions (MFs). It contains adaptive nodes with node functions described as:

$$O_{1,i} = \mu_{A_i}(T_1), \quad \text{for } i = 1, 2 \quad (3.1)$$

$$O_{1,i} = \mu_{B_{i-2}}(T_2), \quad \text{for } i = 3, 4 \quad (3.2)$$

where  $T_1$  and  $T_2$  are the input node, A and B are the linguistic labels associated with this node,  $\mu(T_1)$  and  $\mu(T_2)$  are the MFs, There are many types of MFs that can be used. However, a Gaussian shaped function with maximum and minimum equal to 1 and 0 is usually adopted. Parameters in this layer are defined as premise parameters.

**Layer 2:** Every node in this layer is a fixed node, marked by a circle and labelled by  $\Pi$ , with the node function to be multiplied by input signals to serve as output signal.

$$O_{2,i} = w_i = \mu_{A_i}(T_1) \cdot \mu_{B_{i-2}}(T_2), \text{ for } i = 1, 2 \quad (3.3)$$

where the  $O_{2,i}$  is the output of Layer 2. The output signal  $w_i$  represents the firing strength of the rule.

**Layer 3:** Every node in this layer is considered a fixed node, marked by a circle and labelled by N, with node function to normalise the firing strength by computing the ratio of the  $i^{\text{th}}$  node firing strength to sum of all rules' firing strength.

$$O_{3,i} = \bar{w} = \frac{w_i}{w_1 + w_2}, \text{ for } i = 1, 2 \quad (3.4)$$

where the  $O_{3,i}$  is the output of Layer 3. The quantity  $\bar{w}$  is known as the normalised firing strength.

**Layer 4:** Every node in this layer is an adjustable node, marked by a square, with node function as following:

$$O_{4,i} = \bar{w}_i \cdot f_i, \text{ for } i = 1, 2 \quad (3.5)$$

where  $f_1$  and  $f_2$  are the fuzzy “if-then” rules as follows:

Rule 1. IF  $T_1$  is  $A_1$  and  $T_2$  is  $B_1$ , THEN  $f_1 = p_1 T_1 + q_1 T_2 + r_1$

Rule 2. IF  $T_1$  is  $A_2$  and  $T_2$  is  $B_2$ , THEN  $f_2 = p_2 T_1 + q_2 T_2 + r_2$

where  $p_i, q_i$  and  $r_i$  are the parameters set, referred to as the consequent parameters.

**Layer 5:** Every node in this layer is a fixed node, marked also by a circle and labelled by  $\Sigma$ , with node function to calculate the overall output by:

$$O_{5,i} = \sum_i \bar{w}_i \cdot f_i = \frac{\sum_i w_i f_i}{w_i} = f_{out} = \text{Overall output} \quad (3.6)$$

The simplest learning rule of ANFIS is “back-propagation” which computes error signals recursively from the output layer (Layer 5) backward to the input nodes (Layer 1). This learning rule is exactly the same as the back-propagation learning rule used in the common feedforward neural networks [50, 64]. Although this method can be applied to identify the parameters in an ANFIS network, the method is generally slow and likely to become trapped in local minima [80]. Different learning techniques, such as a hybrid-learning algorithm [87] or genetic algorithm [88], can be adopted to solve this training problem. Better performance of ANFIS models has been shown by adopting a rapid hybrid learning method, which integrates the gradient descent method and the least squares method to optimise parameters [64, 89, 90]. Thus in this thesis, the hybrid learning method is used for constructing the proposed models.

### 3.3.2 Extraction of the Initial Fuzzy Model

In order to start the modelling process, an initial fuzzy model has to be derived. This model is required to select the input variables, input space partitioning or clustering, choosing the number and type of membership functions for inputs, creating fuzzy rules, and their premise and conclusion parts. For a given dataset, different ANFIS models can be constructed using different identification methods such as grid partitioning, and fuzzy c-means clustering [64].

A. The ANFIS-Grid partition method is the combination of grid partition and ANFIS. The data space divides into rectangular sub-spaces using axis-paralleled partitions based on a pre-defined number of MFs and their types in each dimension [91]. The limitation of this method is that the number of rules rises rapidly as the number of inputs (sensors) increases. For example, if the number of input sensors is  $n$  and the partitioned fuzzy subset for each input sensor is  $m$ , then the number of possible fuzzy rules is  $m^n$ . While the number of variables raises, the number of fuzzy rules increases exponentially, which requires a large computer memory. According to Jang [80], grid partition is only suitable for problems with a small number of input variables (e.g. fewer than 6).

B. The ANFIS-fuzzy c-means clustering is the most common method of fuzzy clustering [89]. Essentially, it works with the principle of minimising an objective function that defines the distance from any given data point to a cluster centre. This distance is weighted by the value of MFs of the data point [89]. In the FCM method, which is proposed to improve ANFIS performance, the data are classified into pertinent groups based on their degrees of MFs. In this clustering method, it is assumed that the number of clusters,  $n_c$ , is known or at least fixed. It divides a given dataset  $X=\{x_1, \dots, x_n\}$  into  $c$  clusters. More detail can be found in the next section.

In order to obtain a small number of fuzzy rules, a fuzzy rule generation technique that integrates ANFIS with FCM clustering can be used, where the FCM is used to systematically identify the fuzzy MFs and fuzzy rule base for ANFIS model. In this work, to identify premise membership functions, the two aforementioned methods were used and compared.

### 3.3.2.1 Fuzzy C-Means (FCM) Clustering

Fuzzy C-Means (FCM) is a soft clustering method in which each data point belongs to a cluster, with a degree specified by a membership grade. Dunn introduced this algorithm in 1973 [92] and it was improved by Bezdek [93]. FCM algorithm is the fuzzy mode of K-means algorithm and it does not consider sharp boundaries between the clusters [94, 95]. Thus, the significant advantage of FCM is the allowance of partial belongings of any object to different groups of the universal set instead of belonging to a single group totally.

FCM partitions a collection of  $n$  vectors  $x_i, i = 1, 2, \dots, n$  into fuzzy groups, and determines a cluster centre for each group such that the objective function of dissimilarity measure is reduced.

$i = 1, 2, \dots, c$  are arbitrarily selected from the  $n$  points. The steps of the FCM method are now briefly explained: firstly, the centres of each cluster  $c_i$ ,  $i = 1, 2, \dots, c$  are randomly selected from the  $n$  data patterns  $\{x_1, x_2, x_3, \dots, x_n\}$ . Secondly, the membership matrix ( $\mu$ ) is computed with the following equation:

$$\mu_{ij} = \frac{1}{\sum_{k=1}^c \left( \frac{d_{ij}}{d_{kj}} \right)^{2/m-1}}, \quad (3.7)$$

where,

$\mu_{ij}$ : the degree of membership of object  $j$  in cluster  $i$ ;

$m$ : the fuzziness index varying in the range  $[1, \infty]$ ; and

$d_{ij} = \|c_i - x_j\|$ : the Euclidean distance between  $c_i$  and  $x_j$ .

Thirdly, the objective function is calculated with the following equation. The process is stopped if it falls below a certain threshold:

$$J(U, c_1, c_2, \dots, c_c) = \sum_{i=1}^c J_i = \sum_{i=1}^c \sum_{j=1}^n \mu_{ij}^m d_{ij}^2. \quad (3.8)$$

Finally, the new  $c$  fuzzy cluster centres  $c_i$ ,  $i = 1, 2, \dots, c$  are calculated using the following equation:

$$c_i = \frac{\sum_{j=1}^n \mu_{ij}^m x_j}{\sum_{j=1}^n \mu_{ij}^m}. \quad (3.9)$$

In this thesis, the FCM algorithm will be used to separate whole training data pairs into several subsets (membership functions) with different centres. Each subset will be trained by the ANFIS, as proposed by Park et al. [96]. Furthermore, the FCM algorithm will be used to find the optimal temperature data clusters for thermal error compensation models.

The proposed method has the following merits:

- Using fuzzy c-mean clustering with ANFIS can be regarded as extracting knowledge or information from the experimental data form to the linguistic interpretation form. This is important in that the learning strategies can be started from a point where the risk of getting trapped in a local minimum can be avoided compared to that if the initial membership functions are chosen at random (which is often the case for ANNs).

- Unlike the Mamdani fuzzy model, where the rules of the model are built using the expert knowledge, in ANFIS model, the learning rules calibrate and adjust the membership functions and rules of the fuzzy model from the data it is modelling.

### 3.4 Grey Models

The Grey system theory, established by Deng in [48, 97], is a methodology that focuses on solving problems involving incomplete information or small samples. The technique can be applied to uncertain systems with partially known information by generating, mining, and extracting useful information from available data so that system behaviours and their hidden laws of evolution can be accurately described. It uses a Black-Grey-White colour to describe complex systems [98]. GM (1, N) is the most widely used implementation in literature [98], which can establish a first-order differential equation featured by comprehensive and dynamic analysis of the relationship between system parameters. The Accumulated Generating Operation (AGO) is the most important characteristic of the Grey system theory, and its benefit is to increase the linear characters and reduce the randomness of the samples. Based on the existing GM (1, N) model, Tien [98, 99] proposed a model, which is an improved Grey prediction model. The modelling values by GM (1, N) are corrected by including a convolution integral GMC (1, N).

#### 3.4.1 Accumulation Generation Operation (AGO)

Accumulation generation is a technique used to uncover a development tendency existing in the process of accumulating Grey quantities so that the features and laws of integration hidden in the raw data can be discovered [70]. The dynamic characteristic of the proposed model results from the accumulation generation operation (AGO). The technique transforms the original data to first order 1-AGO data, which reduces the randomness of the samples, so making it easier to design the Grey model. The output value of the model can be associated with Inverse Accumulated Generating Operation, abbreviated as IAGO, the procedure of AGO and IAGO is summarised as follows:

Step 1: consider the original series as:

$$X^{(0)} = x^{(0)}(1), x^{(0)}(2), \dots, x^{(0)}(k-1), x^{(0)}(k). \quad (3.10)$$

Step 2: from the original series, selecting the first value as the first value of the new series, selecting the first value plus the second one of the original series as the second value of the

new series, selecting the sum of the first three values of the original series as the third value of the new series, and so on, as follows:

$$X^{(1)} = x^{(1)}(1), x^{(1)}(2), \dots, x^{(1)}(n-1), x^{(1)}(n). \quad (3.11)$$

By so doing, the new 1-AGO series  $X^{(1)}$  will be obtained from the original data  $X^{(0)}$ , which have more regular series for the benefit of modelling instead of modelling with original data.

Step 3: 1- IAGO can be applied to obtain the original series, selecting the first value as the first value of the new series, selecting the second value minus the first one of the original series as the second entry of the new series, selecting the third value minus the second one of the original series as the third value of the new series, and so on. The mathematical expressions are as the following:

$$X^{(0)} = x^{(1)}(k) - x^{(1)}(k-1), \quad (3.12)$$

Where  $k = 2, 3, \dots, n$ .  $x^{(0)}(1) = x^{(1)}(1)$

Therefore, by applying AGO transformation, the following important advantages can be obtained: (i) removing extreme fluctuation and noise so that the new series is more stable for modelling, (ii) the new series has a linear characteristic which makes it easier to model instead of modelling with the original non-linear data, (iii) and it has the characteristic of determining realistic governing laws from the available data [70, 100]. The emphasis is to discover the true properties of the system under the condition of small training data.

To understand this property in more detail, [Figure 3-3](#) shows an example of original (temperature changes) and converted series of data.

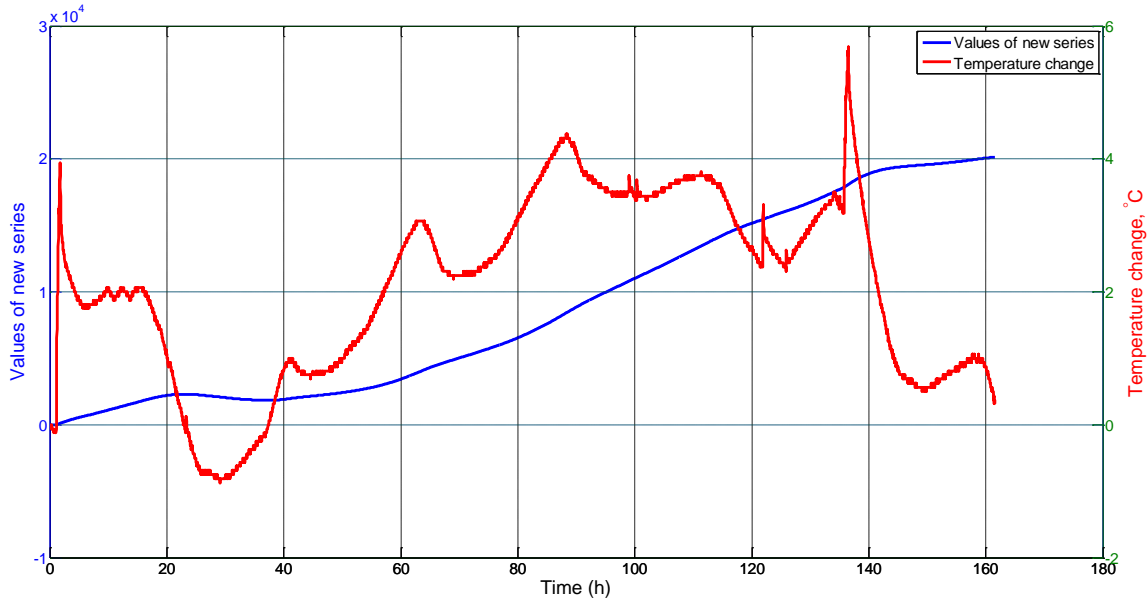


Figure 3-3: The original data vs AGO converted data.

### 3.5 Optimisation Methods

Traditionally, the Grey models have been calibrated by the least squares method. However, due to the nonlinearity of the problem, the least squares solution may not provide a satisfactory result. In order to avoid the tedious trial and error approach, the Particle Swarm Optimisation (PSO) algorithm will be used in order to improve the performance of the Grey models. The PSO algorithm will be reviewed in the next section and will then follow with the main steps of GMC (1, N) learning algorithm using PSO.

#### 3.5.1 The Particle Swarm Optimisation (PSO)

The Particle Swarm Optimisation (PSO) algorithm was introduced by Eberhart et al. [101] as an alternative to other evolutionary techniques. The PSO algorithm is inspired by the behaviour of natural swarms, such as the formation of flocks of birds and schools of fish. The advantages of the PSO algorithm is that it does not require the objective function to be differentiable as in the gradient descent method, which makes few assumptions about the problem to be solved. Furthermore, it has a simple structure and its optimisation method illustrates a clear physical meaning. PSO consists of a population formed by individuals called particles, where each one represents a possible solution of the problem. Each particle tries to search the best position with time in D-dimensional space (solution space). During flight or swim, each particle adjusts its "flying" or "swimming" in light of its own experience

and its companions' experience, including the current position, velocity and the best previous position experienced by itself and its companions.

### 3.6 GMC (1, N) and its Learning Algorithm

In this section, the main steps of GMC (1, N) modelling are illustrated and discussed. The model can reveal the long-term trend of data and, by driving the model by the AGO, rather than raw data, can minimise the effect of some of the random occurrences. Therefore, the first step for building GMC (1, N) is to carry out 1-AGO (first-order Accumulated Generating Operation) to the data, so as to increase the linear characteristics and reduce the randomness from the measuring samples. PSO algorithm, with capability to optimise complex numerical functions, is adopted to calibrate the GMC (1, N) model. Finally, an IAGO (Inverse Accumulated Generating Operation) is performed to predict the thermal error and generate the final compensation values. Figure 3-4 shows a schematic diagram of PSO-based Grey model. The modelling detail is described as follows:

Step 1: Consider the original data series as:

$$X_1^{(0)} = \{x_1^{(0)}(1+r), x_1^{(0)}(2+r), \dots, x_1^{(0)}(n+r)\}, \text{ and}$$

$$X_i^{(0)} = \{x_i^{(0)}(1), x_i^{(0)}(2), \dots, x_i^{(0)}(n), \dots, x_i^{(0)}(n+m)\}, \text{ where } i = 2, 3, \dots, N, r \text{ is the period of delay, } n \text{ gives the length of original data series and } m \text{ denotes the number of entries to be predicted.}$$

Step 2: The above sequences of each variable are processed using 1-AGO to obtain the 1<sup>st</sup>-order AGO sequences as follows:

$$X_1^{(1)} = \{x_1^{(1)}(1+r), x_1^{(1)}(2+r), \dots, x_1^{(1)}(n+r)\}, \text{ and}$$

$$X_i^{(1)} = \{x_i^{(1)}(1), x_i^{(1)}(2), \dots, x_i^{(1)}(n), \dots, x_i^{(1)}(n+m)\},$$

$$\text{where } X^{(1)} = \sum_{j=1}^t x^{(0)}(j), \quad t = 1, 2, \dots, n+m.$$

Since the details of GMC (1, N) can be found in [98], this work only briefly mentions the core equations of this method.

$$\frac{dX_1^{(1)}(t+r)}{dt} + b_1 X_1^{(1)}(t+r) = b_2 X_2^{(1)}(t) + b_3 X_3^{(1)}(t) + \dots + b_N X_N^{(1)}(t) + u, \quad (3.13)$$

where  $t = 1, 2, \dots, n + m$ ,  $b_1$  is the development coefficient,  $b_i, (i = 2, 3, \dots, N)$  the driving coefficient, and  $u$  is the Grey control parameter. Therefore, time response sequences can be obtained.

$$\hat{X}_1^{(1)}(t + r) = x_1^{(0)}(1 + r)e^{-b_1(t-1)} + \frac{1}{2} \times e^{-b_1(t-1)} \times f(1) + \sum_{\tau=2}^{t-1} [e^{-b_1(t-\tau)} \times f(\tau)] + \frac{1}{2} \times f(t), \quad (3.14)$$

where  $f(\tau) = \sum_{j=2}^N b_j X_j^{(1)}(\tau) + u$ .

To calculate the coefficients  $b_1, b_i$  and  $u$ , the PSO can be used to calibrate the equation (3.14). Then, the Grey model is optimised until the performance is satisfactory. Finally, the optimal corresponding coefficients are used as the Grey model coefficients to predict the thermal error. The calibrating process of GMC (1, N) can be summarised as follows:

In PSO algorithm, a particle refers to a coefficient in the model that changes its position from one move to another based on velocity updates. The mathematical description of the PSO algorithm is as follows: suppose that the search space is D-dimensional, and then the current position and velocity of the  $i$ th particle can be represented by  $B_i = [b_{i1}, b_{i2}, \dots, b_{iD}]^T$  and  $V_i = [v_{i1}, v_{i2}, \dots, v_{iD}]^T$  respectively, where  $i = 1, 2, \dots, M$  and  $M$  is the number of particles in the swarm.

Particle  $i$  can remember the best position so far, which is known as the local best position  $Pbest_i = [pbest_1, pbest_2, \dots, pbest_{iD}]^T$ . It can also obtain the best position that the whole swarm establish, known as the global best position  $Gbest_i = [gbest_1, gbest_2, \dots, gbest_{iD}]^T$ . The first position and velocity of particle  $i$  are randomly initialised by the uniformly distributed variables. Afterwards, particle  $i$  adjusts its velocity of iteration  $k+1$  according to the local and global best positions, as well as the velocity and position of iteration  $k$ , as follows:

$$V_i(k + 1) = \omega V_i(k) + C_1 R(Pbest_i(k) - B_i(k)) + C_2 R(Gbest_i(k) - B_i(k)) \quad (3.15)$$

where  $\omega$  is the inertia factor which is used to manipulate the impact of the previous velocities on the current velocity,  $C_1$  and  $C_2$  are the self-confidence factor and the swarm-confidence factor, respectively.  $R$  is a uniformly distributed random real number that can take any values between 0 and 1. With the updated velocity, the position of particle  $i$  in the iteration  $k+1$  can be obtained as follows:

$$B_i(k + 1) = B_i(k) + V_i(k + 1) \quad (3.16)$$

The fitness of particle is measured using a fitness function that quantifies the distance between the particle and its optimal solution as follows:

$$f(B_i) = \sum_{k=1}^N [\hat{x}^{(0)}(k) - x^{(0)}(k)]^2 \quad (3.17)$$

where  $f$  is the fitness value,  $\hat{x}^{(0)}(k)$  is the target output; and,  $x^{(0)}(k)$  is the predicted output based on model parameters (particles) updating.

Step 3: Update the velocity and position of each particle based on equations (3.15) and (3.16). Adjusting the model parameters in equation (3.14).

Step 4: If the value of the error meets the requirement of the model, or a pre-determined number of epochs are passed, then the model calibration will end. If not, then return to Step 3.

Step 5: Export the optimal solution  $B_i$ .

Step 6: 1- IAGO can be applied to obtain the predicted values. The mathematical expression is as the following.

$$\hat{x}_1^{(0)}(t+r) = \hat{x}_1^{(1)}(t+r) - \hat{x}_1^{(1)}(t-1+r), \text{ and } \hat{x}_1^{(0)}(1+r) = \hat{x}_1^{(1)}(1+r). \quad (3.18)$$

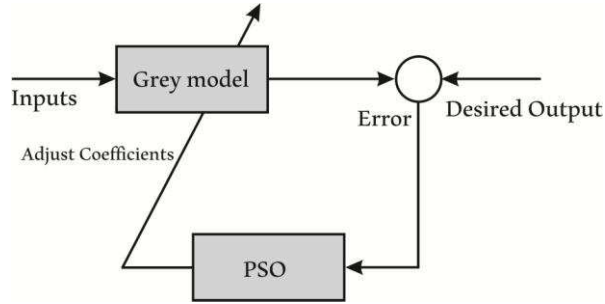


Figure 3-4: Schematic diagram of PSO-based Grey model.

### 3.7 Variables Selection Using Grey Models

A large number of thermal sensors may have a negative influence on predication accuracy and robustness of a thermal prediction model. One of the difficult issues in thermal error modelling is the selection of appropriate locations for the temperature sensors, which is a key factor in the accuracy of the thermal error model. This study adopts Grey system theory to identify the proper sensor positions for thermal error modelling.

The Grey system theory is a methodology that focuses on studying the Grey system by using mathematical methods with a only few datasets and poor information. The technique works on uncertain systems that have partial known and partial unknown information. Its most significant advantage is that it needs a small amount of experimental data for accurate prediction, and the requirement for the data distribution is also low [70]. There are many types of Grey models; the Grey GM (0, N), GM (1, N), GMC (1, N), and Grey Relational Analysis (GRA) models will be used in this work and are described in the following subsections.

### 3.7.1 Grey Model GM (0, N)

The Grey Model GM (h, N) is based on the Grey system theory, where h is the order of the difference equation and N is the number of variables [102]. The GM (h, N) model is defined as follows:

If in sequences  $x_i^{(0)}(k)$ ,  $i = 1, 2, \dots, N$ .  $x_1^{(0)}(k)$ , is the main factor in the system, and sequences  $x_2^{(0)}(k), x_3^{(0)}(k), x_4^{(0)}(k), \dots, x_N^{(0)}(k)$  are the influence factors of the same system, then the GM (h, N) model is described as [70, 102]:

$$\sum_{i=0}^h a_i \frac{d^{(i)} x_1^{(1)}}{dt^{(i)}} = \sum_{j=2}^N b_j x_1^{(1)}(k), \quad (3.19)$$

where,

$a_1$  and  $b_j$  are determined coefficients;

$b$  is defined as the Grey input;

$x_1^{(1)}(k)$ : The major sequence;

$x_j^{(1)}(k)$ : The influence sequences; and

The accumulation generating operation (AGO)

$$x^{(0)} = x^{(1)} = \left[ \sum_{k=1}^1 x^{(0)}(k), \sum_{k=1}^2 x^{(0)}(k), \sum_{k=1}^3 x^{(0)}(k), \dots, \sum_{k=1}^{n_1} x^{(0)}(k) \right]. \quad (3.20)$$

According to the previous definition of GM (h, N), the GM (0, N) is a zero-order Grey system, which can be described as follows:

$$z_1^{(1)}(k) = \sum_{j=2}^N b_j x_j^{(1)}(k) = b_2 x_2^{(1)}(k) + b_3 x_3^{(1)}(k) + \dots + b_N x_N^{(1)}(k), \quad (3.21)$$

Where,

$$z_1^{(1)}(k) = 0.5x_1^{(1)}(k-1) + 0.5x_1^{(1)}(k), \quad k = 2, 3, 4, \dots, n.$$

Equation (3.21) can be written as:

$$\begin{aligned} a_1 z_1^{(1)}(2) &= b_2 x_2^{(1)}(2) + \dots + b_N x_N^{(1)}(2), \\ a_1 z_1^{(1)}(3) &= b_2 x_2^{(1)}(3) + \dots + b_N x_N^{(1)}(3), \\ &\dots \dots \dots \\ a_1 z_1^{(1)}(n) &= b_2 x_2^{(1)}(n) + \dots + b_N x_N^{(1)}(n). \end{aligned} \quad (3.22)$$

Dividing equation (3.22) by  $a_1$  in both sides, then transfer into matrix form as follows:

$$\begin{bmatrix} 0.5x_1^{(1)}(1) + 0.5x_1^{(1)}(2) \\ 0.5x_1^{(1)}(2) + 0.5x_1^{(1)}(3) \\ \vdots \\ 0.5x_1^{(1)}(n-1) + 0.5x_1^{(1)}(n) \end{bmatrix} = \begin{bmatrix} x_2^{(1)}(2) & \dots & x_N^{(1)}(2) \\ x_2^{(1)}(3) & \dots & x_N^{(1)}(3) \\ \vdots & \dots & \vdots \\ x_2^{(1)}(n) & \dots & x_N^{(1)}(n) \end{bmatrix} \begin{bmatrix} \frac{b_2}{a_1} \\ \frac{b_3}{a_1} \\ \vdots \\ \frac{b_N}{a_1} \end{bmatrix}. \quad (3.23)$$

Assume  $\frac{b_j}{a_1} = \theta_m$ , where  $m=2, 3, \dots, N$ , then equation (3.23) can be simplified as follows:

$$\begin{bmatrix} 0.5x_1^{(1)}(1) + 0.5x_1^{(1)}(2) \\ 0.5x_1^{(1)}(2) + 0.5x_1^{(1)}(3) \\ \vdots \\ 0.5x_1^{(1)}(n-1) + 0.5x_1^{(1)}(n) \end{bmatrix} = \begin{bmatrix} x_2^{(1)}(2) & \dots & x_N^{(1)}(2) \\ x_2^{(1)}(3) & \dots & x_N^{(1)}(3) \\ \vdots & \dots & \vdots \\ x_2^{(1)}(n) & \dots & x_N^{(1)}(n) \end{bmatrix} \begin{bmatrix} \theta_2 \\ \theta_3 \\ \vdots \\ \theta_N \end{bmatrix}. \quad (3.24)$$

The coefficients of the model can then be estimated from the following equation:

$$\hat{\theta} = (B^T B)^{-1} B^T Y, \quad (3.25)$$

where,

$$Y = \begin{bmatrix} 0.5x_1^{(1)}(1) + 0.5x_1^{(1)}(2) \\ 0.5x_1^{(1)}(2) + 0.5x_1^{(1)}(3) \\ \vdots \\ 0.5x_1^{(1)}(n-1) + 0.5x_1^{(1)}(n) \end{bmatrix}, \quad B = \begin{bmatrix} x_2^{(1)}(2) & \dots & x_N^{(1)}(2) \\ x_2^{(1)}(3) & \dots & x_N^{(1)}(3) \\ \vdots & \dots & \vdots \\ x_2^{(1)}(n) & \dots & x_N^{(1)}(n) \end{bmatrix}, \quad \hat{\theta} = \begin{bmatrix} \theta_2 \\ \theta_3 \\ \vdots \\ \theta_N \end{bmatrix}.$$

Therefore, the influence ranking of the major sequences (input sensors) on the influencing sequence (thermal response) can be known by comparing the model values of  $(\theta_2 \sim \theta_N)$ .

### 3.7.2 The GM (1, N) Model

The first-order Grey model, GM (1, N), is a multivariable Grey model for multi-factor forecasting. GM (1, N) means a Grey model that has N variables including one dependent

variable and  $N-1$  independent variables. Assume that there are  $N$  variables,  $x_i (i = 1, 2, \dots, N)$ , and each variable has  $n$  initial sequences as:

$$x_i^{(0)} = \{x_i^{(0)}(1), x_i^{(0)}(2), \dots, x_i^{(0)}(n)\} \quad (i = 1, 2, \dots, N) \quad (3.26)$$

First, in order to reduce the randomness and increase the smoothness of the sequence, the accumulative generation operation (AGO) is also applied to convert the sequences to be strictly monotonic increasing sequences (see section 3.4.1). Then, the GM (1,  $N$ ) model can be expressed by the following Grey differential equation [70]:

$$x_1^{(0)}(k) + az_1^{(1)}(k) = \sum_{j=2}^N b_j x_j^{(1)}(k) = b_2 x_2^{(1)}(k) + b_3 x_3^{(1)}(k) + \dots + b_N x_N^{(1)}(k), \quad (3.27)$$

In which,  $z_1^{(1)}(k)$  is defined as:

$$z_1^{(1)}(k) = 0.5x_1^{(1)}(k-1) + 0.5x_1^{(1)}(k) \quad k = 2, 3, 4, \dots, n.$$

where the coefficients  $a$  and  $b_j$  are called the system development parameter and the driving parameters, respectively.

Equation (3.27) can be written as:

$$\begin{aligned} x_1^{(0)}(2) + az_1^{(1)}(2) &= b_2 x_2^{(1)}(2) + \dots + b_N x_N^{(1)}(2), \\ x_1^{(0)}(3) + az_1^{(1)}(3) &= b_2 x_2^{(1)}(3) + \dots + b_N x_N^{(1)}(3), \\ &\dots \dots \dots \\ x_1^{(0)}(n) + az_1^{(1)}(n) &= b_2 x_2^{(1)}(n) + \dots + b_N x_N^{(1)}(n). \end{aligned} \quad (3.28)$$

Equation (3.28) can be written in the matrix form as:

$$\begin{bmatrix} x_1^{(0)}(2) \\ x_1^{(0)}(3) \\ \vdots \\ x_1^{(0)}(n) \end{bmatrix} = \begin{bmatrix} z_1^{(1)}(2) & x_2^{(1)}(2) & \dots & x_N^{(1)}(2) \\ z_1^{(1)}(3) & x_2^{(1)}(3) & \dots & x_N^{(1)}(3) \\ \vdots & \vdots & \ddots & \vdots \\ z_1^{(1)}(n) & x_2^{(1)}(n) & \dots & x_N^{(1)}(n) \end{bmatrix} \begin{bmatrix} a \\ b_2 \\ \vdots \\ b_N \end{bmatrix}. \quad (3.29)$$

The coefficients of the model can then be obtained using the least squares estimate method as:

$$\hat{\theta} = (B^T B)^{-1} B^T Y, \quad (3.30)$$

where,

$$\hat{\theta} = \begin{bmatrix} a \\ b_2 \\ \vdots \\ b_N \end{bmatrix}, \quad Y = \begin{bmatrix} x_1^{(0)}(2) \\ x_1^{(0)}(3) \\ \vdots \\ x_1^{(0)}(n) \end{bmatrix}, \quad B = \begin{bmatrix} z_1^{(1)}(2) & x_1^{(1)}(2) & \cdots x_N^{(1)}(2) \\ z_1^{(1)}(3) & x_1^{(1)}(3) & \cdots x_N^{(1)}(3) \\ \vdots & \vdots & \vdots \\ z_1^{(1)}(n) & x_2^{(1)}(n) & \cdots x_N^{(1)}(n) \end{bmatrix}.$$

Therefore, the influence ranking from the independent variables to the dependent variable can be known by comparing the model values of  $(b_2 \sim b_N)$ .

### 3.7.3 Grey Relational Analysis (GRA) Method

Grey Relational Analysis (GRA) is a method to capture the correlations between the reference factor and other compared factors of a system with a relatively small amount of data [98]. On the basis of Deng's initial models of Grey incidences, Liu et al. [103] proposed a new type of GRA model to investigate the closeness of connection between sequences using the geometric shapes of the sequences. The GRA model can be summarised as follows:

Step 1: Assume sequences:

$X_i = (x_i(1), x_i(2), x_i(3), \dots, x_i(n))$ , is a sequence of data representing a system's characteristics, and,

$X_j = (x_j(1), x_j(2), x_j(3), \dots, x_j(n))$ , is a sequence of relevant factors.

Step 2: The initial point zeroing images are:

$$X_i^0 = (x_i^0(1), x_i^0(2), x_i^0(3), \dots, x_i^0(n)),$$

$$X_j^0 = (x_j^0(1), x_j^0(2), x_j^0(3), \dots, x_j^0(n)),$$

where,  $x_i^0(k) = x_i(k) - x_i(1)$ ,  $x_j^0(k) = x_j(k) - x_j(1)$ ,  $k = 1, 2, \dots, n$ .

Step 3: The grey similitude degree is calculated as follows:

$$\varepsilon_{ij} = \frac{1}{1 + |s_i - s_j|}, \quad \text{where } s_i - s_j = \int_1^n (X_i^0 - X_j^0) dt.$$

The similitude degree of the GRA model is used to measure the geometrical shape similarity between sequence  $X_i$  and  $X_j$ . The  $\varepsilon_{ij}$  is called the similitude degree of  $X_j$  with respect to  $X_i$ . According to the above equations, the similitude degree  $\varepsilon_{ij}$  between thermal error of CNC

machine tool and the various temperature sensors can be calculated. The bigger  $\varepsilon_{ij}$  the greater impact on thermal error.

### 3.8 Model Validation

Once a model has been trained, it is necessary to check the prediction quality of the resulting model and to assess the parameter accuracy. This will give the confidence behind the model, and tell the designer if he needs to revise the training process. This procedure is called model validation, which consists of several steps.

#### 3.8.1 Direct Validation

The first test is to examine whether the obtained model can predict the experimental dataset that has been used for the training process. Otherwise, there is clearly something wrong in the training procedure, and it has to be modified and repeated.

In order to compare the prediction results of the thermal model and its deviation from the measured data, statistical indices can be used. One of the most commonly used methods is the residual value: the model has to follow well the experimental data while smoothing off the noise (a model that tends to remember the noise is over-fitted model and will fail later on in cross-validation tests). A number of performance criteria such as a Root Mean Square Error (RMSE), correlation coefficient (R), and Nash–Sutcliffe Efficiency coefficient (NSE) [104] can also be used for testing the model performance.

The coefficient of correlation (R) describes the degree of collinearity between predicted and measured data, which ranges between (-1, 1), is an index of the degree of linear relationship between measured and predicted data. Systems with good correlations have an absolute magnitude approaching 1.

The Nash–Sutcliffe efficiency coefficient is a normalised statistic that determines the relative magnitude of the noise compared to the measured data variance, which ranges between  $(-\infty, 1)$ . Systems with a good efficiency have an NSE approaching 1.

The root mean square error is used to measure the difference between values predicted by a model and those measured from the experimental test. Actually, the RMSE has been the sole tool used to evaluate the model fit in several studies [50, 104]. Systems with high accuracy have RMSE approaching 0.

The performances of the models used in this study were computed using four performance criteria: Root Mean Square Error (RMSE), Nash-Sutcliffe Efficiency coefficient (NSE), correlation coefficient (R) and also residual value. The equations of first two are defined as:

$$RMSE = \sqrt{\frac{\sum_{k=1}^n (Z - P)^2}{n}}, \quad (3.31)$$

$$NSE = 1 - \frac{\sum (Z - P)^2}{\sum (Z - \bar{Z})^2}, \quad (3.32)$$

where,

$Z$ : The thermal response;

$P$ : The predicted thermal response;

$\bar{Z}$ : Average of the thermal response; and

$n$ : The number of measured data samples.

### 3.8.2 Cross Validation

Direct validation is an essential condition, but by no means a sufficient condition to accept a model as being one that can predict the thermal error under different operation conditions. It may well be that the model predicts the data that has been used for training stage, but performs poorly with new unseen dataset. Cross validation is used to examine the performance of the model, to check its generalisation capability. Therefore, enough dataset must be used and divided these into two subsets, one for training stage (and afterward direct validation), and the other for cross validation. This procedure has been applied to check the obtained model validity, especially when complex models, such as thermal error models, are considered [105].

## 3.9 Summary

The aim of the work presented in this chapter is to provide a complete and thorough description of the AI tools that will be used thought this thesis. Fuzzy models allow one to utilise qualitative knowledge (words) in form of “if-then” rules. Typically, qualitative engineering knowledge is not sufficient in order to build a fuzzy model with high accuracy. Therefore, often measurement data is needed for fuzzy model calibration. Data-driven fuzzy models are commonly referred to as neuro-fuzzy models.

Clustering procedures can be considered as extracting knowledge or information from the data forms to the linguistic interpretation form. After knowledge extraction using clustering

or partition, fuzzy models calibrate the knowledge by using training processes, and then their knowledge of the modelled system can be represented. The learning performed by the fuzzy models can be considered a process of calibrating the given knowledge, which refines it to fit the experimental data.

The Grey system theory is a methodology that focuses on studying the Grey systems by using mathematical methods with an only few datasets and poor information. The technique works on uncertain systems that have partial known and partial unknown information. Its most significant advantage is that it needs a small amount of experimental data for accurate prediction, and the requirement for the data distribution is also low. In this thesis, the Grey models and fuzzy c-means clustering will be used to determine the major sensors influencing thermal errors of a CNC machine tool, which is capable of simplifying the system prediction model.

The following chapter explores the experimental work and thermal characterisation of machine tools.

## **Chapter 4: Thermal Characterisation of Machine Tools**

### **4.1 Introduction**

It is important to understand thermal characteristics of machine tools before attempting to reduce thermal deformation or apply a thermal error compensation system. Appropriate selection of input variables is an important task in modelling. In fact, not all input variables are equally important; some may have no significant effect on the system being modelled. In this thesis, thermography will be used extensively, both qualitatively and quantitatively, for selection of the optimal sensor locations and developing thermal error models.

This chapter outlines the experimental considerations taken into account when collecting the data to build the compensation models of the CNC machine tool. Details are also provided on the equipment setup used during the various experimental tests. This is followed by a systematic methodology for a precise selection of thermal sensors and their positions in order to ensure the prediction accuracy and robustness of compensation models. The effect of using different physical quantities (temperature and strain) is also explored.

### **4.2 Measurements of Thermal Deformation of Machine Tools**

In order to meet the wider aims of the research, it is necessary to be able to measure the thermal displacement of the machine, and also the temperature changes causing those errors. A number of different measurement devices have been used to achieve the testing requirements.

#### **4.2.1 Measurement of Temperature**


Usually for investigation of thermal error, discrete temperature sensors, such as thermocouples or resistance thermometers (Pt100, Pt1000) are attached on the machine surface to measure the temperature [31]. Some of these sensors are so small that they can be installed in the machine structure very close to the heat source. However, the exact temperature distribution within the machine structure can only be measured by discrete temperature sensors if they are densely deployed, which can be impractical. An appropriate method to provide richness of temperature data is the use of a thermal imaging approach.

Thermal imaging is an important part of this research work and is used both qualitatively and quantitatively for developing models on wide range of machine tools with different configurations.

#### 4.2.1.1 Thermal Imaging Camera

A thermal imaging camera provides a visible image of otherwise invisible infrared light that is emitted by all bodies due to their thermal state. The thermal imaging camera has become a powerful tool for researchers and has applications in various fields such as medicine, biometrics, computer vision, building maintenance and so on [10, 106]. In this research work, a high-specification thermal imaging camera, namely a FLIR ThermaCAM®S65, was used to record a sequence of thermal images of temperature distributions across the parts of the machine structure. This camera provides a sensitivity of 0.08 °C, and an absolute accuracy of  $\pm 2\%$ . Full camera specifications are provided in Table 4-1. The thermal imaging camera offers a continuous picture of the temperature distribution in the image field-of-view. This is important as it provides the distribution of heat during heating and cooling cycles across the whole machine structure. This allows the machine's structural elements to be measured online during the test. As well as the camera providing live continuous thermal images, they can also be recorded for further analysis. The thermal images are saved as a matrix of temperatures with a specific resolution of one pixel (equivalent to 2.25 mm<sup>2</sup>), which equates to over 76000 temperature measurement points for this 320 x 240 resolution camera. These thermal images can be transferred to a personal computer for analysis. Figure 4-1 shows a general overview of the experimental setup.

Table 4-1: Thermal imaging camera specification.

Field of view/min focus distance	24° x 18° / 0.3 m	
Spatial resolution (IFOV)	1.5 mrad	
Thermal sensitivity @ 50/60 Hz	0.08 °C at 30 °C	
Electronic zoom function	2, 4, 8, interpolating	
Focus	Automatic or manual	
Digital image enhancement	Normal and enhanced	
Detector type	Focal plane array (FPA) uncooled microbolometer; 320 x 240 pixels	
Spectral range	3.5 to 13 μm	

In this research work, the data has been analysed using MATLAB. One disadvantage of thermal imaging is that it can have low absolute accuracy, usually in the order of  $\pm 2$  °C. A

number of MATLAB functions have been developed to enhance this accuracy, including averaging the images to reduce pixel noise, alignment of images and extraction from the temperature data by averaging groups of pixels at a specific point [107].

The radiation measured by the thermal camera depends on the temperature of the machine tool structure, but is also affected by the emissivity of the machine surfaces. Additionally, radiation reflects from shiny surfaces (ballscrew, test mandrel, etc.), and is directly captured by the thermal camera and appearing as very hot areas. In order to measure the temperature of the machine structure precisely it is therefore necessary to know the emissivity accurately, for which the application of masking tape with a known emissivity (0.95) is a common and effective solution. The camera parameters are then set according to the measurement conditions considering the emissivity of the machine tool material, the distance between the machine and the camera, the relative humidity and the ambient temperature, as illustrated in Table 4-2.

Table 4-2: Thermal imaging camera parameters.

Distance	1.5 m
Emissivity	0.95
Ambient temperature	23 °C
Relative humidity:	30%

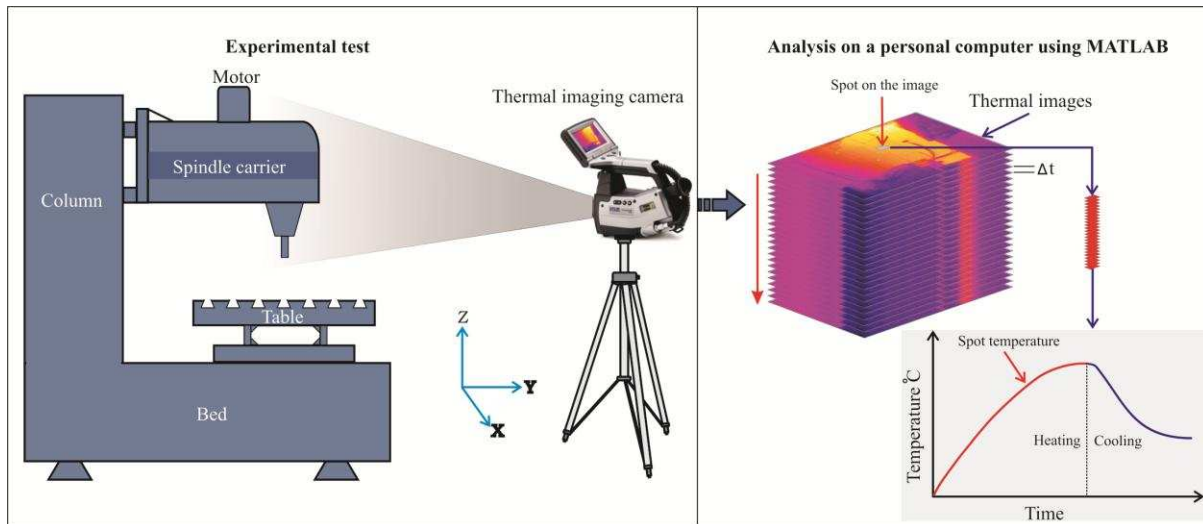


Figure 4-1: A general overview of a typical thermographic experimental setup.

The advantages of using thermal imaging approach are:

- It is a remote and a non-contact temperature measuring technique that enables simultaneous monitoring a large area of the machine structure. It has the benefits of no temperature sensor placed on a machine surface, and that a whole image field-of-view can be characterised in a single measurement.
- Thermal imaging requires minimal instrumentation. The essential requirements for such temperature measurement are a thermal imaging camera with its tripod. Nowadays, an infrared handheld camera is also available with the benefit of being lightweight and portability.
- Thermal imaging enables recording of live, continuous thermal images and interpretations of the acquired pseudo colour coded thermal images are easier to understand. The thermal images can be transferred to a personal computer for further analysis.
- Thermal imaging allows simultaneous acquisitions of a great number of the picture's elements (pixels). These elements equate to great numbers of possible temperature measurement points, depending upon the camera specifications and field of view.
- It is worth mentioning that use of thermography only shows the surface temperature which means it is unable to obtain the temperature of the internal elements of the machine tool. Therefore, in a practical compensation system, temperature sensors will be physically placed in drilled holes to obtain a better response of internal temperature variation.

### 4.2.1.2 Discrete Temperature Sensors

Thermocouples are the most commonly used sensor for measuring temperature on machine tool thermal response. Although these sensors have low cost and easy to fix to the machine tool surface, their accuracy is relatively low, which is unsuitable for this type of application because a temperature change of a small magnitude on a machine can equate to tens of microns of error [108]. Moreover, thermocouples require a complex wiring effort when several sensors are being used, which is often the case in the numerical compensation (data-driven) approach.

Fletcher [108] used digital temperature sensors from Dallas Semiconductor LTD. These temperature sensors have a diameter of 1 mm and are of type “Dallas DS18S20”, capable of measuring in a range of -55 °C to +125 °C, with an accuracy of  $\pm 0.5$  °C over the range of -10 °C to +85 °C and resolution of 0.063 °C. Each sensor has a unique 64-bit serial code, which allows multiple sensors to function on the same 1-Wire bus. This feature significantly reduces the complexity of wiring and interface effort.

## 4.2.2 Measurement of Displacement

The movement of the machine as it changes shape can be measured using various pieces of metrology equipment such as the on-machine probe, high accuracy displacement transducers, laser interferometer, etc.

### 4.2.2.1 Non-Contact Displacement Transducers (NCDTs)

Non-Contact Displacement Transducers (NCDTs) have been used to measure the displacement of a precision test bar, representing the tool, in the X, Y and Z axes [3, 39, 65]. Capacitive sensors can be used, but the ones selected for this research work on the eddy current principle. When an alternating current is fed through a coil embedded in the head of the sensor, it creates an alternating magnetic field in the conductive target (see Figure 4-2). As a consequence, the alternating current resistance of the sensor coil change. This change of impedance produces an electrical signal proportional to the distance from the target [109]. The non-contacting nature of the measurement allows the position of a rotating test bar to be constantly monitored during a spindle running test. The sensor can measure the distance of any conductive target and with re-calibration, any other metallic target. This position measurement device is ideal for harsh industrial environments due to its resistance to dirt, oil, dust, moisture, interference fields, etc. Furthermore, it is often less expensive than capacitive sensors and much smaller than laser triangulation devices [110]. The sensor has the measurement range of 0-1 mm and a fundamental resolution of 0.1  $\mu\text{m}$ .

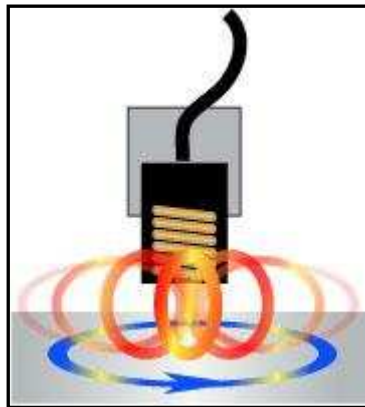


Figure 4-2: Principle of eddy current sensor [111].

#### 4.2.2.2 Laser Triangulation Sensor (LTS)

A Laser Triangulation Sensor (LTS) is an NCDT, which can measure and detect the relative distance to a target or surface. LTS works by firing a laser beam at the target under study. A common arrangement of the laser triangulation sensor is shown in Figure 4-3. The laser beam is projected on the surface, on which the light from a laser source scatters, and the scattered light can be recorded by a detector. The signal from the detector is used to determine the relative distance between the sensor and the target [110].

The main benefit of LTS is the speed with which the measurement can be taken and their robustness for harsh environments. Furthermore, LTS has a relatively large standoff (i.e. distance between the sensor and the target surface), in which the risk of damage during setup is reduced. However, LTSs are susceptible to self-heating, and are sensitive to the ambient property of the medium in the gap between the sensor and the target [110].

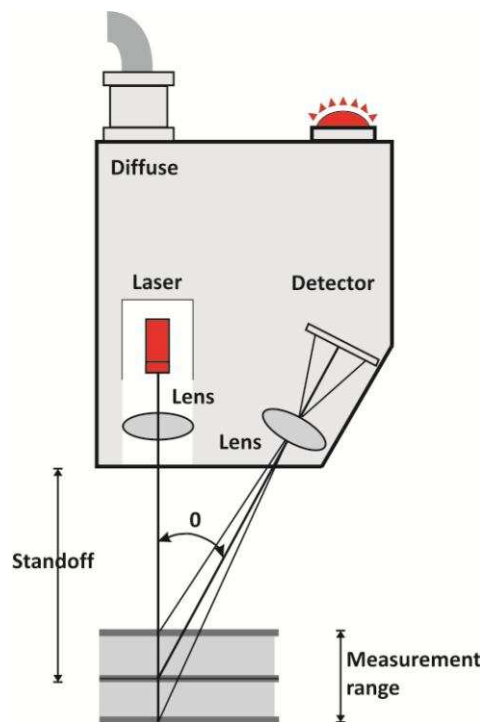


Figure 4-3: Laser triangulation principle.

#### 4.2.2.3 Fiber Bragg Grating (FBG) Sensors

Fiber Bragg Grating (FBG) sensors are gaining increasing attention in the field of real-time temperature measurement of machine tools [77, 112]. FBG sensors belong to the optical strain gauges family, are a promising technology in thermal error compensation systems. The working principle of these sensors is described in detail in [75], as one of the most exciting

developments in recent years. In the field of thermal error compensation, having a large number of temperature sensors would affect normal operation of machine tool, however FBG sensors prove to be an interesting solution for placing a large number of temperature sensors on the machine structure [77, 113]. The great advantage of this measurement technology is that a single FBG sensor is able to provide a set of measurements of distortion at many positions, providing distributed measurement along the structure [114]. In literature, the most common applications of FBG sensors are structure health monitoring, damage detection and strain measurement in harsh environments [75, 76].

However, the FBG sensor itself is also affected by temperature by a factor that equates to  $8.64 \mu\text{m}/\text{m}/^\circ\text{C}$ . One method of compensating temperature is to use an unconstrained grating to measure temperature. Nevertheless, this was unviable for this application because it would require additional gratings to be mounted, incurring additional cost and requiring additional mounting space, which was not readily available. Instead, the low-cost temperature sensors used for the temperature-based model were used to correct for change in the grating temperature.

### 4.3 Test Machines

A CNC machine tool usually has three main groups of parts: machine tool structure, drives, and control system. The machine structure consists of stationary and moving elements. The stationary elements include columns, bridges, beds, gear box housings, etc. They usually carry moving elements, such as spindles, tables, slides, gears, bearings, and carriages. Moving mechanisms can be grouped into spindle and feed drives in machine tools. The spindle drive provides sufficient angular speed, torque, and power to a rotating spindle shaft, which is connected to the spindle with different configurations [115]. The feed drives carry the table or the carriage. Generally, the table is connected to the nut, and the nut houses a ballscrew. The screw is connected to the drive motor either directly or via a gear system depending on the feed speed, inertia, and torque reduction requirements. The detailed design of machine tool structures will not be covered in this thesis.

In this thesis, the modelling methods have been applied and validated on three different machine tools. The different configurations of these machines are described as follows:

### 4.3.1 Machine A - Vertical Milling Centre (VMC)

In this thesis, the initial experiments were performed on a small, three-axis vertical milling centre. Figure 4-4 shows the block diagram of the machine, whose configuration is often known as C-frame due to its shape. This is a very common form of machine in industry. The Z-axis maximum tool travel is 330 mm, and the machine table X-axis maximum travel and Y-axis maximum travel are 500 mm and 400 mm, respectively. The spindle is rotated by a DC motor mounted on the top of the spindle carrier. The spindle speed can be controlled from 80 rpm to 9000 rpm. The motors for the axes are directly coupled to a ballscrew that is supported by bearings at each end. The position feedback for each axis is from a rotary encoder mounted on the axis motor. This means that the ballscrew forms part of the feedback device.

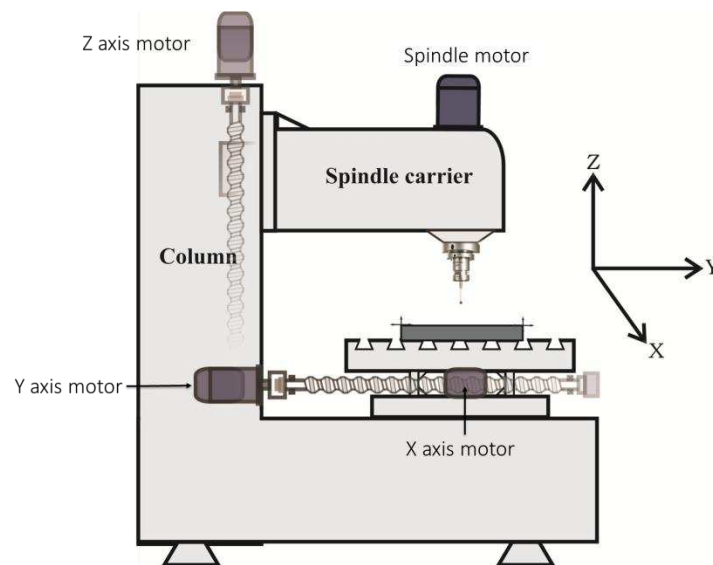


Figure 4-4: A general overview of Machine A.

### 4.3.2 Machine B - Vertical Milling Centre (VMC)

Figure 4-5 shows the block diagram of a three-axis vertical milling machine, this machine is similar in concept to Machine A. The motors for the axes are directly coupled to a ballscrew that is supported by bearings at each end. The spindle is rotated by a DC motor mounted on the top of the spindle carrier. Nevertheless, in this machine the spindle is rotated using a belt drive which may acts as a heat source by which the heat flows into the spindle through the contacting areas. The spindle speed can be controlled from 60 rpm to 8000 rpm. Unlike Machine A, the axis feedback on Machine B is via linear scales, which means that ballscrew expansion is directly compensated by the CNC's control loop. In order to obtain the

temperature data of this machine tool, a total of 77 thermal sensors were already placed on the machine [107]. The sensors can be classified into different categories according to their positions as illustrated in Table 4-4.

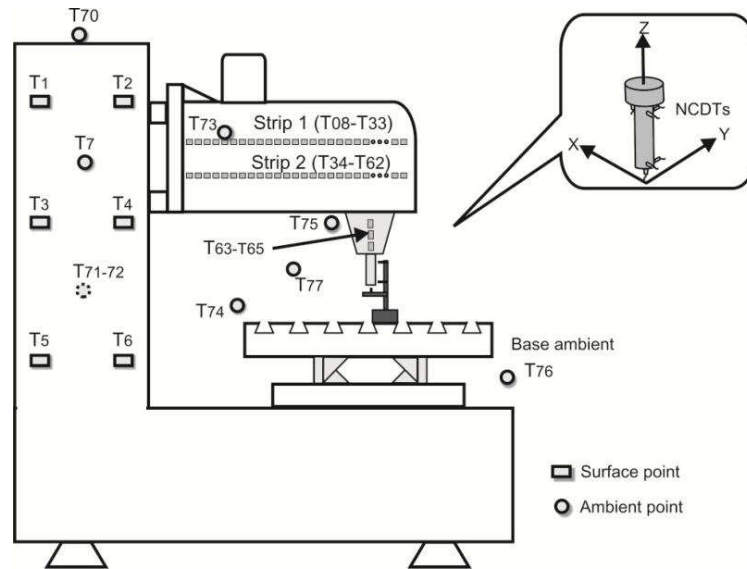


Figure 4-5: Location of thermal sensors on the Machine B.

### 4.3.3 Machine C – A 5-axis Gantry Milling Machine

Machine C is a 5-axis gantry milling machine as shown in Figure 4-6. The machine is constructed of three linear axes X, Y, Z, and two rotary axes B and C. The tool-carrying spindle is mounted on the B axis and for this configuration, all axes move the tool. The maximum speeds along the X-axis, Y-axis, and Z-axis of the machining centre are 75 m/min, 75 m/min, and 70 m/min, and the travels are 2.5 m, 1.2 m, and 0.7 m, respectively. The spindle has a maximum rotational speed of 3200 revolutions per minute. This machine has linear scale feedback for the three axes and directly mounted rotary encoder for the B and C axes.

To improve the accuracy of the proposed model, and to avoid the need for a large number of temperature sensors, additional feedback information is supplied by FBG as shown in Figure 4-6 and Figure 4-22. This can detect the change in length by measuring the detectable strain. Three FBG sensors were placed on the ram structure in order to measure the distortion of each side of the structure. Another four FBG sensors were placed on the cross-beam structure to monitor the thermal response with change in the ambient temperature. These on-line distortion measurements will be used as input to the proposed model in order to predict the growth of the ram.

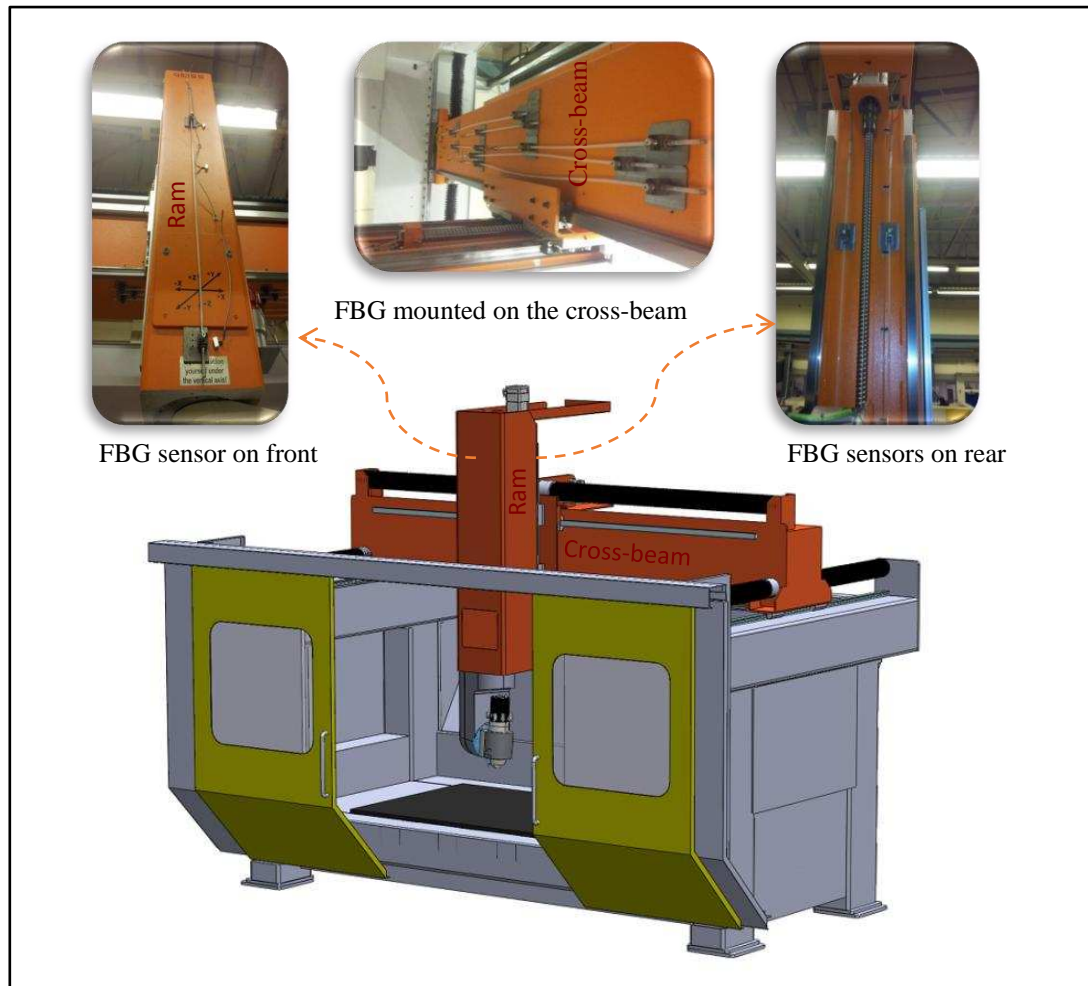


Figure 4-6: A general overview of the 5-axis milling machine and location of the (FBG).

#### 4.4 Key Thermal Measurement Points

The selection of temperature variables is a key factor to the accuracy of the thermal error model, which will be adversely affected if there is insufficient coverage of the temperature distribution. At the same time, the calibration/training time and the relative cost of the system will increase if the number of input variables is large. Therefore, the location of suitable temperature sensors should be determined before the modelling process.

In this section, experiments were performed on Machine A. The thermal imaging camera was used to record a sequence of temperature distributions across the spindle-carrier structure of the machine tool. Three NCDTs were used to measure the resultant displacement of a solid test bar, used to represent the tool. Two sensors, vertically displaced by 100 mm, measure both displacement and tilt in the Y-axis direction and a third measures displacement in the Z-axis direction (see [Figure 4-7](#)). Distortions in the X-axis direction were not measured during

this study, since experience has shown that the symmetry of the machine structure renders this effect negligible. A general overview of the experimental setup is shown in [Figure 4-8](#).

The use of masking tape on the machine provides areas of known emissivity. In particular, in some locations such as on the rotating test bar, the tape is required to provide a temperature measurement, which would be difficult to achieve by other means.

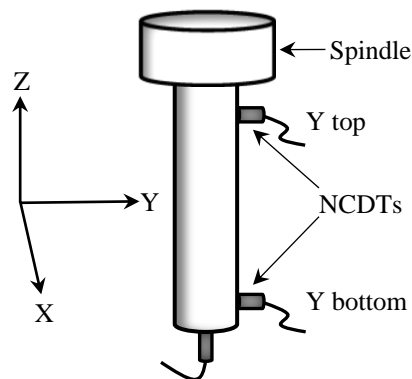


Figure 4-7: Measurement of the thermal effect using a test bar and NCDTs.



Figure 4-8: A general overview of the experimental setup.

The VMC was examined by running the spindle at its highest speed of 9000 rpm for 120 minutes to excite the thermal behaviour. The spindle was then stopped for approximately 70 minutes for cooling. The thermal imaging camera was positioned approximately 1500 mm from the spindle carrier to ensure that the parts of the machine of interest were within the field of view. Images were captured and stored to the camera's memory card during the experiment at 10 second intervals. The thermal displacement at the spindle was measured

simultaneously and is shown in Figure 4-9. The effects of test mandrel run-out and measurement noise should be considered (see the oscillation in the Y bottom-axis) during the test when the spindle is rotating. The elimination of the effects of this error can be achieved by use of time averaging or a low-pass filter. The maximum displacement for the Y top-axis is 20  $\mu\text{m}$ , the Y bottom-axis is 23  $\mu\text{m}$ , and the Z-axis is 35  $\mu\text{m}$ . A change in tilt is also found by measuring the difference between the Y top-axis and Y bottom-axis after the spindle was stopped. This is likely to have been caused by non-uniform distortions in the complex geometry of the machine structure [39].

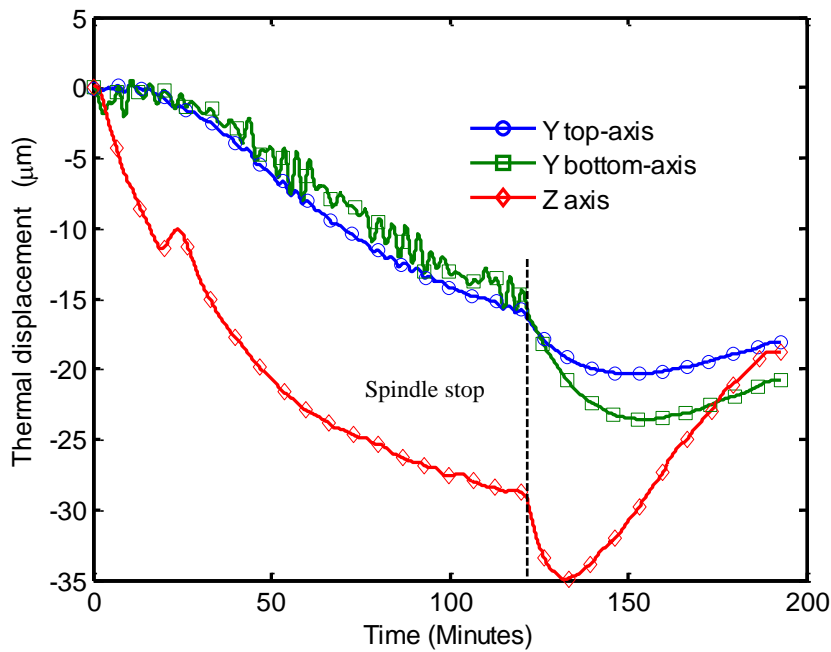


Figure 4-9: Thermal response of the spindle.

MATLAB functions were developed to enhance and analyse the temperature data [107]. These functions include image averaging (to reduce noise from individual pixels), image alignment and the ability to extract a discrete point precisely by averaging groups of pixels. In addition, efficient methods of creating virtual sensors were created, including the ability to draw “lines” of temperature sensor spots representing strips. This is important in order to obtain sufficient temperature data readings across the carrier structure. A Grey model was applied to the measured temperature data to quantify the influence of each spot across the carrier structure. Figure 4-10 shows thermal images with 525 discrete spots on the carrier and Figure 4-11 shows some extracted readings from these spots taken over the duration of the whole test.

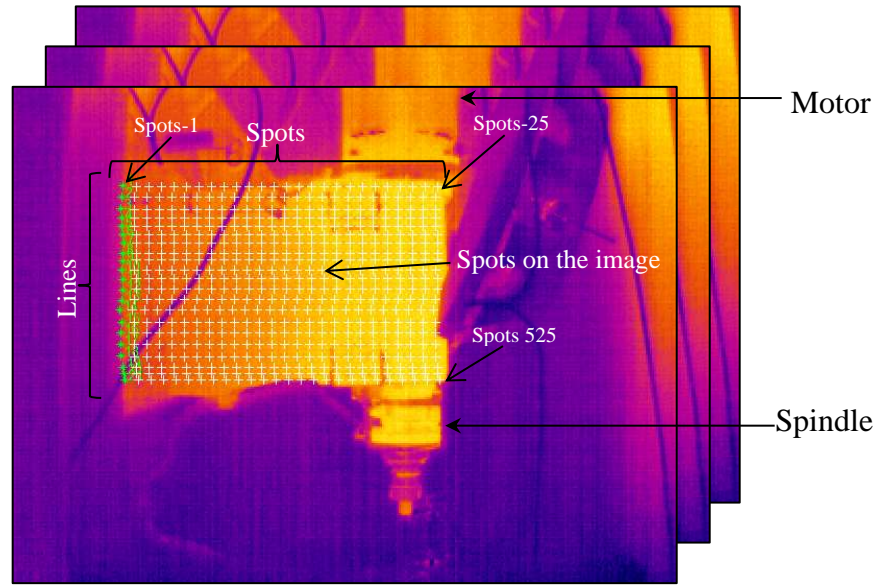


Figure 4-10: Thermal images captured during the experiment with 525 selected spots.

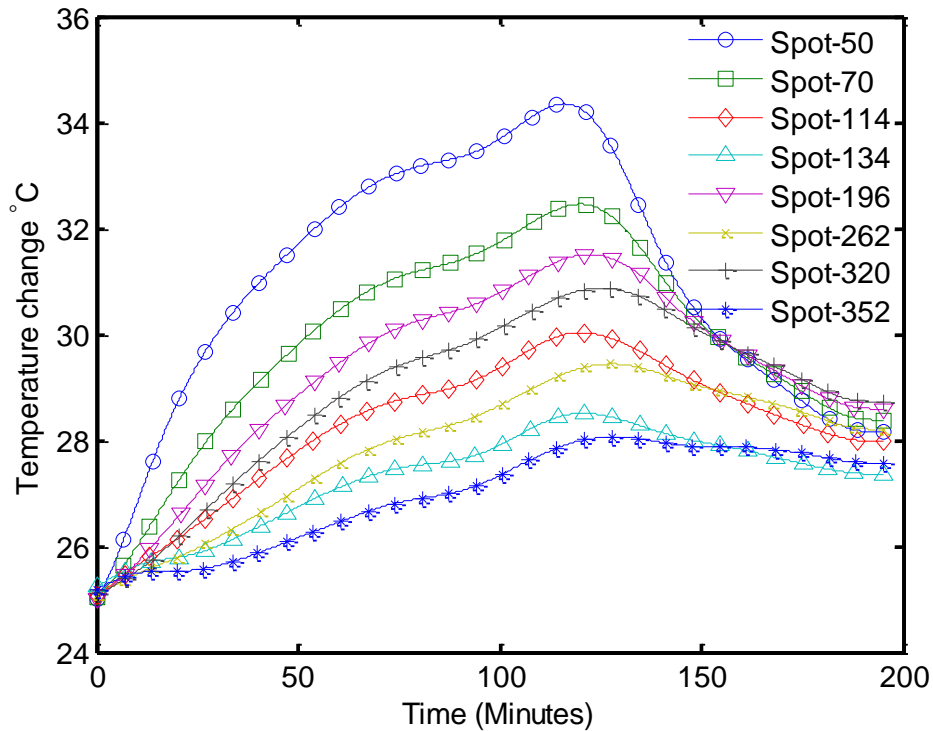


Figure 4-11: Thermal data extracted from images using MATLAB.

The machine was run through a test-cycle of 120 minutes heating and approximately 70 minutes cooling. The temperature change and displacement of the spindle relative to the table in the Z-axis was captured throughout the test. This was used in the GM (h, N) model to determine which parts within the machine structure contribute most significantly to the total thermal displacement. Further analysis then concentrated on the influence coefficient of discrete points using the FCM method. The process is as follows:

First, the GM (0, N) model of Grey system theory is calculated using the temperature changes and displacement of spindle nose in the Z-axis.

Suppose that Spot-1~Spot-525 represents the major variables (inputs)  $x_2^{(0)} \sim x_{526}^{(0)}$  and the measurement of the NCDT sensors are the target variable (output)  $x_1^{(0)}$ . The norm values of the influence coefficient matrix  $\hat{\theta}$  can be obtained using equation (3.25), as  $|\theta_2| \sim |\theta_{526}|$ , indicating the influence weighting of the input data against the output data, respectively. The greater the influence weight, the greater the impact on the thermal error, and the more likely it is that the temperature variable can be regarded as a possible modelling variable. Figure 4-12 shows a 3D plot of the influence coefficient matrix.

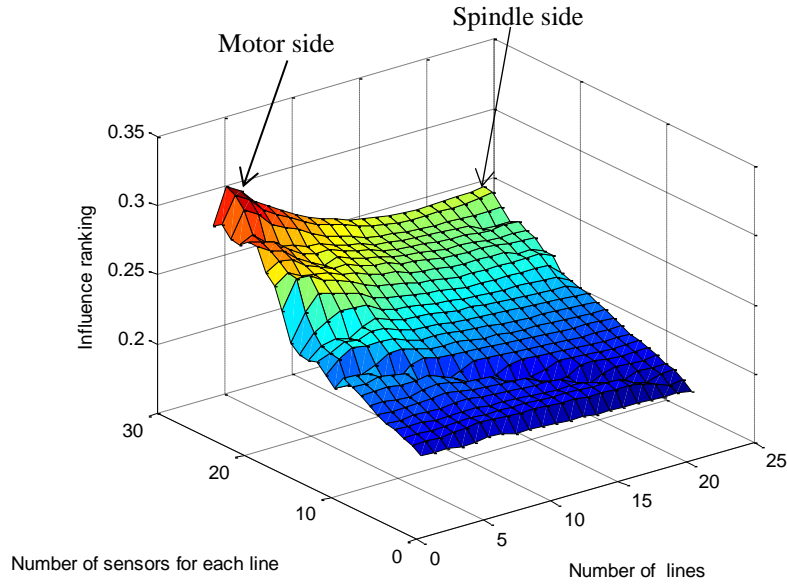


Figure 4-12: Surface of Influence ranking of temperature data using GM (0, N).

From Figure 4-12, the flow of heat across the carrier can be clearly seen. Different points have different influence on thermal error in the Z-direction; the points near the motor are the highest factors. During the cooling cycle, it can be seen (Figure 4-9) that the test bar shows some movement which occurred immediately after the spindle was stopped. This movement is probably caused by the expansion of the test bar itself; the localised heat from the motor and spindle bearings flow into the bar and there is no cooling effect from air turbulence. This flow of heat into the test bar is a significant contributor to the response in the Z-direction as the tool continues to expand after the spindle has stopped. An investigation of the source of this growth of the test bar was carried out by extracting ten spots during the same heating and

cooling test as show in Figure 4-13. The GM (0, N) model of the Grey system theory was applied again on a specific period “snapshot” of the test as shown in Figure 4-14.

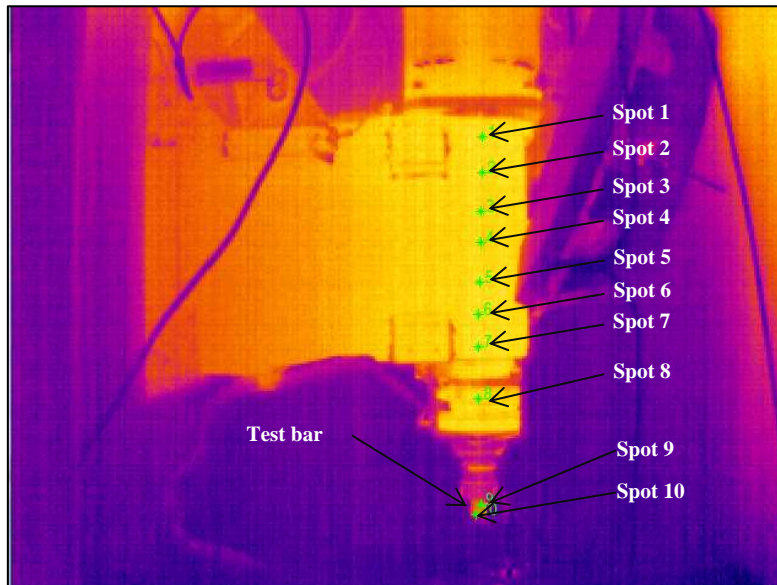


Figure 4-13: Thermal image captured during the experimental with 10 selected points.

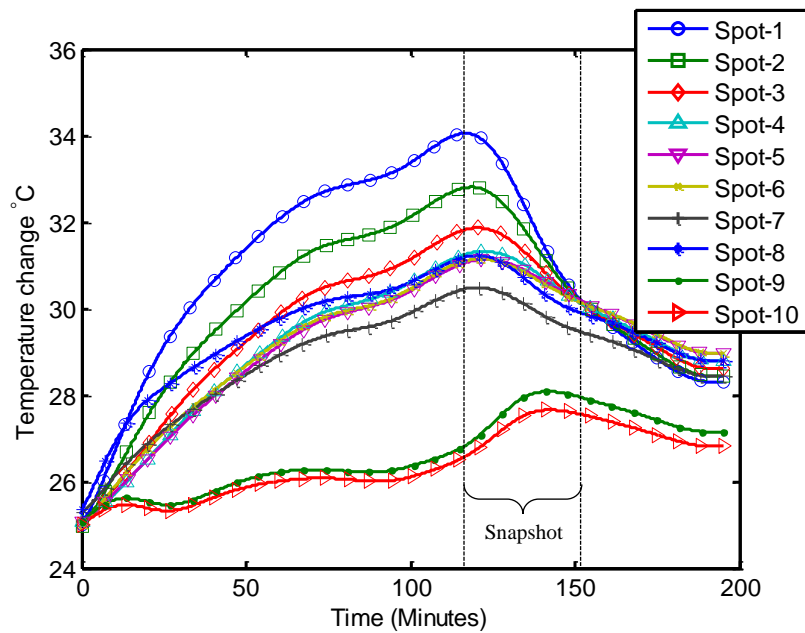


Figure 4-14: Thermal data extracted from images with 10 selected points.

Figure 4-15 shows the GM (0, N) model output for the selected period. It can be observed that the temperature change of different selected spots on the carrier has different influence on the thermal error in the Z-axis direction and the spots 9 and 10 on the test bar are the most important factors, while spot 7 is the most significant location on the machine structure. The GM (0, N) model provides a method to analyse systems where traditional methods such as the correlation coefficient do not seem appropriate. It is applicable irrespective of the size of

datasets and independent of requirement for a specific distribution. The results of this investigation indicate that the GM (0, N) model is a good optimisation tool for finding the proper selection of thermal sensors and their location.

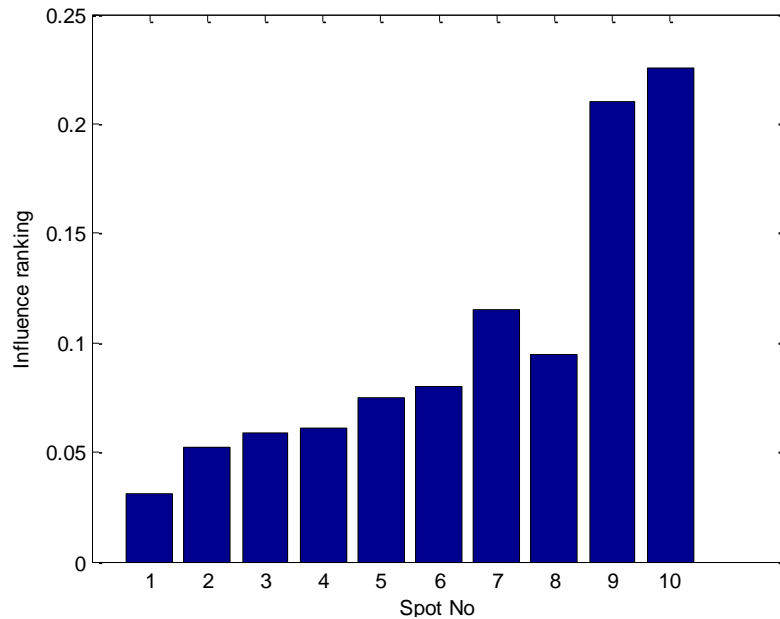


Figure 4-15: Influence ranking of ten temperature spots using GM (0, N).

The temperature sensors were clustered into a different number of groups using FCM as described in section 3.7, starting with one cluster for group 1 up to eight clusters for group 8. Then, one sensor from each cluster was selected according to its correlation with the thermal response to represent the temperature sensor of the same category (see Table 4-3); different number of compensation models can be constructed from these representative spots which will be discussed in the next chapter. An example of the clustering procedure for four clusters is shown in Figure 4-16.

Table 4-3: The cluster results.

No. of groups	Representative spots
Group 1 (one cluster)	Spot-50
Group 2 (two clusters)	Spot-50, Spot-214
Group 3 (three clusters)	Spot-50, Spot-84, Spot-398
Group 4 (four clusters)	Spot-50, Spot-107, Spot-249, Spot-493
Group 5 (five clusters)	Spot-50, Spot-140, Spot-225, Spot-263, Spot-283
Group 6 (six clusters)	Spot-50, Spot-109, Spot-200, Spot-240, Spot-348, Spot-407
Group 7 (seven clusters)	Spot-50, Spot-96, Spot-136, Spot-305, Spot-335, Spot-443, Spot-474
Group 8 (eight clusters)	Spot-50, Spot-70, Spot-114, Spot-134, Spot-196, Spot-262, Spot-320, Spot-352

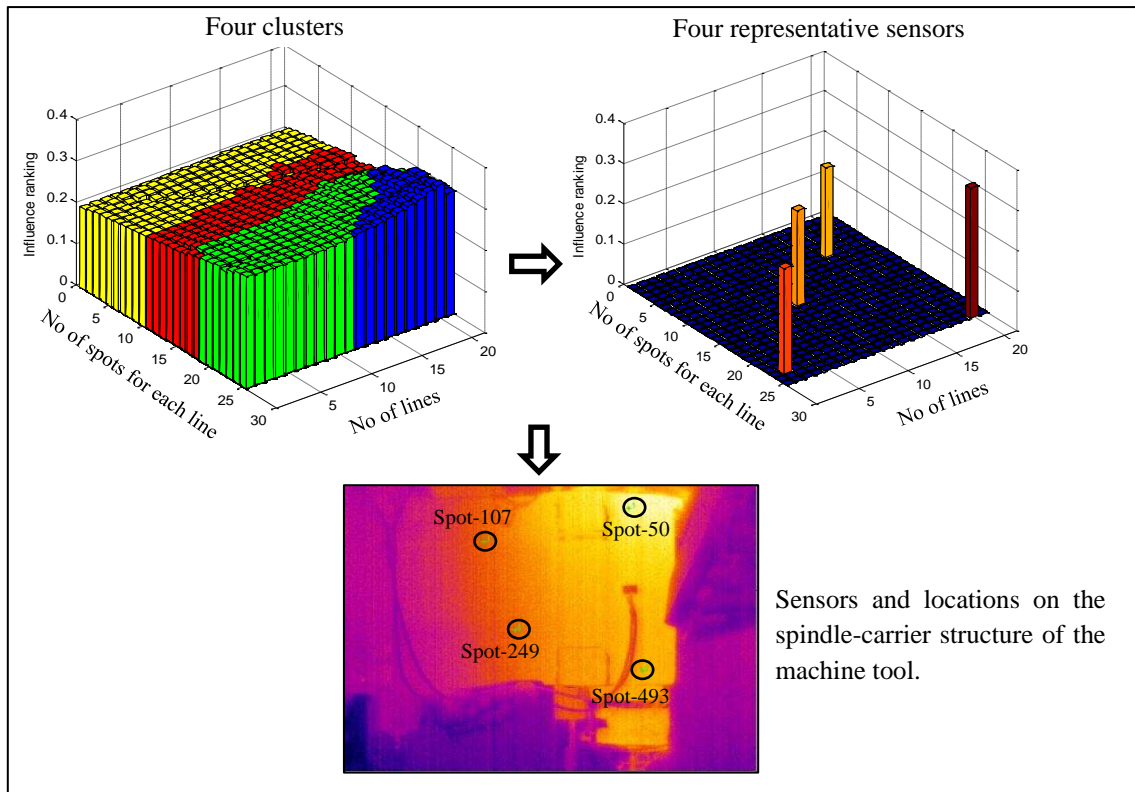


Figure 4-16: An example of clustering procedure for four clusters.

#### 4.4.1 Summary of the Proposed System

In this section, a thermal imaging camera was used to record temperature distributions across the machine structure during the experiments. The thermal images were saved as a matrix of temperatures with a specific resolution of one pixel, each of which can be considered as a possible temperature measurement point. The size of a temperature sensor means that, in a practical compensation system, sensing could not be physically applied at that spatial resolution. However, the locations can be centred on the optimal position and it is possible to use localised averaging of pixels to reduce any noise across the image. The Grey system theory and fuzzy c-means clustering were applied to minimise the number of temperature points and select the most suitable ones for a given target accuracy.

Generally, the following steps would be conducted when developing intelligent thermal model on a CNC machine tool:

- Record a sequence of thermal images using the thermal imaging camera while the machine runs through a range of duty cycle.
- Save the thermal images as a matrix of temperatures with a specific resolution of one pixel, each of which can be considered as a possible temperature measurement point.

- Analyse the measurement points using the Grey model to determine which parts within the machine structure contribute most significantly to the total thermal displacement. Further analysis then concentrated on the influence coefficient of discrete points using a clustering method.
- Further analyse the representative temperature sensors by constructing different models with different architectures. This is important to understand any uncertainty that is created by variation of the model design. (Chapter 5).
- Validate and test the developed model on a machine tool. (Chapter 6).

Most of these steps are carried out off-line. This modelling approach addresses the problems of the previous empirical models and so offers a cost-effective approach to develop a thermal error compensation that can be implemented on a wide range of machine tools. It is worth reiterating that use of thermal imaging is to help find the optimal locations for temperature measurement when designing a thermal error model. In a practical compensation system, discrete temperature sensors will be physically applied at these optimal locations.

The whole block diagram of the proposed system is shown in Figure 4-17 where spots 1 to N represent the virtual temperature sensor data captured from the thermal imaging camera, and the thermal response obtained from NCDTs.

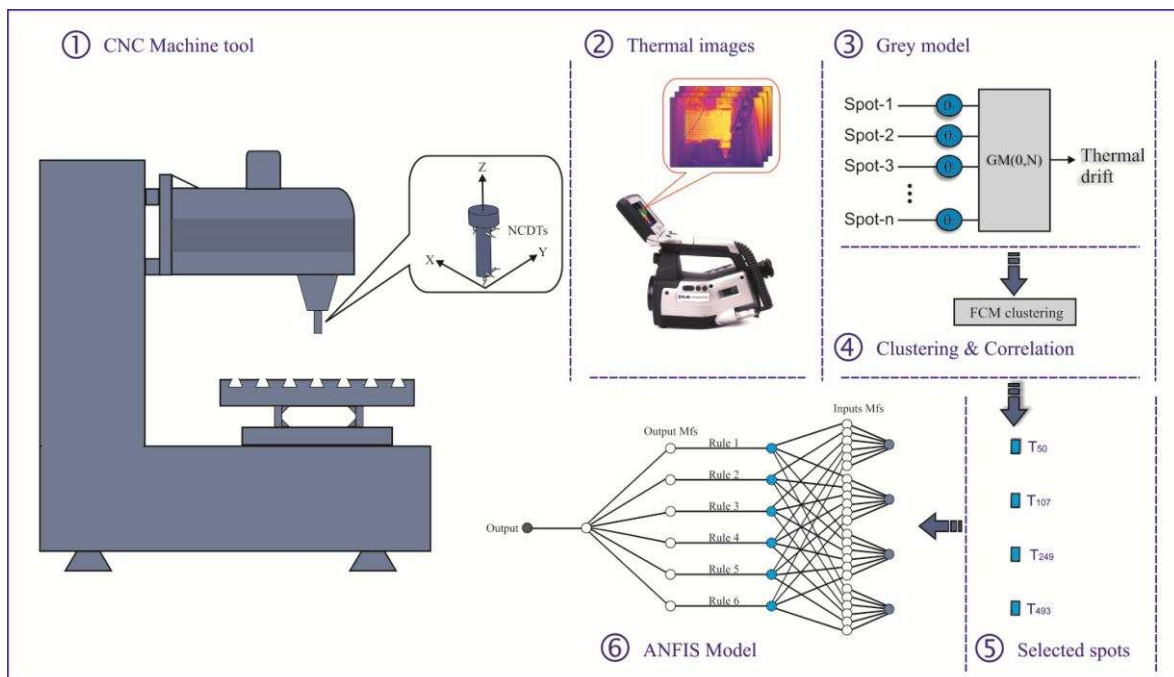


Figure 4-17: Block diagram of the proposed system.

Next, ANFIS using FCM will be used to derive a thermal prediction model. Temperature measurement points will be used as inputs and thermal response data, synchronously measured by NCDTs, as the output. The ANFIS with FCM uses these input/output pairs to create a fuzzy inference system whose membership functions are tuned using either the back-propagation or least squares estimator learning algorithm.

## 4.5 Robustness of Grey Models

A number of Grey models (GM(0,N), GM(1,N), and GRA) have been used throughout this research work (section 3.4, and our published studies in [116, 117]). Among these models, the GRA model provides a simple, less computationally intensive and low-cost approach to analyse systems with the benefit of requiring less experimental data. This is explained by the following example on Machine B.

As has been discussed in the previous sections, a large number of thermal sensors may have a negative influence on predication accuracy and robustness of a thermal prediction model. However, too few sensors will fail to cover the requirement for a comprehensive transfer function. One of the difficult issues in thermal error modelling is the selection of appropriate temperature sensor locations, which is a key factor in the accuracy of the thermal error model. This study adopts Grey relational analysis to identify the proper sensor positions for thermal error modelling. The similarity degree between the thermal error and the temperature sensors is calculated from the experimental data. All of the similarity degrees of thermal sensors will be clustered into their groups. Then, one sensor from each group will be selected according to its similarity degree with the thermal response, to represent the temperature sensors of the same category. Therefore, by selecting these sensors, the ANFIS models can be built easily to predict the thermal response.

### 4.5.1 Setup of Measurement System

As shown in Figure 4-18, in order to obtain the temperature data of the Machine B, a total of 77 thermal measurement points are placed on a small vertical milling machine. The measurement points can be classified into different categories according to their positions as illustrated in Table 4-4:

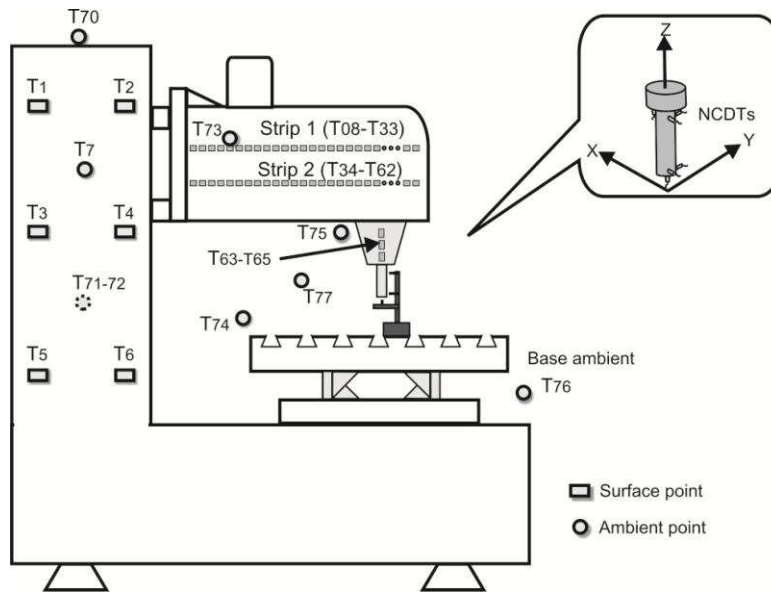


Figure 4-18: Location of thermal points and displacement sensors on the machine.

Table 4-4: The location of the thermal measurement points

Group No.	Point No.	Definition
Column sensors (1)	1-7	Outside the column
	70	Ambient at top of column air
	71-72	Inside the column
Carrier sensors (2),(3)	8-33	Strip 1 Sensors (placed on the carrier)
	34-62	Strip 2 Sensors (placed on the carrier)
Spindle boss points (4)	63,65	Spindle boss
	66,67	Y Scale air
	68,69	Y bed sensor
	73	Carrier air
	74	Table
	75	Spindle air
	76	Base air
Other parts of the machine (5)	77	Tool air

Five NCDTs are used to measure the displacement of a precision test bar, representing the tool in the X, Y and Z axes, respectively. The configuration is shown in [Figure 4-18](#). The vertical milling machine was examined by running at its highest spindle speed of 8000 rpm for one hour to excite the largest thermal behaviour. The temperature measurement points at the selected places on the machine tool and the thermal displacement of the spindle are measured simultaneously; the thermal displacement of the vertical milling machine is shown in [Figure 4-19](#). The maximum displacement of the X-axis is 3  $\mu\text{m}$ , the Y-axis is 60  $\mu\text{m}$  and the Z-axis is 24  $\mu\text{m}$ . In this example, the X-axis thermal displacement is ignored because it is

much smaller than that of the Y-axis and the Z-axis due to their mechanical symmetry; only the Y-axis and Z-axis are considered.

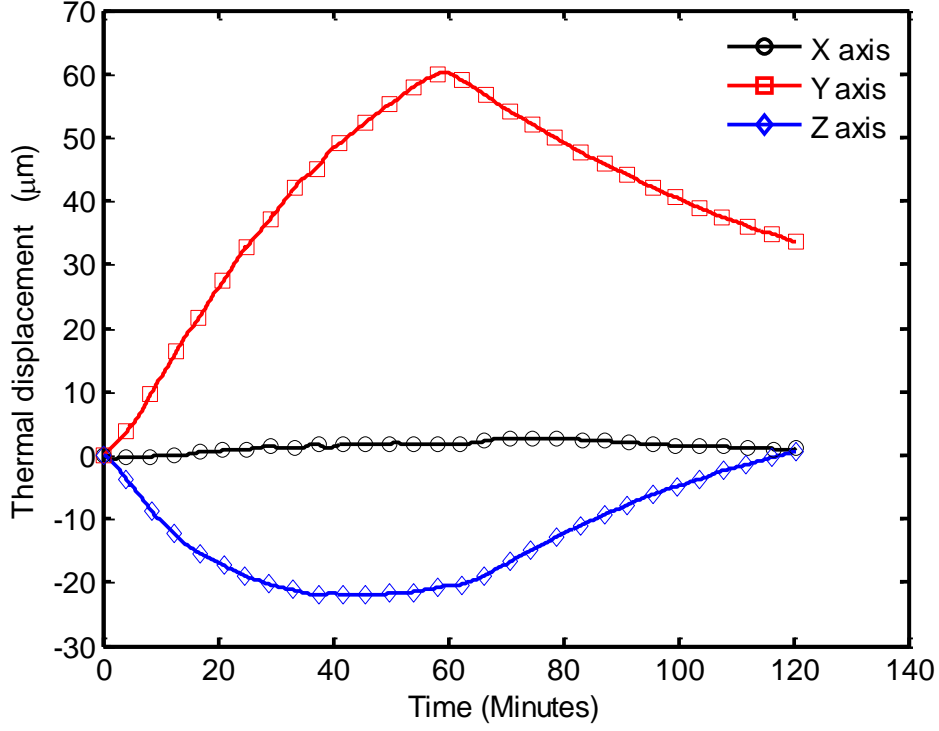


Figure 4-19: Thermal response of the spindle.

#### 4.5.2 Thermal Key Point Identification Using GRA Model

Suppose that the measurement of the NCDTs sensor in the Y-direction is the reference sequence and T1-T77 represents the comparative sequences. According to the GRA method explained in section 3.7.3, the algorithm is summarised as follows:

Step1: Pre-processing the experimental data; the reference sequence ( $X_0$ ) and  $m$  comparative sequences ( $X_m$ ) are pre-processed and represented as:

$$\begin{aligned}
 X_0 &= (x_0(1), x_0(2), \dots, x_0(n)), \\
 X_1 &= (x_1(1), x_1(2), \dots, x_1(n)), \\
 &\vdots \\
 &\vdots \\
 &\vdots \\
 X_m &= (x_m(1), x_{m1}(2), \dots, x_m(n)).
 \end{aligned}$$

Step 2: Computing the initial images with zero initial provides:

$$X_0^0 = (x_0^0(1), x_0^0(2), \dots, x_0^0(n)),$$

$$\begin{aligned} X_1^0 &= (x_1^0(1), x_1^0(2), \dots, x_1^0(n)), \\ &\vdots \\ X_m^0 &= (x_m^0(1), x_m^0(2), \dots, x_m^0(n)), \end{aligned}$$

where,  $x_i^0(k) = x_i(k) - x_i(1)$ ,  $k = 1, 2, \dots, n$ , and  $i = 0, 1, 2, \dots, m$ .

Step 3: Compute  $|s_0 - s_m|$  as follows:

$$|s_0 - s_m| = \left| \sum_{k=2}^{n-1} x_0^0(k) - x_m^0(k) + \frac{1}{2} [x_0^0(n) - x_m^0(n)] \right|.$$

Step 4: Calculation of similarity degrees of sequences  $n \times m$  are as follow:

$$\varepsilon_{0m} = \frac{1}{1 + |s_0 - s_m|} \quad (4.1)$$

Step 5: Sort/cluster the similarity degrees of all the sequences. Then, one point from each group is selected according to its similarity degree with the thermal response to represent the temperature measurement point of the same category.

To facilitate processing of calculation, MATLAB Graphical User Interface (GUI) functions have been developed to aid in the processing of variables selection for modelling. Input data into the presented GUI can have different origins, but they have to be MS Excel .xlsx formatted, specifically named and saved in the same directory as the other GUI files. Then, the first column of the MS Excel file is presented as time, the second column as reference factor, and the rest of the columns as compared factors of a system. By loading the file, it will display brief information about a particular system (number of inputs, output and the number of samples).

This allows a sequence of data, captured using NCDTs sensors and temperature measurement points to be loaded into the MATLAB GUI directly. The GRA method can be applied with different lengths of data; the results can be plotted and/or exported to MS Excel file.

Different tests were carried out with different input-output dataset sizes using the GRA model: a sixty minute test (350 samples); 30 minute test (175 samples) and; a one minute test (6 samples) respectively. The similarity degrees, the group-sorting and representative temperature sensors are illustrated in [Figure 4-20](#), [Table 4-5](#), and [Table 4-6](#), respectively.

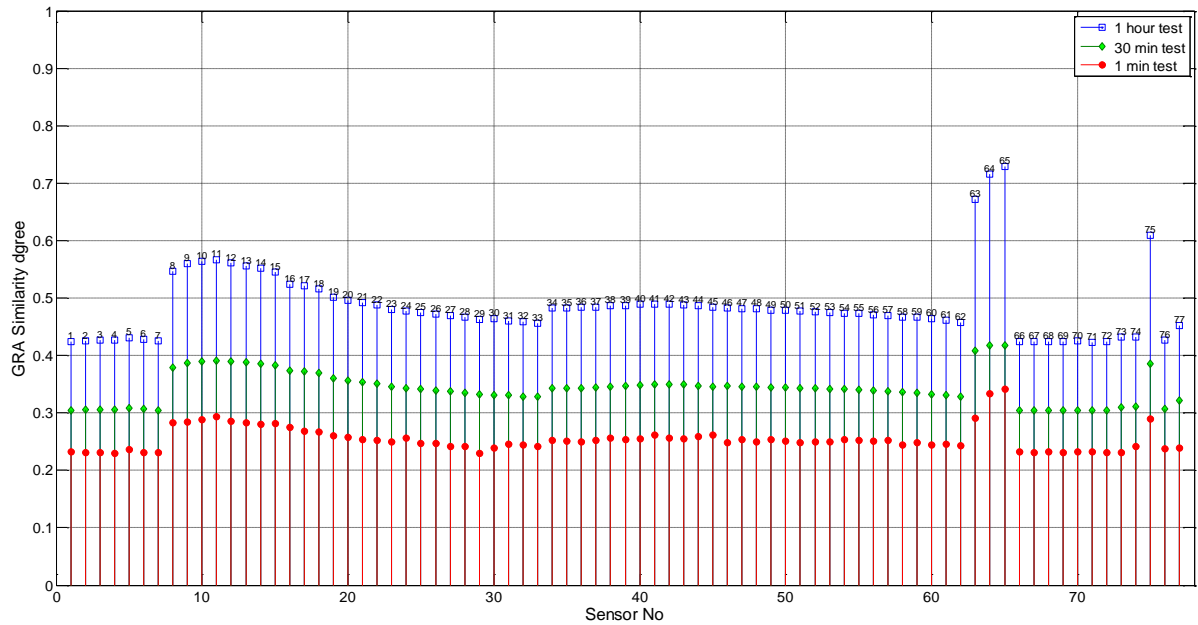


Figure 4-20: Similarity ranking of temperature points using GRA model.

Table 4-5: The clustering result.

Group No	Measurement points order
Group 1	5>6> 3>4>7>2>70>1>72>71
Group 2	11>10>12>9>13>14>8>15>16>17>18>19>20>21>22>23>24>25>26>27>28>30>29>31>32>33
Group 3	40>41>42>43>39>38>44>45>37>36>35>46>34>46>34>47>48>49>50>51>52>53>54>55>56>57>59>58>60>61>62
Group 4	65>64>63
Group 5	75>77>73>74>76>69>66>68>67

Results in [Figure 4-20](#) can be well explained by the physical construction and expected thermal behaviour of the machine tool. They indicate that the temperature measurement points located close to the heat source give a higher similarity degree than the temperature measurement points located relatively far away from the heat source. Results also indicate that GRA is applicable irrespective of the size of datasets and independent of requirements for a specific distribution. It provides a method to analyse systems where traditional methods such as the correlation coefficient do not seem appropriate. GRA is a useful tool to determine the degree of similarity between the reference sequence and comparative sequences.

According to the degrees of similarity between the temperature sequences and the thermal error sequence of the Y-direction listed in [Table 4-5](#), the thermal measurement point with the biggest value in each group is selected; they are 5, 11, 40, 65, and 75 (see [Table 4-6](#)). Therefore, the 77 measurement points placed for academic investigation were decreased to 5.

For practical purposes, the main representative points can be used as a basis for constructing the models, which could simplify the thermal prediction models. The above analysis indicates that the GRA model is a good optimisation tool for finding the proper selection of thermal measurement points.

Table 4-6: Selected temperature sensors.

Sensor No.	Definition	Group name
5	measuring the temperature of the column	GROUP 1
11	measuring the temperature of point on line 1	GROUP 2,3
40	measuring the temperature of point on line 1	
65	measuring the temperature of the spindle boss	GROUP 4
75	measuring the temperature of the spindle air	GROUP 5

Figure 4-21 shows the influence ranking of temperature data presented in section 4.4 using GRA model. It can be also well explained by the physical construction of the machine tool; the temperature spots located close to heat sources (e.g. spindle motor, bearing) give a higher similarity degree than the temperature measurement points located relatively far away from the heat source (spindle-carrier rear) at the beginning of the test. Therefore, this observation confirms to the results obtained by GM (h, N) model in the section 4.4.

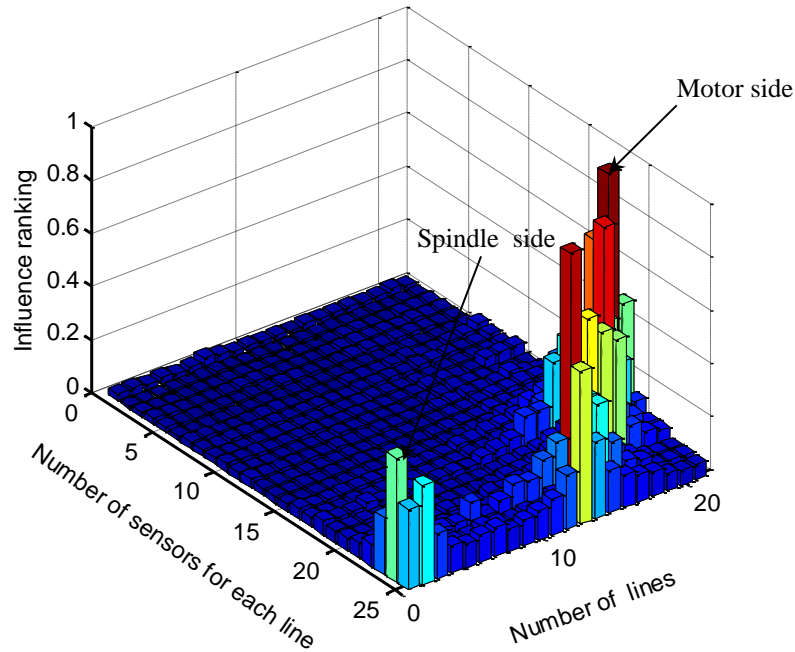


Figure 4-21: Influence ranking of temperature data using GRA model.

#### 4.6 Example of the Fusion Measurement on Machine C

In most previous research work, temperature sensing is used as inputs to the compensation models. This is consistent with the approach from a large number of researchers. The philosophy has a merit, since it ensures that the model is driven by changes in temperature profile irrespective of the heat source. However, to improve the accuracy of the predicted model, and to minimise the effects of thermal hysteresis, additional feedback information is supplied by FBG sensors on Machine C.

In this example, the machine under investigation is a 5-axis gantry milling machine (Machine C). The first step was to perform an initial assessment to identify machine structural elements and heat sources that contribute most significantly to the machine errors. A thermal imaging camera was used to record temperature distributions across the machine structure during “dry” operations, i.e. without coolant present. The two main contributors to thermal error were due to C-axis rotation and Z-axis movement of the ram. These two errors are therefore analysed in this work. MATLAB processing routines have been devised to generate “virtual” temperature sensors from the thermographic images, which were used to identify the optimal position to install surface-mount temperature sensors on the surface of the structure (see [Figure 4-22](#)). From related work on this aspect (see [section 4.4](#)) and the initial tests, a total of twelve temperature sensors were placed on the machine. Six sensors were located on or near

the major heat sources: one measured the surface temperature of the ram near the C-axis motor (T1); one (T2) measured the surface temperature of the lower bearing of the ballscrew; two monitored the gradient from the end of the ram (T3, and T4); and two measured the surface temperature of the Z-axis motor (T5, and T6). Another six temperature sensors were placed around the machine to pick up the ambient temperature changes. Four laser displacement sensors were used to measure the displacement of a test bar (attached to the spindle) caused by the thermal distortion of the machine: two measured displacement of the test bar in the Y-axis and Z-axis directions (this study also did not consider the X-axis direction due to symmetry of the machine); two measured any tilt. A general overview of the experimental setup is shown in Figure 4-23. The diagram also indicates the sign convention of all the machine axes.

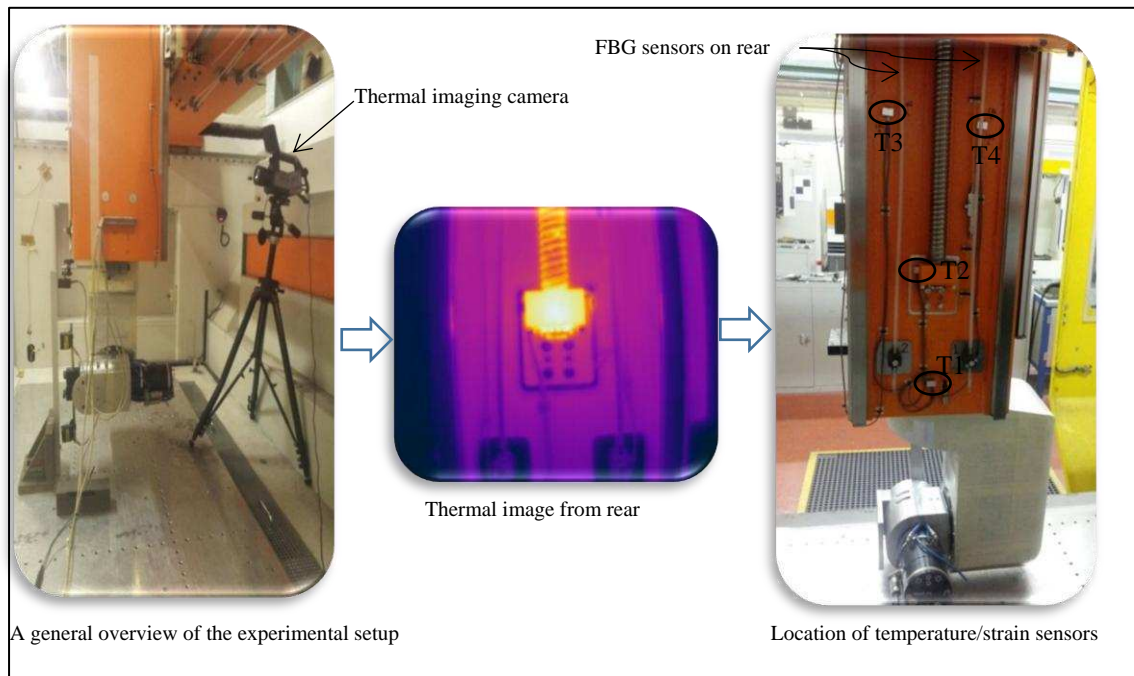


Figure 4-22: Strategy of temperature sensor placement on ram structure.

To improve the accuracy of the proposed models, and to avoid the need for a large number of temperature sensors, additional feedback information is supplied by FBG as shown in Figure 4-6. This can detect the change in length by measuring the detectable strain. However, the FBG sensor itself is also affected by temperature by a factor that equates to  $8.64 \mu\text{m}/\text{m}/^\circ\text{C}$ . One method of compensating temperature is to use an unconstrained grating to measure temperature. Nevertheless, this was unviable for this application because it would require additional gratings to be mounted, incurring additional cost and requiring additional mounting space, which was not readily available. Instead, the low-cost temperature sensors

used for the temperature-based model were used to correct for change in the grating temperature. Three FBG sensors were placed on the ram structure in order to measure the distortion of each side of the structure. Another four FBG sensors were placed on the cross-beam structure to monitor the thermal response with change in the ambient temperature. These on-line measures were used as input to the proposed model in order to predict the growth and distortion of the ram.

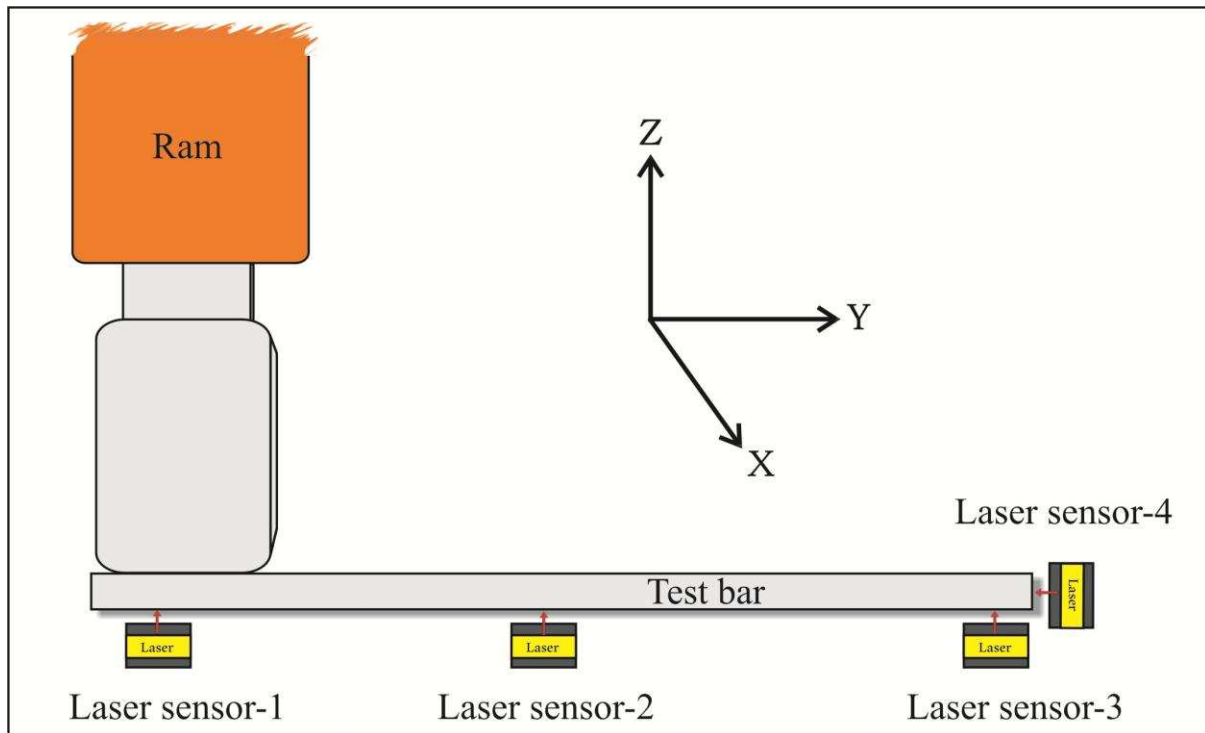


Figure 4-23: Procedures for measuring the thermal errors.

#### 4.6.1 Hysteresis Effect

Figure 4-24 shows test results from a cycle of two hours heating-up and another two hours for cooling down (test detail will be given in section 5.4). Results show that the temperature of the machine tool (T2 Ram rear) changed with a certain delay relative to variation in the machine displacement and FBG sensors (FBG-1, and FBG-2).

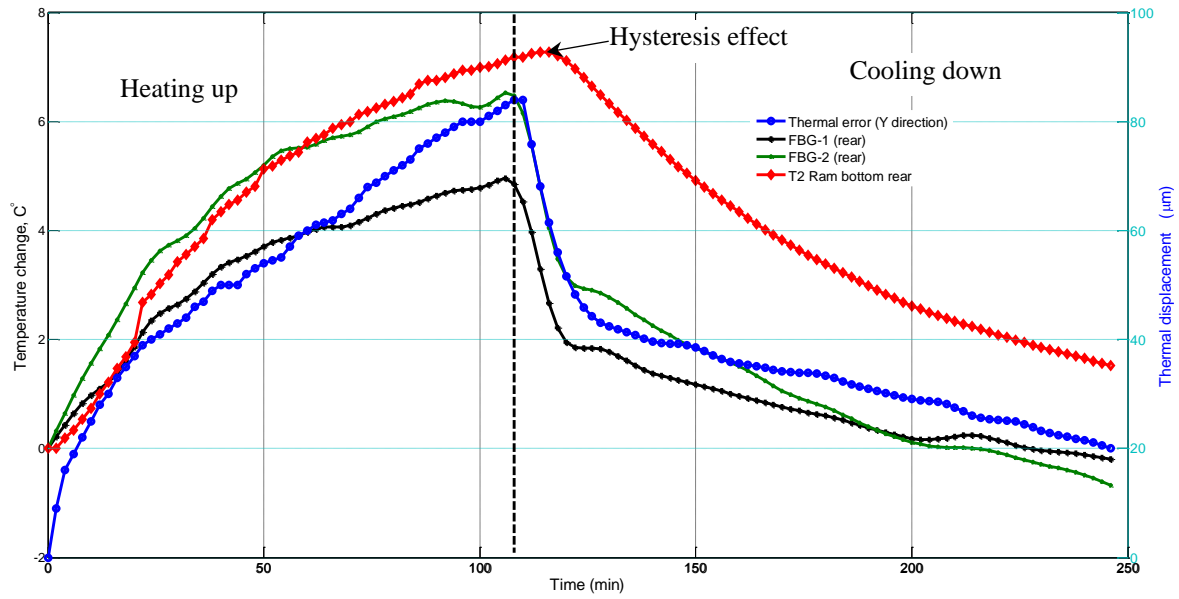


Figure 4-24: Data fusion (temperature and strain).

Furthermore, [Figure 4-25](#) shows hysteresis plot of different sensors, it can be clearly seen that the FBG sensors located on the machine ram exhibit lower hysteresis. For example, (FBG-1, and FBG-2) sensors respond in an almost linear fashion, whether the machine is being heated or cooled. It can also be observed that the temperature at the point of measurement (T2 Ram rear) possess slightly higher hysteresis behaviour relative to other sensors; there is a latency of approximately 10 minutes. By using FBG sensors, the effect of thermal hysteresis could be minimised. Therefore, the application of FBG sensors could allow for a more accurate prediction of thermal error (see next chapter).

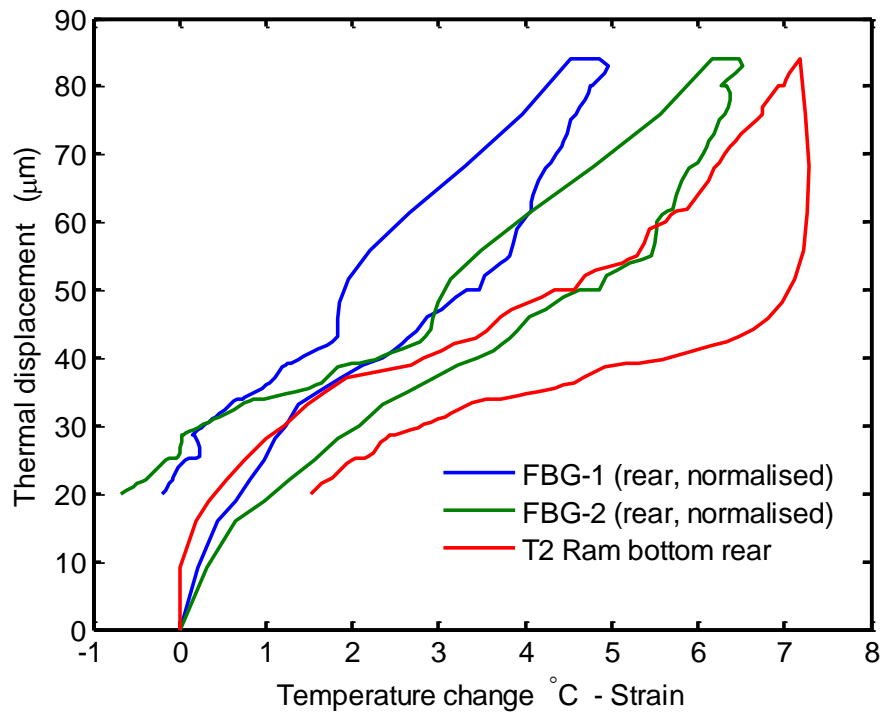


Figure 4-25: Hysteresis plot from different sensors.

## 4.7 Summary

In this chapter, a thermal imaging camera has been used to record temperature distributions across the spindle carrier structure during the experiments. The thermal images are saved as a matrix of temperatures with a specific resolution of one pixel (equivalent to  $2.25 \text{ mm}^2$ ). This system equates to over 76000 possible temperature measurement points. Averaging, which is used to decrease noise, reduces the number of temperature locations to the equivalent of 525 points, depending upon the field of view. This richness of data is exploited to find the optimal location for temperature measurement when designing a thermal error control model.

With the use of Grey model and FCM methods, the influence rankings of recorded temperature data has been found to be applicable to determine which parts within the machine structure contribute most significantly to the total thermal displacement. This eliminates the need for intuitive locating of sensors and significantly reduces implementation time. The principal advantage of this novel technique is to use thermal imaging to assess a machine's thermal behaviour and to build compensation models with different numbers and configurations of sensors. It is worth to notice that use of thermography is to help find the

optimal model structure when designing a thermal error model. In this sense, in a practical, temperature sensors will be physically applied at the key locations on the machine's surface.

This section also has highlighted the use of FBG sensors for strain measurement. They have several advantages over other sensors in terms of sensitivity and quality and could be embedded in a future, commercialised system. Therefore, in the next chapter, temperature measurement at key locations will be supplemented by direct distortion measurement. This fusion measurement will be used as input to the proposed models.

## **Chapter 5: Artificial Intelligence Model Development**

### **5.1 Introduction**

Thermal errors are often quoted as being the largest contributor to CNC machine tool errors, but they can be effectively reduced using error compensation. The performance of a thermal error compensation system depends on the accuracy and robustness of the thermal error model and the quality of the inputs to the model as previously discussed. The location of temperature sensors must provide a representative measurement of the change in temperature that will affect the machine structure. The number of sensors and their locations are not always intuitive and the time required to identify the optimal locations is often prohibitive, resulting in compromise and poor results.

It is likely that when a compensation system is implemented on a machine, each part of the structure will be modelled separately. The final compensation value will be calculated by combining the displacement of all the structural elements. As a next step in this research, the machine is modelled as individual structural elements. For this reason, it was decided to begin the investigation by looking at applying ANFIS modelling to the spindle carrier of Machine A and to concentrate on predicting Z-direction deformation. Another investigation was carried out on Machine B; the experimental tests were carried out throughout different time durations, different ambient temperatures and different spindle rotation speeds in order to validate the robustness of the modelling method. This is followed by an example of fusion sensors modelling on Machine C.

### **5.2 Generating ANFIS Architecture**

In this section, a new intelligent compensation system for reducing thermal errors of machine tools using data obtained from a thermal imaging camera will be introduced. In section 4.4, different groups of key temperature points were identified from thermal images using a novel approach based on a Grey model and fuzzy c-means clustering method. An adaptive neuro-fuzzy inference system with fuzzy c-means clustering will be employed to design the thermal prediction model. In order to optimise the approach, a parametric study was carried out by changing the number of inputs and number of membership functions to the ANFIS-FCM model, and comparing the relative robustness of the designs. Eight models were developed as

follows: representative temperature sensors from [Table 4-3](#) were selected as input variables and the thermal response in the Z-direction was considered as a target variable. The same test (120 minutes heating and 70 minutes cooling) was used for training and validating the models: experimental data are divided into training and checking datasets. The training dataset is used to train (or tune) a fuzzy model, while the checking dataset was used for over-fitting model validation. The Gaussian functions are used to describe the membership degree of these inputs, due to their advantages of being smooth and non-zero at each point [50]. After setting the initial parameter values in the ANFIS-FCM models, the models were adjusted using a hybrid learning scheme.

Extensive simulations were conducted to select the optimal number of MFs (clusters) and number of iterations (epoch) for each model. The performance of the model depends on the combination of these different parameters. Too few MFs do not allow the ANFIS-FCM models to be well mapped. However, too many MFs increase the difficulty of training and lead to over-fitting or memorising undesirable inputs such as noise. The prediction errors were measured separately for each model using the root mean square error (RMSE) index. By varying the simulations, it was determined that the optimal solution was six MFs in the first five models, and three MFs for the remaining models. Different numbers of epochs were selected for each model because the training process only needs to be carried out until the errors converge. An example of selecting MFs with four inputs is presented in [Table 5-1](#).

Table 5-1: Performance of ANFIS-FCM models with various numbers of MFs.

Models	Number of MFs	Convergence epochs	RMSE of the validation data	the RMSE of the testing data
1	2	200	0.8314	3.8456
2	3	200	0.6064	2.0052
3	4	200	0.5380	2.4614
4	5	100	0.5793	2.0534
5	6	100	0.5327	1.7275
6	7	100	0.3494	4.1113
7	8	100	0.3232	4.8818
8	9	100	0.3058	5.0802

In order to examine the performance of all the ANFIS-FCM models on non-training data, another test was carried out on the same machine (Machine A) in an operational cycle as follows. The machine was programmed to run at spindle speed of 8000 rpm for 60 minutes and then 40 minutes with the spindle stopped. It was then run again at spindle speeds of

4000 rpm and 9000 rpm for 30 minutes and 40 minutes respectively. Finally, measurement continued for another 40 minutes with the spindle stopped. During the experiment, the thermal errors were measured by the NCDTs, and the predicted displacements were obtained using ANFIS-FCM models.

In Table 5-2, the prediction performance of eight ANFIS-FCM models was compared for training and non-training data respectively.

Table 5-2: The characteristics of the ANFIS-FCM models.

Model	No. of inputs	No. of MFs for each input	No. of iterations	Training stage		Testing stage			
				NSE	RMSE	NSE	RMSE	R	Residual
ANFIS-FCM 1	1	6	200	0.6780	4.4835	0.4070	5.8847	0.7636	14.09
ANFIS-FCM 2	2	6	200	0.9838	1.0071	0.4929	5.5618	0.8302	13.76
ANFIS-FCM 3	3	6	11	0.9941	0.6223	0.9585	1.5183	0.9904	3.39
ANFIS-FCM 4	4	6	9	0.9939	0.6069	0.9764	1.4139	0.9912	2.95
ANFIS-FCM 5	5	6	12	0.9941	0.6254	0.9351	1.8981	0.9806	4.53
ANFIS-FCM 6	6	3	2	0.9881	0.8634	0.7154	3.9754	0.9595	8.00
ANFIS-FCM 7	7	3	2	0.9880	0.8659	0.7352	3.8346	0.9635	8.21
ANFIS-FCM 8	8	3	10	0.9847	0.9789	0.6439	4.4463	0.9332	10.42

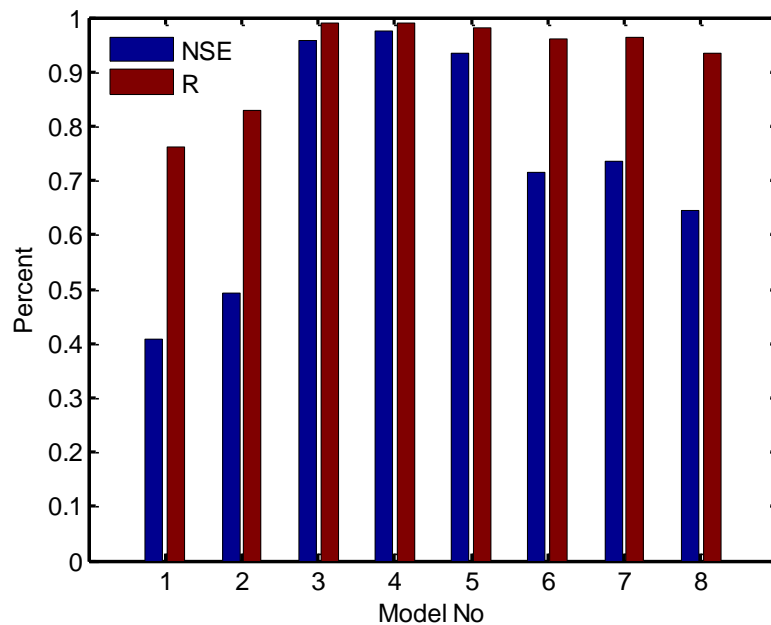


Figure 5-1: The characteristics of the ANFIS models during testing stage.

Table 5-2 and Figure 5-1 illustrate the obtained results from all eight developed models. From these results, it can be observed that both NSE and RMSE have promising values

during the training stage for all the models. However, during the testing stage the models with one and two input variables gave low efficiency, low correlation coefficient and high residual value due to insufficient data regarding the system behaviour. In addition, the seven and eight inputs models did not give as good results as the other models due to redundancy of input data. The ANFIS-FCM model with four inputs gives the best estimation, taking into account the performance indices (higher efficiency coefficient  $NSE=0.97$  higher correlation coefficient  $R=0.9912$ , and lower root mean square error  $RMSE=1.4139$ ) and lowest residual value amongst others as shown in Figure 5-2.

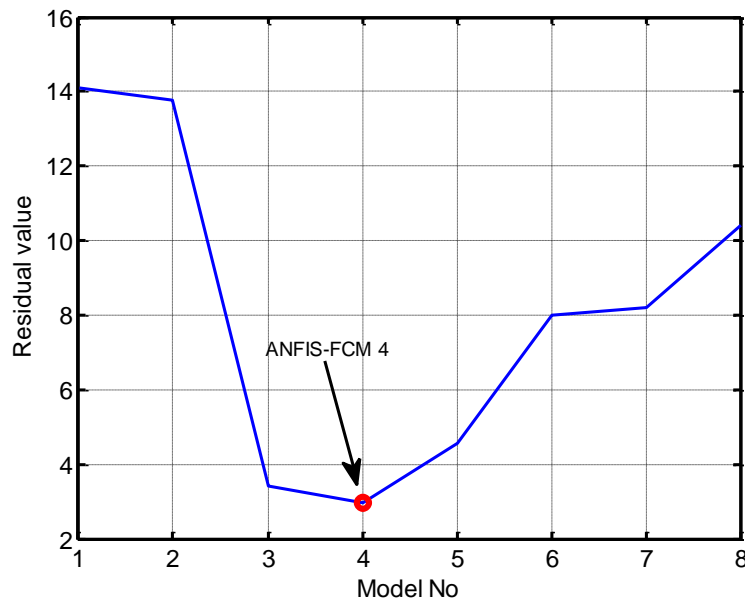


Figure 5-2: Residual values for all eight models.

The structure of the ANFIS-FCM model with four inputs is shown in Figure 5-3. There are four input neurons, corresponding to as found in section 4.4 (see Figure 5-4). In the second layer, six neurons are connected to each input neuron (in total 24 neurons), which correspond to six Gaussian membership functions for each input sensor as shown in Figure 5-5. The next layer contains six neurons equivalent to six fuzzy "if-then" rules. The result of the prediction process is presented by six neurons in the output layer. A weighted average method is used for the defuzzification stage in order to obtain the final predicted thermal response.

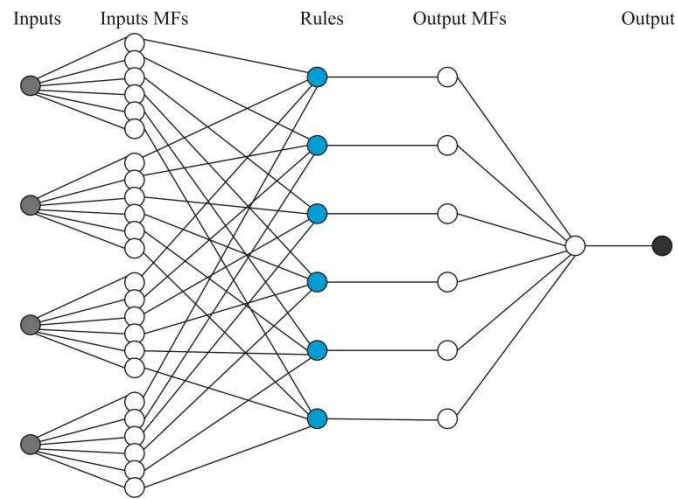


Figure 5-3: The structure of associated network model.

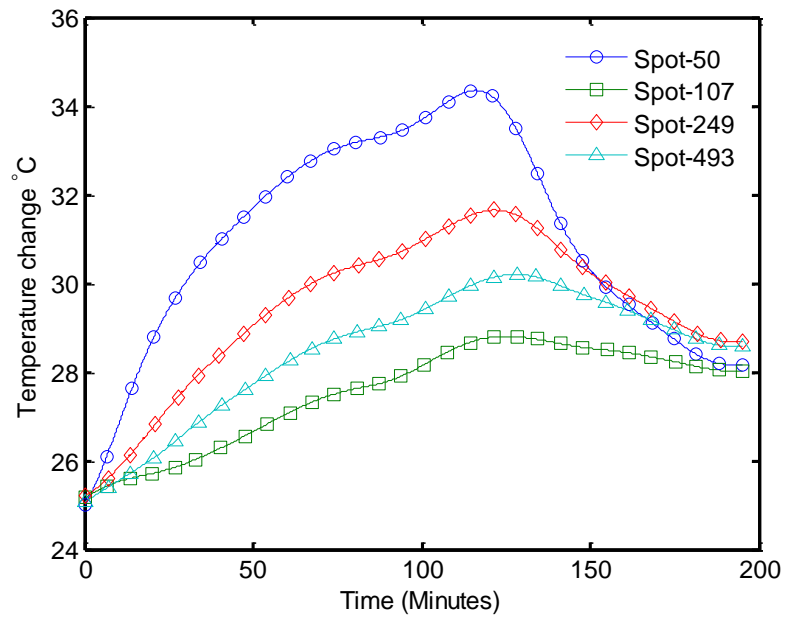


Figure 5-4: Thermal data extracted from four points.

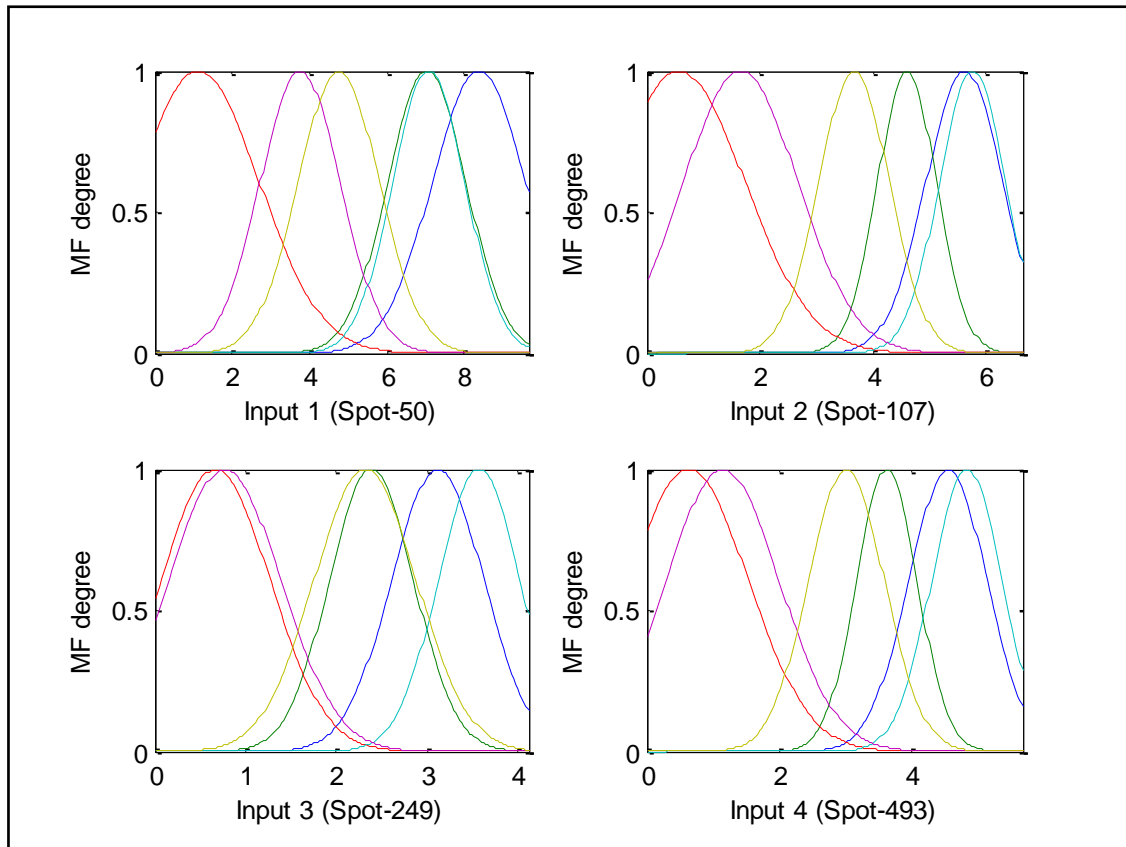


Figure 5-5: Membership functions obtained through FCM.

Figure 5-6 describes the temperature rise during the testing experiment. It can be seen that the temperature extracted from the representative sensors fluctuated due to change of the spindle speed, which causes sudden change in the resultant displacement in the Z-axis direction. The simulation result shows that the proposed ANFIS-FCM model can predict the error accurately and can also track the rapid changes of thermal error precisely (see Figure 5-7, the maximum residual is approximately  $\pm 2 \mu\text{m}$ ). Thus, a model with four representative temperature sensors is therefore a powerful and precise predictor of the thermal errors of the machine tool.

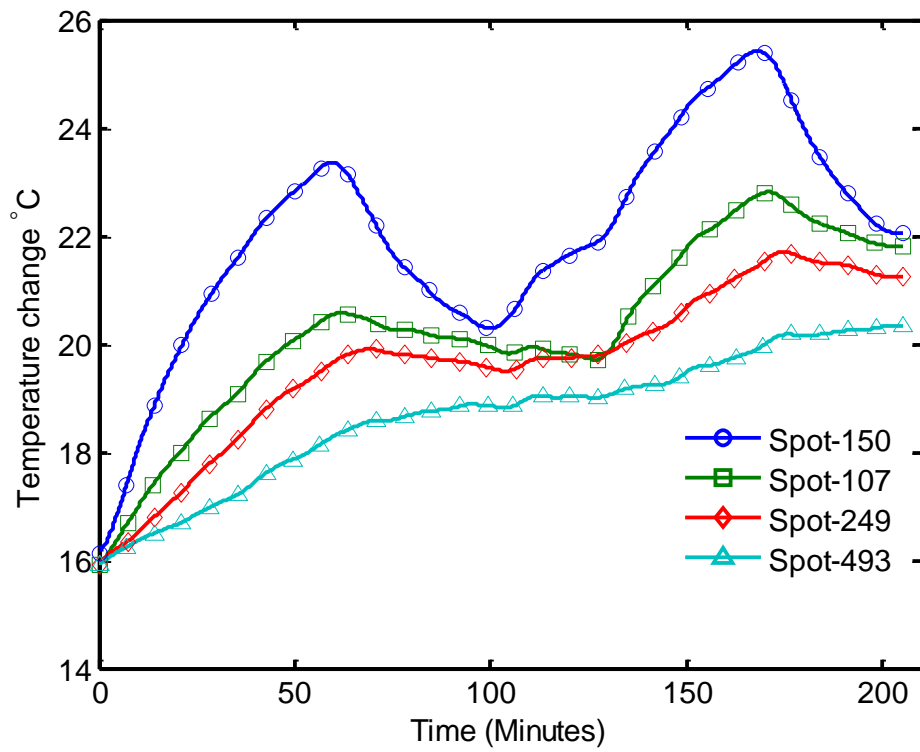


Figure 5-6: Thermal data extracted from images from selected points.

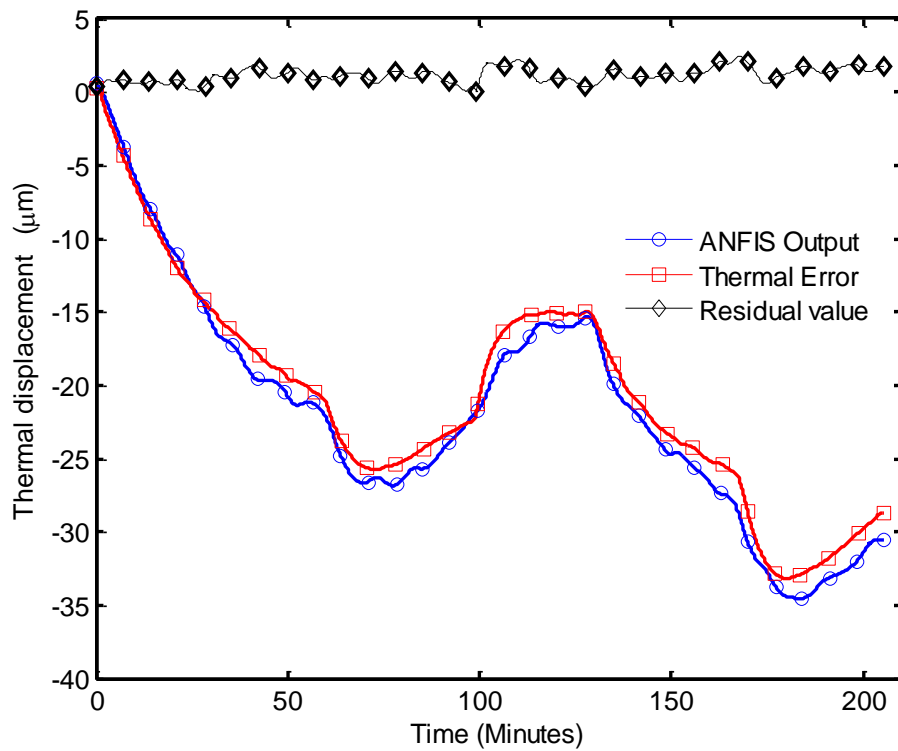


Figure 5-7: ANFIS-FCM model output vs the actual thermal response.

The prediction of the ANFIS-FCM model with four selected key temperature points can significantly reduce the thermal error from an independent test under different conditions of varying rotational spindle speeds and dwells on the machine tool. To emphasise the importance of correctly finding the optimal sensor locations, one of the virtual sensors was arbitrarily moved from the location determined by this method to another location that could have been selected intuitively, i.e. with some engineering justification. The model was retrained with this new sensor location. By changing just one temperature point from the key temperature points gives unsatisfactory prediction ability (residual value  $\pm 9 \mu\text{m}$ ), which implies that the proposed methods (Grey model and FCM) are a valid and important combination to build an accurate model.

In the following section, a number of experimental tests were carried out throughout different time durations, different ambient temperatures and different spindle rotation speeds in order to validate the robustness of the modelling method. Additionally, different types of ANFIS model will be discussed and compared.

### 5.3 Robustness of the Model to Machining Parameters

The machine tool is subjected to continuously changing operation conditions. It is rarely maintained at steady state and the heat generated internally will vary significantly as the spindle rotation speed, axis feedrate, etc. is changed. When this is combined with the effect of ambient changes, the result is the complex thermal behaviour of the machine. Five NCDTs are used to measure the displacement of a precision test bar, representing the tool, in the X, Y and Z axes. The configuration was shown in [Figure 4-5](#) (Machine B).

In this work, a thermal model was created for Machine B using the model described in section [5.2](#). A variety of heating and cooling tests were then carried out in different ambient conditions and different spindle speeds of the VMC (see [Table 5-3](#)). Brief appraisal of the methodology shows the variation considered in this study. Comparing Test I and Test VI shows that a higher spindle rotation speed causes a larger thermal error for the same time duration. Whereas comparing Test II with Test III and Test V with Test VI, it can be seen that the same spindle rotation speed, and the same time duration, gave rise to different thermal error. This was due to change of the ambient conditions and hysteresis effect. More detail of these differences can be observed by examining a selected temperature sensor on the spindle

carrier (T11); Figure 5-8 shows different initial conditions of the machine and Figure 5-9 shows the different magnitude of temperature changes in different tests.

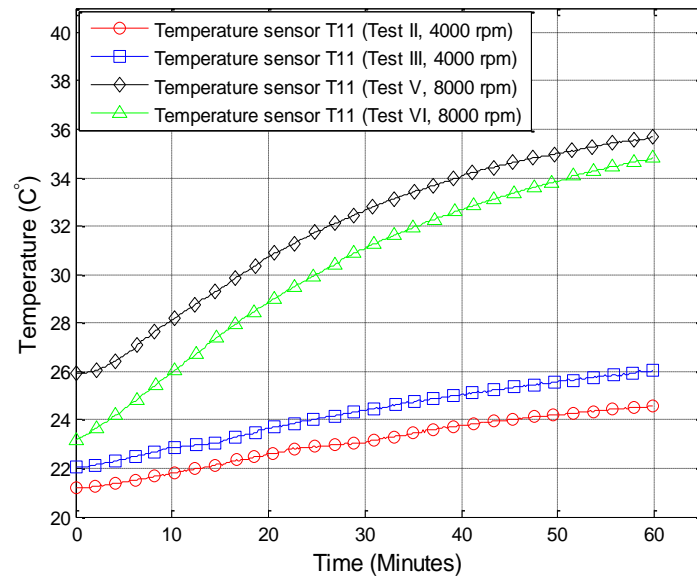


Figure 5-8: Absolute temperature of the selected sensor in different tests.

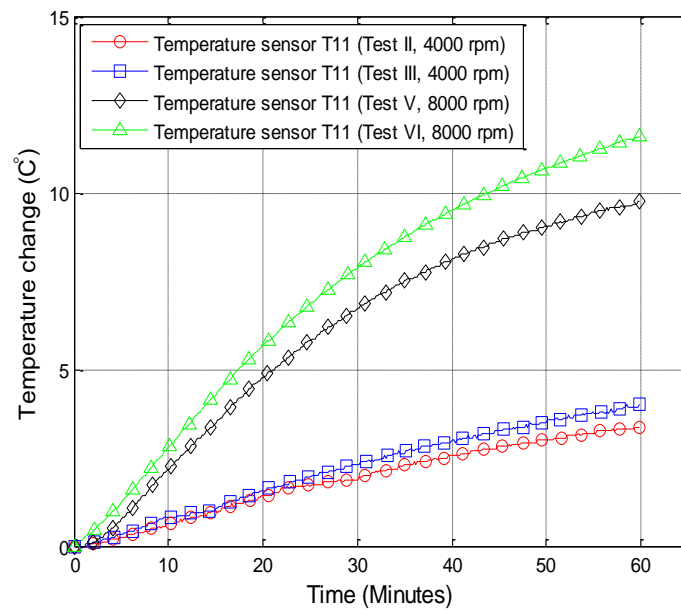


Figure 5-9: Magnitude of temperature changes in different tests.

Table 5-3: The various heating and cooling tests

Spindle speed	Test description	Total Time (hours)	Maximum error	Test name
			Y-direction	
4000 rpm	1 hour heating/1 hour cooling	2 h	25 $\mu\text{m}$	Test I
	3 hours heating/2 hours cooling	5 h	35 $\mu\text{m}$	Test II
	3 hours heating/2 hours cooling	5 h	40 $\mu\text{m}$	Test III
	2 hours heating/1 hour cooling/2 hours heating/3 hours cooling	8 h	39 $\mu\text{m}$	Test IV
8000 rpm	1 hour heating/1 hour cooling	2 h	64 $\mu\text{m}$	Test V
	1 hour heating/1 hour cooling	2 h	79 $\mu\text{m}$	Test VI

An example of heating and cooling test is illustrated as follows: the vertical milling machine was examined by running at its highest spindle speed of 8000 rpm for one hour to excite the largest thermal behaviour. The temperature sensors at the selected points on the machine tool and the thermal displacement of the spindle were measured simultaneously; the thermal displacement of the vertical milling machine is shown in Figure 5-10. The maximum displacement of the X-axis is 3  $\mu\text{m}$ , the Y-axis is 79  $\mu\text{m}$  and the Z-axis is 22  $\mu\text{m}$ . The X-axis thermal displacement is much smaller than that of the Y-axis and the Z-axis due to the mechanical symmetry of the machine and therefore is not investigated further in this work; only the Y-axis and Z-axis errors are considered.

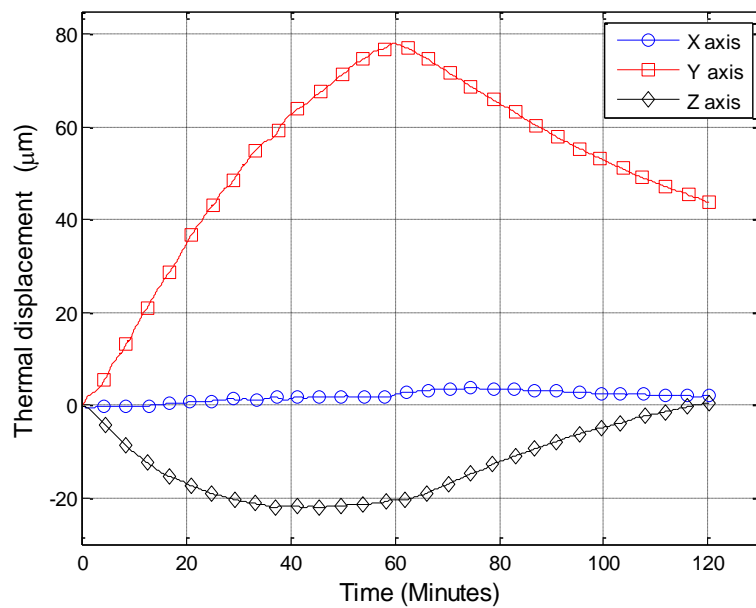


Figure 5-10: Thermal response of the spindle (spindle speed 8000 rpm)

The selection of temperature variables is a key factor to the accuracy of the thermal error model, which will be adversely affected if there is insufficient coverage of the temperature distribution. At the same time, the calibration/training time and the relative cost of the system will increase if the number of input variables is large. Therefore, the location of suitable temperature sensors should be determined before the modelling process.

By applying the Grey model on the experimental data from Test VI, the influence coefficients can be obtained. Next, the influence weightings are clustered to five clusters by using fuzzy c-means clustering analysis (see examples in [Table 4-5](#) and [Table 5-4](#)). Afterward, one sensor from each cluster is selected according to its influence weight with the thermal displacement to represent the temperature sensors of the same category. In this case they are T05, T11, T40, T65 and T75. These temperature sensors are located on the column, spindle carrier (Strip 1, and Strip 2), spindle boss, and ambient near the spindle, respectively. The whole block diagram of the proposed system is shown in [Figure 3-1](#), where variables T1 to TN represent the temperature data captured from the temperature sensors, and the thermal response obtained from NCDTs.

Table 5-4: The clustering result.

Group 1	T18- T23, T33-T53, T72
Group 2	T24-T32, T54-T61
Group 3	T8-T17, T62, T63
Group 4	T5, T4, T68, T69, T76
Group 5	T1-T3, T6, T7, T64-T67, T70, T71, T73-T75

### 5.3.1 ANFIS Models Design

One of the main concerns with designing a thermal error compensation model using ANFIS, or any other self-learning algorithm, is whether the training data that was measured at one particular operating condition of the CNC machine tool would be sufficient to train the model fully for other operational conditions. In other words, is the measured data sufficient for the model to be applicable for all operating conditions?

Ideally, an ANFIS model is trained by a training set that includes many training pairs collected from all likely conditions. However, the cost of machine downtime to capture the training data is a significant concern, because the impact on productivity can have a high penalty. For this reason, reducing the number of training pairs required is very attractive.

Test IV was considered to validate the method of reducing the number of training cycles. Measurements of thermal error and corresponding temperatures were recorded while the machine was run through a range of duty cycle as follows: It was allowed to run at spindle speed 4000 rpm for 120 minutes, and then paused for 60 minutes before running for another 120 minutes; and then stopped for 180 minutes. Hence, the data obtained from this test is divided into three parts which were training, checking, and testing dataset. The checking dataset was used for over-fitting model validation, while the testing dataset was used to verify the accuracy and the effectiveness of the trained model.

Five temperature sensors from section 4.5 were used as input variables to the models and the thermal displacement in the Y-direction was chosen as a target variable. The Gaussian functions are used to describe the membership degree of these inputs, due to their advantages of being smooth and non-zero at each point (see section 5.2). After setting the initial parameter values in the ANFIS models, the input membership functions were adjusted using a hybrid learning scheme.

Extensive simulations were conducted to determine the optimum structure of the FIS models through various experiments. The optimal number of MFs was determined by assigning different numbers of MFs for the ANFIS-Grid model, and different values to the number of clusters ( $n_c$ ) for the ANFIS-FCM model, respectively. Too few MFs will not allow an ANFIS model to be mapped well. However, too many MFs will increase the difficulty of training and will lead to over-fitting or memorising undesirable inputs such as noise. The prediction errors were measured separately for each model using the root mean square error (RMSE) index with the testing dataset. An example of selecting the optimum structure for the ANFIS-FCM model is presented as follows:

In this modelling method, the optimum size of the FIS model was determined, and the results are shown in Table 5-5. Different numbers of epochs were selected for each model because the training process only needs to be carried out until the errors converge. As can be seen in Table 5-5, it cannot simply be stated that better results will be obtained with more clusters. It was found that the FIS model with three ( $n_c=4$ ) clusters exhibited the lowest RMSE value (1.7) for the testing dataset. Consequently, this FIS model with 3 rules was considered to be the optimal. The corresponding rules of the optimum model are provided in Table 5-6.

Similarly, the optimum FIS model for ANFIS-Grid model was determined by arbitrarily varying the number of MFs from 2 to 4. The FIS model with three MFs per input (243 rules) was found to be the optimum.

Table 5-5: Performance of ANFIS-FCM models with various numbers of  $n_c$

Models	Number of clusters ( $n_c$ )	Convergence epochs	RMSE of testing dataset
Model-1	2	200	2.3
Model-2	3	200	1.8
Model-3	4	100	1.7
Model-4	5	300	2.1
Model-5	6	200	5.6

Table 5-6: Linguistic rules

Linguistic rules
1. If (T05 is T05cluster1) and (T11 is T11cluster1) and (T40 is T40cluster1) and (T65 is T65cluster1) and (T75 is T75cluster1) then (out1 is out1cluster1)
2. If (T05 is T05cluster2) and (T11 is T11cluster2) and (T40 is T40cluster2) and (T65 is T65cluster2) and (T75 is T75cluster2) then (out1 is out1cluster2)
3. If (T05 is T05cluster3) and (T11 is T11cluster3) and (T40 is T40cluster3) and (T65 is T65cluster3) and (T75 is T75cluster3) then (out1 is out1cluster3)

### 5.3.2 Results and Discussion

In this section, the aim is to use the structure of the ANFIS models described in the previous section to derive a thermal error compensation system. With the purpose of evaluating the prediction performance of the models generated using dataset Test IV, the remaining datasets Test I, Test II, Test III, Test V, and Test VI were used to run the models. The experimental tests were carried out throughout different time durations, different ambient temperatures and different spindle rotation speeds in order to validate the robustness of the modelling method. The performance of the models used in this study were computed using four performance criteria, including root mean square error (RMSE), Nash–Sutcliffe Efficiency coefficient (NSE), correlation coefficient (R) and also the residual value.

#### 5.3.2.1 Same Spindle Speed under Different Operation Conditions

The prediction models established using the dataset from Test IV are used to forecast the thermal error of Test I, Test II, and Test III, respectively. In all experiments, the machine was

examined by running the spindle at a speed of 4000 rpm, but the duration and ambient temperature is different between each test and different from the training data, as illustrated in Table 5-3. This is representative of a machine that manufactures similar parts, but in varying factory conditions. This is would be the case, for example, of a model trained in the summer, but tested in winter, or day vs night. The temperature sensors at the selected points on the machine tool and the thermal displacement of the test bar are measured simultaneously.

Predictive results for the three tests using ANFIS-Grid model and ANFIS-FCM model are shown in Figure 5-11, Figure 5-12, and Figure 5-13. Results show that these two models are competitive. The performance of each of the two thermal prediction models is presented in Table 5-7. They both can predict the new observations and reduce the residual value to less than  $\pm 5 \mu\text{m}$  for each test. It is clear that the ANFIS-FCM model has a smaller RMSE, residual value and higher correlation coefficient than the ANFIS-Grid model. It is also better able to cope during the cool-down phase; a time during which on-machine probing is likely to be taking place.

Table 5-7: Performance calculation of the used models

Test name	Model	Number of rules	Performance indices			
			R	RMSE	NSE	Residual
Test I	ANFIS-Grid model	243	0.96	1.53	0.92	$\pm 3 \mu\text{m}$
	ANFIS-FCM model	3	0.99	1.23	0.94	$\pm 2 \mu\text{m}$
Test II	ANFIS-Grid model	243	0.99	2.72	0.96	$\pm 4 \mu\text{m}$
	ANFIS-FCM model	3	0.99	0.57	0.99	$\pm 2 \mu\text{m}$
Test III	ANFIS-Grid model	243	0.98	2.78	0.95	$\pm 5 \mu\text{m}$
	ANFIS-FCM model	3	0.99	1.06	0.98	$\pm 2 \mu\text{m}$

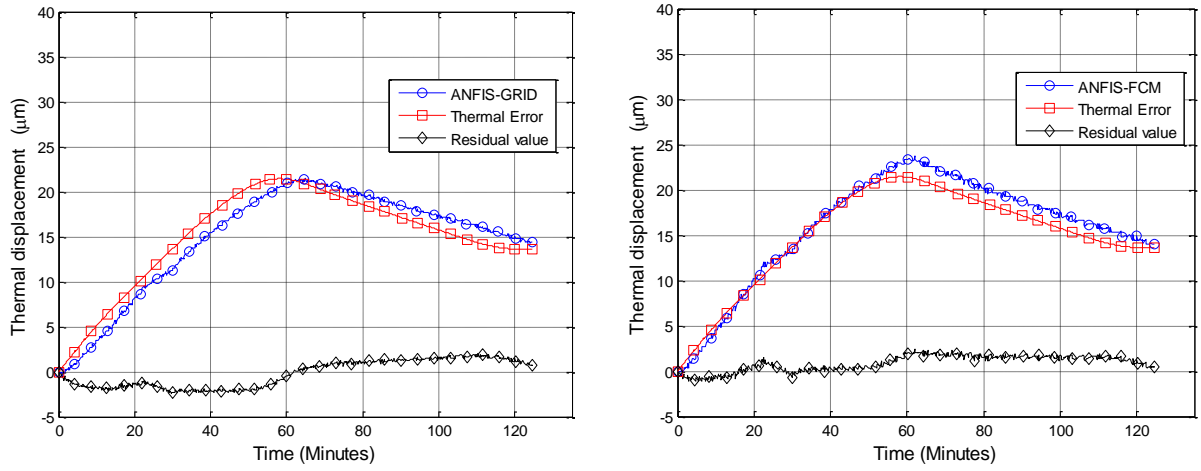


Figure 5-11: (a) ANFIS-Grid model output vs the actual thermal response. (b) ANFIS-FCM model output vs the actual thermal response. (Two hours, Test I).

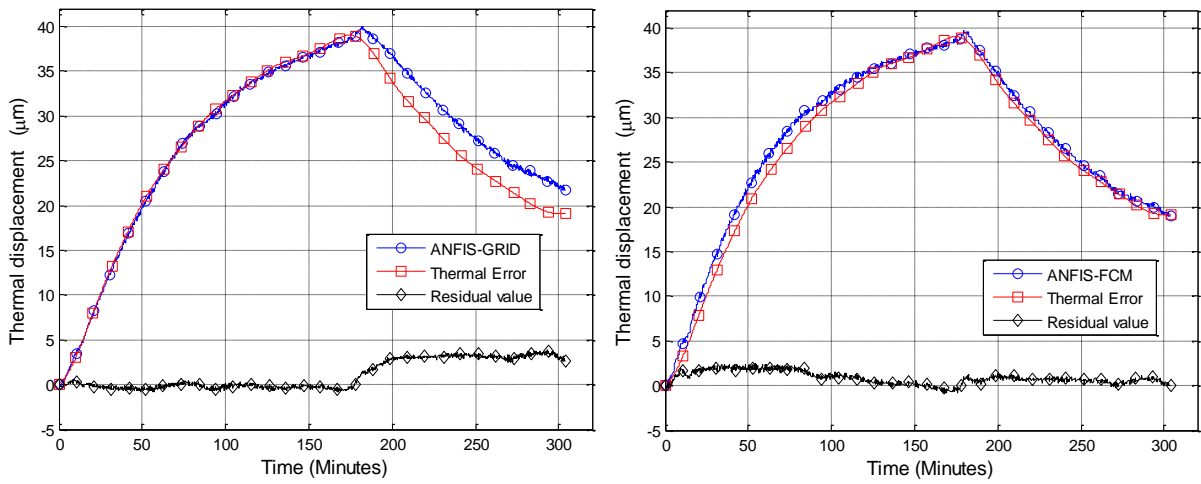


Figure 5-12: (a) ANFIS-Grid model output vs the actual thermal response. (b) ANFIS-FCM model output vs the actual thermal response. (Five hours, Test II).

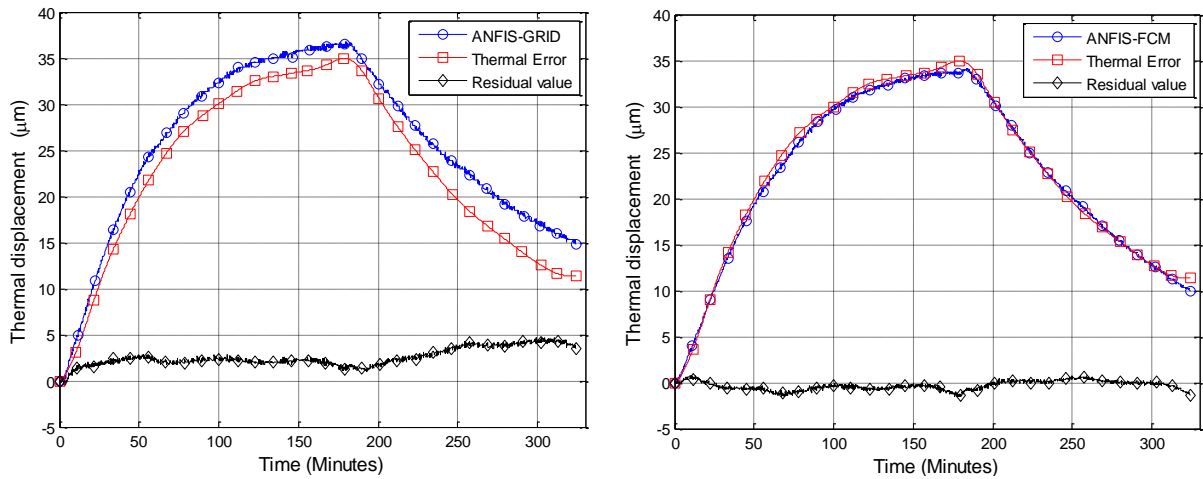


Figure 5-13: (a) ANFIS-Grid model output vs the actual thermal response. (b) ANFIS-FCM model vs the actual thermal response. (Five hours, Test III).

### 5.3.2.2 Different Spindle Speed under Different Operation Conditions

The prediction models established using the dataset from Test IV were further tested to represent a machine that has different manufacturing parameters, also in varying factory conditions. The machine was run at its highest spindle speed of 8000 rpm for one hour to excite more thermal response than during the training data, and then paused for another hour for cooling (see Test V and Test VI). Predictive results using the ANFIS-Grid model and ANFIS-FCM model are shown in Figure 5-14 and Figure 5-15. The evaluation criteria values are provided in Table 5-8. The residual error obtained using the ANFIS-FCM model was again better than the ANFIS-Grid model. In addition, the ANFIS-FCM model has a lower RMSE and slightly higher correlation coefficient and NSE than the ANFIS-Grid model. This indicates that the ANFIS-FCM model is a good modelling choice for predicting the thermal error of the machine tools.

Table 5-8: Performance calculation of the used models

Test name	Model	Number of rules	Performance indices			
			R	RMSE	NSE	Residual
Test V	ANFIS-Grid model	243	0.97	3.98	0.95	$\pm 8 \mu\text{m}$
	ANFIS-FCM model	3	0.99	2.78	0.97	$\pm 4 \mu\text{m}$
Test VI	ANFIS-Grid model	243	0.98	3.88	0.95	$\pm 7 \mu\text{m}$
	ANFIS-FCM model	3	0.99	2.78	0.97	$\pm 5 \mu\text{m}$

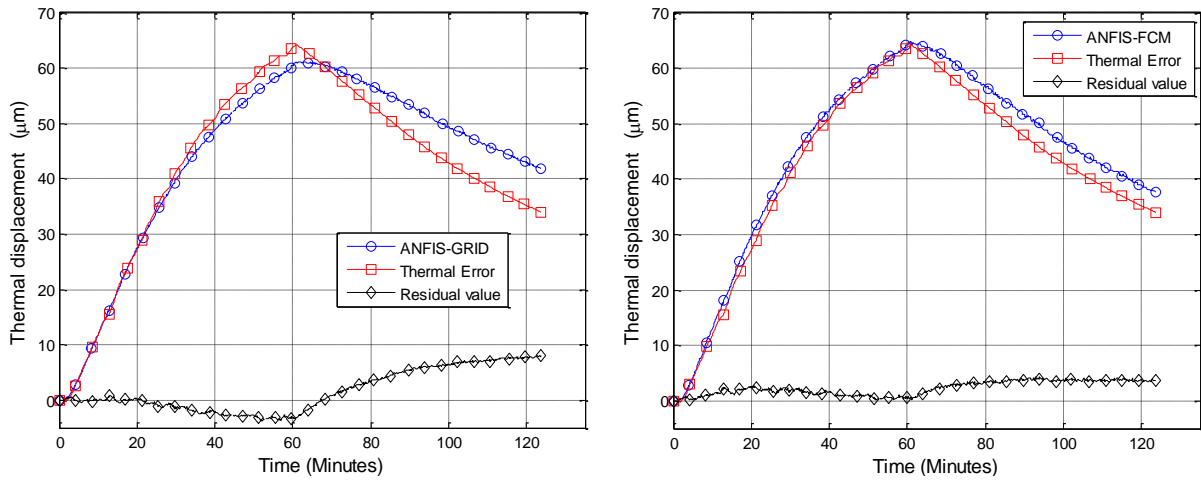


Figure 5-14: (a) ANFIS-Grid model output vs the actual thermal response. (b) ANFIS-FCM model output vs the actual thermal response. (Five hours, Test V).

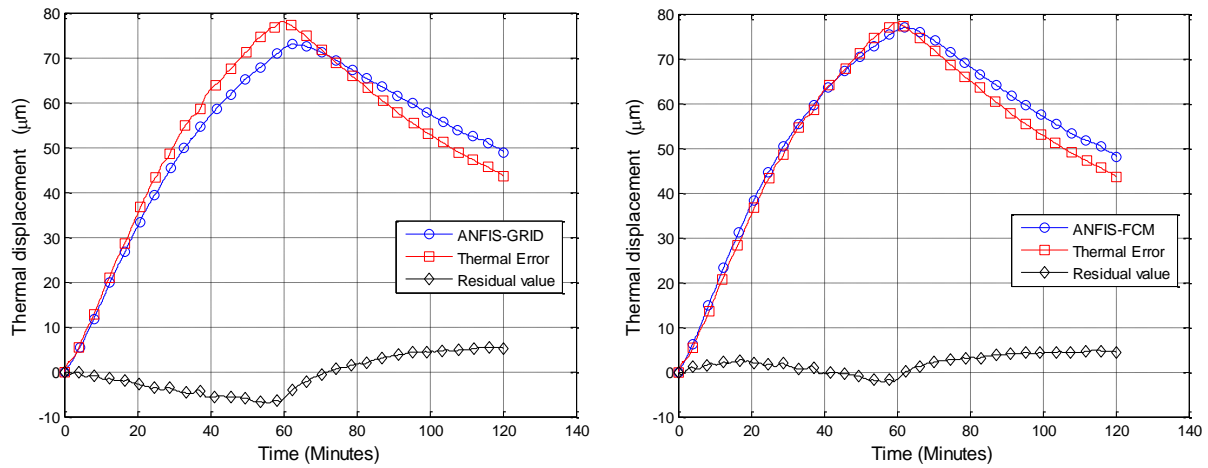


Figure 5-15: (a) ANFIS-Grid model output vs the actual thermal response. (b) ANFIS-FCM model output vs the actual thermal response. (Five hours, Test VI).

In this section, a single training test was validated with a variety of heating and cooling tests under different ambient conditions and different spindle speeds of the VMC (see [Table 5-3](#)). According to the results in the work, the proposed ANFIS model can predict the new observations and reduce the residual value to less than  $\pm 5 \mu\text{m}$  for all tests. This shows that as expected the spindle motor generates different amounts of heat at different speeds. Nevertheless, monitoring the effect of different speeds using temperature sensors, rather than using the programmed value, still yields very good results.

In this piece of work, only temperature sensors are used as inputs to the model. This is consistent with the approach from a large number of researchers. This philosophy has some merit, since it ensures that the model is driven by changes in temperature profile irrespective

of the heat source. However, applying some prior knowledge in designing self-learning algorithms can yield improved results. In this research work, fusion of other sensor types and machine control values here also considered.

In the following section, to improve the accuracy of the predicted model, and to minimise the effects of thermal hysteresis, additional feedback information is supplied by FBG sensors.

## 5.4 Fusion of Temperature and Distortion Measurement

This work develops an error compensation model for the gantry type 5-axis machine tool (Machine C). The machine operates in a non-temperature controlled environment. Changes in temperature cause the machine to change shape and result in a loss of accuracy. In the initial work on this machine, only temperature sensors were used as inputs to the model. Temperature sensors described in section 4.6 were used as input to the model, and the thermal error in the Z-direction was used as a target variable. The proposed ANFIS model was used to predict the thermal response of the machine as shown in Figure 5-16. Although, the ANFIS model based on temperature measurement works well in the previous sections, the result is not as good as demanded in the case of Machine C (the maximum residual value is approximately  $\pm 30 \mu\text{m}$ ). The ANFIS model established by only temperature sensors has high residual value due to complexity of the machine thermal behaviour, as a result of bigger volumes, and longer strokes, which have to be considered. It was anticipated that further improvement in accuracy could be achieved by including strain information as part of the training data. Figure 5-17 shows the output result of the simulation; the maximum residual value is approximately  $\pm 10 \mu\text{m}$ . Therefore, in the next section, temperature measurement at key locations will be supplemented by direct distortion measurement at accessible locations.

The modelling approach mentioned in this section is a preliminary work with a scope to be extended in the next sections by considering a variety of modelling methods such as modular approach.

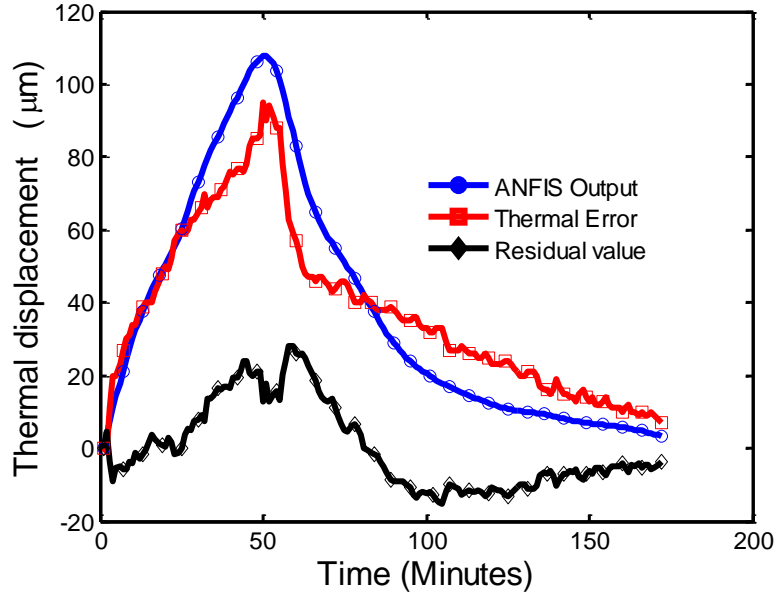


Figure 5-16: ANFIS model output vs the actual thermal response (only temperature).

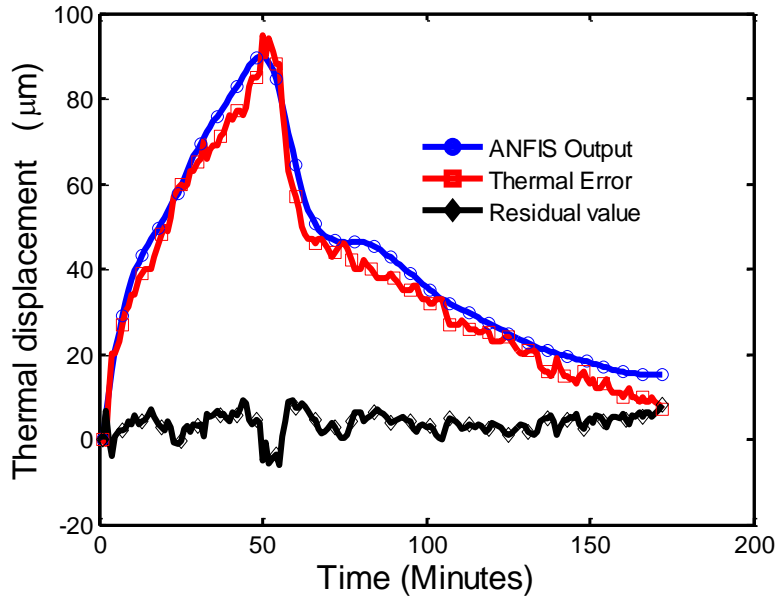


Figure 5-17: ANFIS model output vs the actual thermal response (temperature and strain).

A new prediction model “Grey Neural Network Model with Convolution Integral (GNNMCI (1, N))” is proposed, which makes full use of the similarities and complementarity between Grey models and artificial neural networks to overcome the disadvantage of applying either a Grey model or an artificial neural network individually. A particle swarm optimisation algorithm is also employed to optimise the Grey neural network. As discussed in section 4.6, different physical inputs will be applied to the proposed model. This is because different physical inputs (temperature and strain) have different correlation efficiency and

their effective and cooperative fusion is expected to produce a better prediction results. The architecture of the GNNMCI (1, N) is presented in Appendix A.

The optimal sensor locations were selected based on work presented in section 4.4. The thermal compensation model is designed and simulated in the MATLAB environment. The integrated model was designed as follows:

Step 1: A 1-AGO (first-order Accumulated Generating Operation) is applied to the raw data to increase the linear characteristics and reduce the randomness from the measuring samples.

Step 2: The GNNMCI (1, N) model is trained with a PSO algorithm as discussed in Appendix A.

Step 3: An IAGO (Inverse Accumulated Generating Operation) is performed to calculate the thermal error and generate the final compensation value.

To demonstrate the modelling of thermal error using GNNMCI (1, N) model, five variables (temperature and strain) were selected based on their influence coefficient value using the Grey model (see section 4.5). The selected sensors were used as input variables for the GNNMCI (1, N) model and the machine movement were used as a target variable.

In this work, two compensation procedures were used to predict the thermal errors. The first method was to obtain the GNNMCI (1, N) model at the first stage of the test regime, and then to use this model to predict the machine movement during the remainder of the same test or for other regimes. The other was to obtain the model parameters during a short test, and then predict the thermal displacement for all other tests. The advantage of using a short test to calibrate the model is that it reduces non-productive downtime of the machine. The potential disadvantage is the lack accuracy of the model due to low training experience.

In order to optimise the GNNMCI (1, N) parameters (weights), the experimental datasets were divided into training set (and afterward direct validation), validation set (cross validation), and testing set. An example of training dataset from a short test of five samples is illustrated in Table 5-9; four FBG sensors and one temperature sensor are used as inputs, and Z-axis displacement as output.

Table 5-9: The training data from first 5 readings.

Number of sample	FBG-1	FBG-2	FBG-3	FBG-4	Temp	Displacement
0	0	0	0	0	0	0
1	-0.0072	0.2091	0.0573	0.086	0.0620	-0.2282
2	-0.0217	0.3173	-0.1719	-0.344	0.1870	-0.5766
3	0.2031	0.2019	0.0143	0.0502	0.3120	-0.8127
4	0.1378	0.4903	-0.2220	0.0215	0.5000	-1.1718

In the PSO algorithm, the number of the particles is set to be 90 whilst the self-confidence factor and the swarm-confidence factor are  $C_1=1.5$  and  $C_2=2$ , respectively. The inertia weight  $\omega$  was taken as a decreasing linear function in iteration index  $k$  from 0.9 to 0.4, which were the same as those suggested by other papers [118, 119] and these values did not depend on the problems. After 100 training epochs, the total error was at an acceptable level. The Grey neural network weights obtained using PSO algorithm are:

weights	$w_{11}$	$w_{21}$	$w_{22}$	$w_{23}$	$w_{24}$	$w_{25}$	$w_{26}$	$w_{27}$
Values	0.1244	0.001	0.8787	1.5390	0.8830	0.1567	0.7005	1.7403
weights	$w_{31}$	$w_{31}$	$w_{32}$	$w_{33}$	$w_{34}$	$w_{35}$	$w_{36}$	$w_{37}$
Values	1.5855	1.5855	1.5855	1.5855	1.5855	1.5855	1.5855	1.5855

Training and validation errors diminish through the initial phase of training stage. The first test was to check whether the model is able to reproduce the training dataset that has been used for training stage (direct validation). Subsequently, cross validation has been applied to check the model validity. When the validation error becomes minimum, the most appropriate model is achieved. The prediction results of the next six values of thermal errors derived by these weights based on this GNNMCI (1, 6) model are listed in Table 5-10.

Table 5-10: The modelling values of thermal errors based on GNNMCI (1, 6) model.

No. of sample	Model inputs (AGO)					GNNMCI(1,6) model ( $\mu\text{m}$ )	Thermal error ( $\mu\text{m}$ )	Residual value ( $\mu\text{m}$ )
	FBG-1	FBG-2	FBG-3	FBG-4	Temp ( $^{\circ}\text{C}$ )			
5	0.4642	0.618	0.1432	0.1361	0.5620	-0.9017	-1.4144	0.5127
6	0.5512	0.8581	-0.0430	-0.0573	0.6870	-1.2606	-1.7823	0.5217
7	0.6165	0.8220	-0.2578	-0.1433	0.8120	-1.5017	-2.0300	0.5283
8	0.5802	1.0528	-0.1934	-0.3081	0.8750	-1.8693	-2.4049	0.5356
9	0.9429	1.4494	-0.0573	-0.1720	1.0000	-2.5568	-2.6566	0.0998
10	0.9211	1.1321	-0.0358	-0.2938	1.1250	-2.7040	-3.0366	0.3326

The final GNNMCI (1, 6) model being trained and validated in this work has been tested by new unseen dataset. The independent variables are shown in Figure 5-18 (a). Simulation results show that the thermal error in the Z direction can be significantly reduced to less than  $\pm 5 \mu\text{m}$  using testing dataset (see Figure 5-18 (b)). Furthermore, this result shows that the PSO algorithm can act as an alternative training algorithm for Grey neural network that can be used for thermal error compensation.

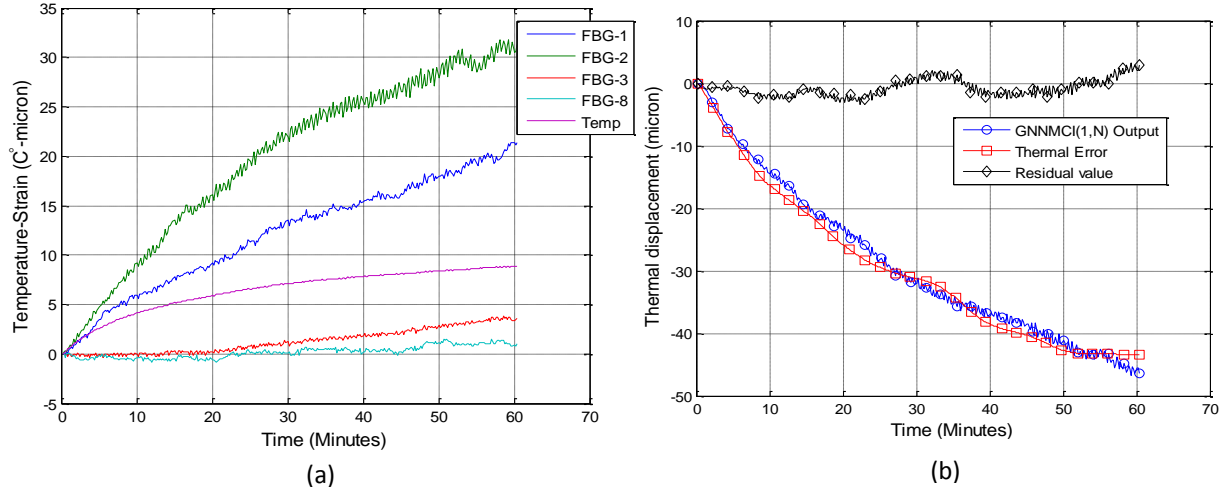


Figure 5-18: (a) Temperature and strain as model inputs. (b) GNNMCI (1, 6) model output vs the actual thermal response.

### 5.4.1 Results and Discussion

Several experiments were conducted on the 5-axis milling machine. The primary motivation of these experiments was to compensate the deformation taking place in the ram of the machine in the Z-axis direction as a result of heat induced by rotation of the C-axis and by motion of the Z-axis. The Z-axis heating test, C-axis heating test, and the combined (helical) movement are considered in this thesis. Detailed procedures and results are as follows:

#### 5.4.1.1 Case 1: Z-axis Heating Test

In this test, the ram reciprocated at a speed of 70 m/min 10 times before dwelling for 10 seconds (to allow stable measurement) to excite the thermal behaviour in the ram. This cycle was repeated for the two hours “heating” cycle. The axes remained stationary for a subsequent two hours cooling cycle. The temperature variation was measured by the temperature sensors and the change in the strain of the ram and crossbeam were measured with FBG sensors. The data is given in Figure 5-19 (a). The heat sources on the ram structure

are friction in the two support bearings of the Z-axis ballscrew, friction in the ball-nut and the power loss of the Z-axis motor. Additionally, there is an effect from change in ambient temperature on the whole structure of the machine. Laser position sensors were used to measure the growth of the ram along the Z-axis direction. It can be seen that the rise in temperature measured by the selected sensors correlates to an error in the Z-axis of more than 100  $\mu\text{m}$ .

The simulation result shows that the GNNMCI (1, 6) model can predict the error accurately and also can track the sudden changes of thermal error precisely (the maximum residual is approximately 16  $\mu\text{m}$ , a 85% improvement see Figure 5-19 (b)), even with such a short training period. Indeed, the greatest loss in model accuracy occurs over one hour after the “heating” cycle. The majority of this thermal error derives from a reaction to ambient changes, for which the model has not been trained. This effect may not be significant in practice since it could be argued that the machine will not be producing parts if the axes are not being used. Nevertheless, this issue will be addressed under further work for those situations where the machining regime excites different parts of the structure during various operations.

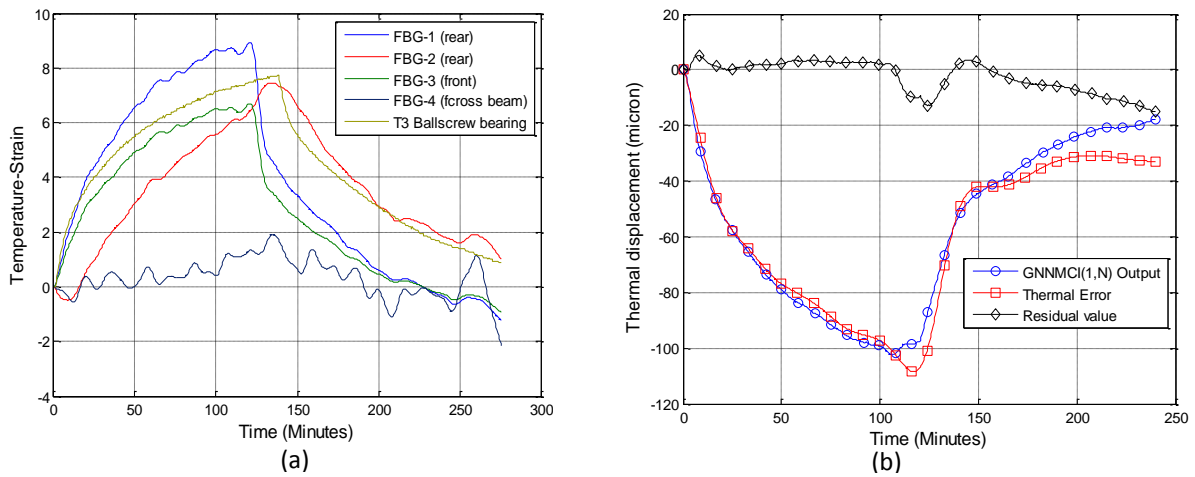


Figure 5-19: (a) Temperature and strain as model inputs. (b) GNNMCI (1, 6) model output vs the actual thermal response.

#### 5.4.1.2 Case 2: C-axis Heating Test

In this test, the C-axis rotated at 2500 rpm ten times before dwelling for 10 seconds (for measurement) to excite the thermal behaviour in the machine ram. This cycle is repeated for the two hours “heating” cycle. The axes remain stationary for a subsequent two hours cooling

cycle. Data collected from temperature sensors and FBG sensors are shown in Figure 5-20 (a). The heat sources in this test are the friction in the C-axis bearings and loss from the motor located inside the ram structure (near the location of temperature sensor T1). Therefore, T1 is the highest temperature (rising by 7 °C). The maximum value of T2 is lower than (4 °C), and the value of T3 and T4 are the lowest (1 °C) because they are relatively further from the heat source. The Z-axis thermal error was greater than 80  $\mu\text{m}$ .

As with the Z-axis heating test, the model weights were obtained at the first stage of the test regime. Simulation results show that the GNNMCI (1, 6) model can provide a good prediction result. Figure 5-20 (b), presents the comparison between thermal displacements from the actual measured data and the output of the model. It can be seen that the prediction ability of the model is excellent, and that the model shows a reduction from 80  $\mu\text{m}$  to  $\pm 8 \mu\text{m}$ .

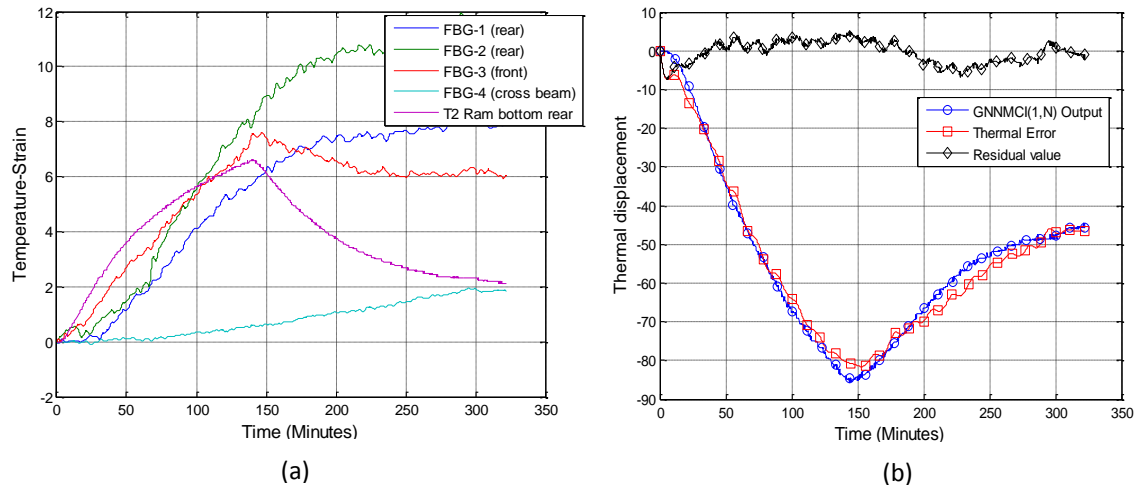


Figure 5-20: (a) Temperature and strain as model inputs. (b) GNNMCI (1, 6) model output vs the actual thermal response.

#### 5.4.1.3 Case 3: Combined Axis (Helical) Test

In this test, the C-axis rotated while the Z-axis was oscillated simultaneously (Helical test). The purpose was to validate the compensation model for the thermal error that was trained from the previous two cases (Case 1, Case 2). This was to demonstrate that the thermal model could be built up in a modular form and so is extensible to the remainder of the structure.

The four hours validation test was again equally divided into two stages of heating and cooling cycles. Figure 5-21 (a) describes the temperature/strain change during the test regime, which induces thermal expansion in the Z-axis direction of approximately 95  $\mu\text{m}$ . The model

weights were obtained from the previous independent C-axis and Z-axis tests. Figure 5-21 (b) shows a reduction in error from  $95\ \mu\text{m}$  to  $\pm 9\ \mu\text{m}$ , with the loss in performance again being prevalent quite some time after the heating part of the cycle. This study validates the modular approach, which means that the combining training data can be superimposed on each other in one model.

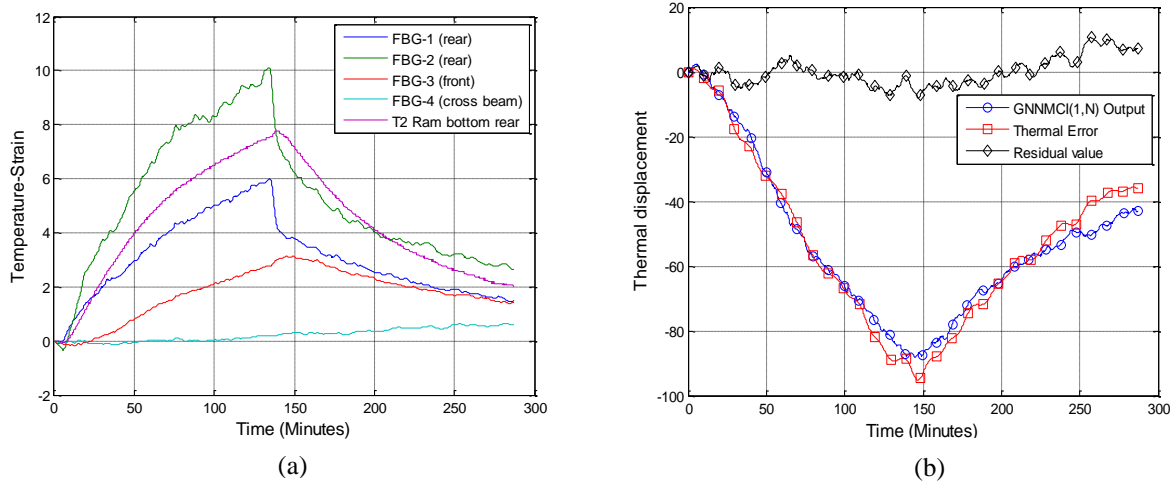


Figure 5-21: (a) Temperature and strain as model inputs. (b) GNNMCI (1, 6) model output vs the actual thermal response.

The experimental results show that the proposed model has an excellent performance in terms of the accuracy of its predictive ability and reduction of machine downtime when compared against traditional and other self-learning techniques.

Consequently, this work develops a simple, less computationally intensive and low-cost approach with a high adaptation rate based on Grey neural model and PSO algorithm to predict the thermal error compensation on CNC machine tools. The results obtained from the proposed model exhibit better performance than conventional ANN model in [50], with far fewer training samples.

This chapter is focused mainly on the spindle unit, which is usually the major heat source, in the next chapter more attention will be paid to environmental temperature variation error and other thermal error sources.

## 5.5 Summary

The principal advantage of this novel technique is to use thermal imaging to assess a machine's thermal behaviour and to build compensation models with different numbers and configurations of sensors. An adaptive neuro-fuzzy inference system with FCM (ANFIS-FCM) has been employed for the prediction of the thermal error in machine tools. The models are built using data obtained from short heating and cooling test, with a wide variety of models being able to be assessed using multiple simulations.

The results on machine indicate that ANFIS-FCM model with four inputs and six rules has the optimal capability to map the input–output data pairs; it can predict thermal displacement under different operational conditions depending on the availability of the empirical data. Perhaps counter-intuitively, the ANFIS model is less well conditioned when additional sensors are included. Minimal effort is then required for practical application of discrete contact sensors that are used for on-line compensation.

The method was further tested by carrying out a number of experimental tests on Machine B. Two types of ANFIS model have been discussed in this work: using grid-partitioning and using fuzzy c-means clustering. Both models were constructed and tested on Machine B. The results from the two sets of validation tests show that both ANFIS-based models, derived from a single heating-and-cooling cycle, can improve the accuracy of the machine tool by over 80% for varying ambient conditions, heating durations and spindle speeds. The ANFIS-FCM produced better results, achieving up to 94% improvement in error with a maximum residual error of  $\pm 4 \mu\text{m}$ . This compares favourably with other compensation methods based upon parametric or self-learning techniques.

In addition to the better absolute accuracy, the ANFIS-FCM has been shown to have the advantage of requiring fewer rules, in this case requiring only three rules as opposed to the 243 found to be optimal for the ANFIS-Grid model. This is a significant benefit, since the latter method is significantly more laborious to construct. Therefore, it can be concluded that the ANFIS-FCM model is a valid and promising alternative for predicting thermal error of machine tools without increasing computation overheads.

Finally, the proposed model was used further to predict the thermal response of the Machine C. The model established by only temperature sensors on this machine has high residual value due to complexity of the thermal behaviour, as a result of bigger volumes, and

longer strokes. The model was improved by fusion of both temperature sensors and direct strain measurement from FBG sensors. Additionally, another model was built up of two component modules. The validation of combined thermal inputs was shown to be as effective as when the individual elements were validated. This is important where changes to the structure are possible, since it means that only that part of the model needs to be retrained. It also means that for greater precision, other structural elements can be conveniently included in the model.

## Chapter 6: Model Validation and Comparison

### 6.1 Introduction

One of the major problems for thermal error modelling is the complex way in which the machine tool distorts due to the environmental change combined with duty cycle effects. It will never reach a true thermal equilibrium condition. For these reasons it was decided to continue the investigation by looking at applying modelling techniques to a machine tool under different conditions; different Environmental Temperature Variation error (ETVE) tests (summer and winter), and more complex duty cycles.

A new concept will be added to the ANFIS modelling by combining ANFIS and Grey system theory in one system. This combination helps to reap the maximum benefit from both systems.

### 6.2 Modelling of ETVE

In this section, an ETVE test was performed on Machine A. This test was conducted to reveal the effects of ambient temperature changes on the machine and to predict the thermal displacement during other performance measurements [3]. In order to obtain the temperature data of the machine tool, a total of 26 temperature sensors were placed on the machine (see section 6.3). Four NCDTs were used to measure the displacement of a test bar (used to represent the tool) while the spindle remained stationary. Three were used to measure displacement of the test bar in each axis direction. A fourth directly monitored displacement of the casting next to the spindle in the Z-axis direction to differentiate expansion of the tool from the machine. A general overview of the experimental setup is shown in [Figure 6-1](#).

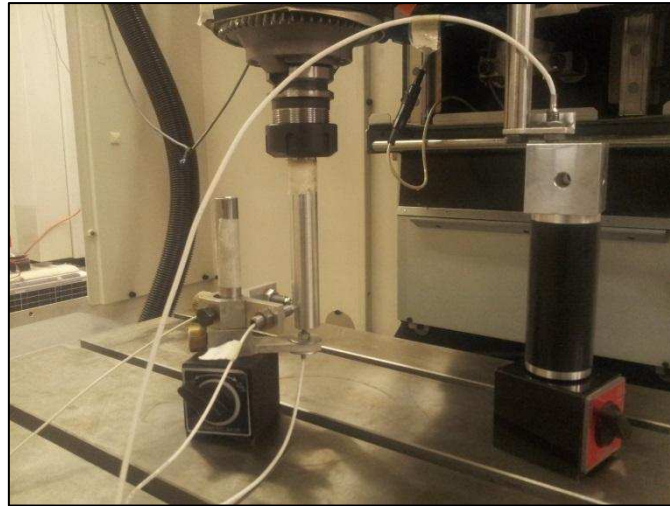


Figure 6-1: A general overview of the experimental setup.

Results of an ETVE test are shown in [Figure 6-2](#). This test was carried out over a five-day period during a three-day holiday, with no significant activity in the workshop, followed by approximately three normal working days (160 hours). This data was sampled once every minute. The environmental temperature conditions for machine shop change due to the day/night cycle, where the temperature fluctuates by about 5 °C throughout the day, with lower temperatures in the morning and higher temperatures in the late afternoon and evening. The strongest response to the ambient change from the machine is in the Z-axis direction. There is a clear relation between the fluctuation in the environmental temperature and the resulting displacement. For example, the anomaly at the beginning of the test can be attributed to a short period (30 minutes) of the workshop door being opened. Externally, the conditions were snowy, which caused a drop in workshop temperature to below 11 °C. The overall movement caused by this phenomenon is 35 µm in the Z-axis and 25 µm in the Y-axis for an overall temperature swing of approximately 9 °C over the 30 minutes. Two similar events can be seen between 120 and 140 hours. The magnitude of the environmental error can be compared to that from two hours spindle-heating test conducted according to ISO 230-3: 2007 which only produced 30 µm of error in the Z-axis.

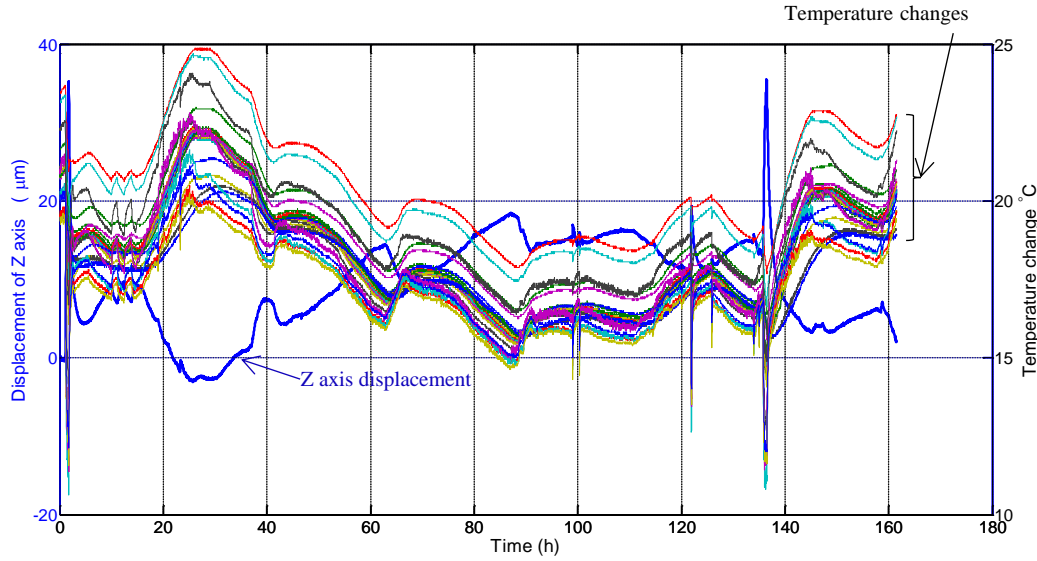


Figure 6-2: Temperature measurements and machine movement due to environment.

### 6.2.1 Grey Model

To demonstrate the modelling of ETVE using the Grey neural network approach, four temperature sensors were selected based on a Grey model. Temperature sensors T1, T2, T5, and T9, which are located on the carrier, column, ambient near spindle, and ambient near the column, were selected according to their influence coefficient value using the Grey model (see section 4.4). They were used as the input variables for the GNNMCI (1, 5) model and the thermal response in Z-direction was used as a target variable.

For this study, a GNNMCI (1, 5) with a structure of 1-1-6-1 was chosen. The details are: layer A has one node, the input time series  $k$ ; layer B has one node; layer C has six nodes, the input variables nodes are from two to five, respectively; T1, T2, T5, and T9 are the input variable data. Layer D has an output variable node, which is the thermal displacement in Z-axis direction. The GNNMCI (1, 5) structure is shown in Appendix A.

Two compensation methods can be used to predict ETVE. The first is an off-line, pre-calibrated method. This means to obtain the GNNMCI (1, 5) model according to the thermal displacement and the temperature change during a short test, and then to use this model to predict the thermal displacement of other processes. The second method is to obtain the GNNMCI (1, N) model at the first stage of the manufacturing process, and then to use this model to predict the machine movement during the rest of the process. This uses additional measurement effort before the process begins.

To apply the first method, another test was carried out for 80 minutes on the same machine during a normal working day. During the experiment, the thermal errors were measured by the NCDTs and the temperature data was measured using the same selected sensors, sampling every ten seconds. The training samples were obtained from the first 5 readings (less than one minute) after the test had been started. All raw data was converted to AGO series, as discussed in section 3.4.1.

After finishing the training of the model, there were two ways to obtain the prediction values: directly obtaining the prediction values from the trained model; or taking out the Grey differential equation parameters from the trained model to the Grey equation and then solving the equation to obtain the prediction values. Although both methods are similar theoretically, a large number of experiments have found that the first method needs less computation. Figure 6-3 shows simulation results for 80 minutes.

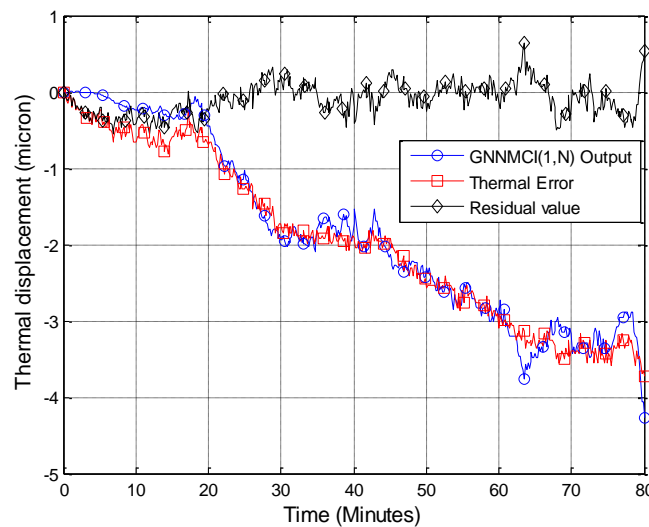


Figure 6-3: Simulation results for 80 minutes.

The process was repeated to create a GNNMCI (1, 5) model for the Y-axis direction. To validate the robustness of these models on non-training data, a normal environmental simulation was run using the temperature data presented in Figure 6-2. The measured and simulated profile results were plotted for the Z-axis and Y-axis. Compared to the measured results, the correlations were 97% for the Z displacement profiles Figure 6-4, and 98% for the Y displacement profiles Figure 6-5. The residual errors were less than  $\pm 10 \mu\text{m}$  for the Z axis and less than  $\pm 6 \mu\text{m}$  for the Y-axis even when considering the rapid changes due to the opened workshop door. Under more predictable conditions, which could be achieved by

better management of the environment,  $\pm 3 \mu\text{m}$  would be achieved in each axis. Thus, the proposed GNNMCI (1, 5) model can predict the normal daily cyclic error accurately and also can track sudden changes of thermal error from a relatively small training sample.

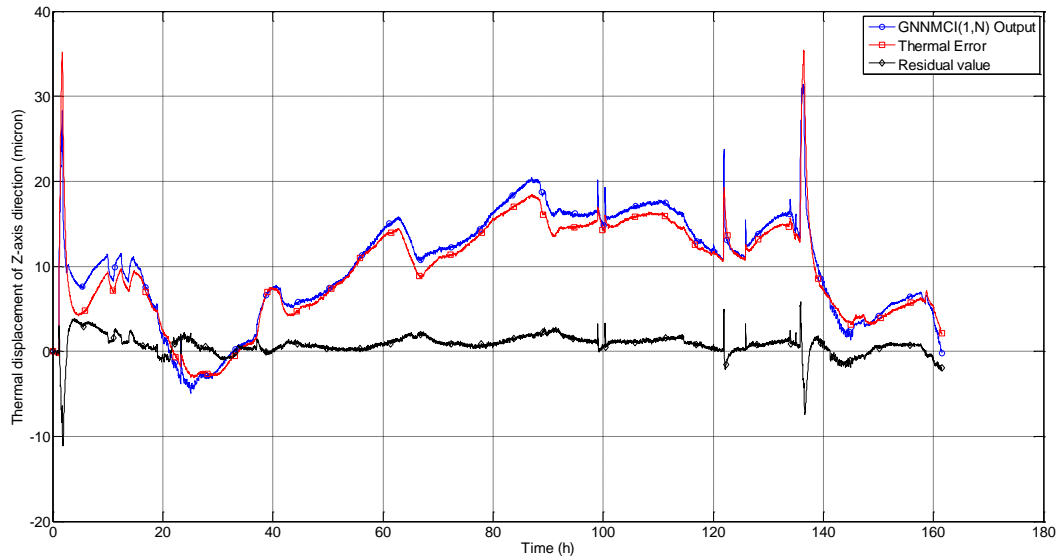


Figure 6-4: Correlation between the measured and simulated Z-axis displacement using GNNMCI model.

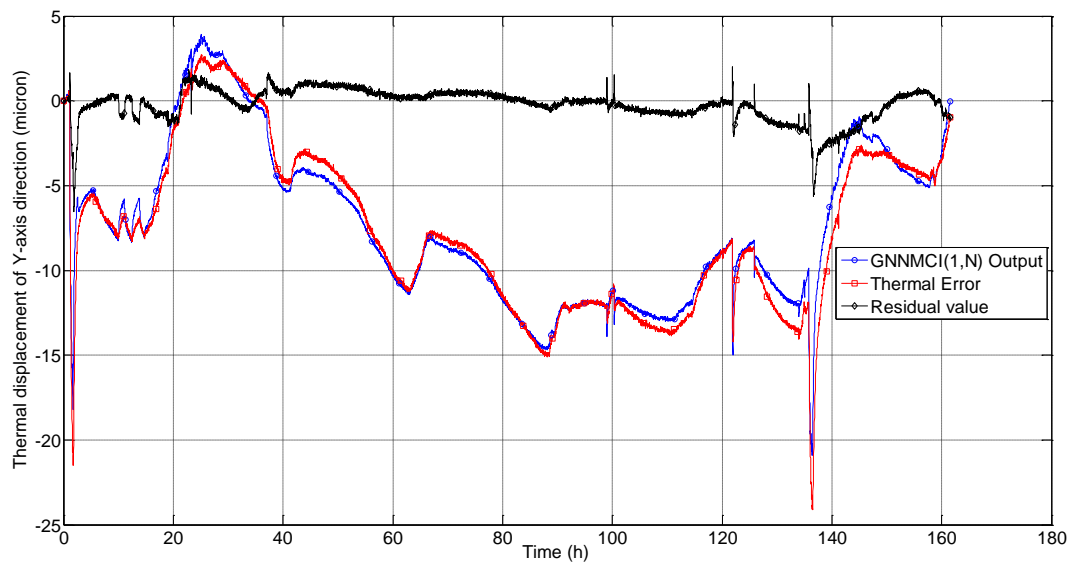


Figure 6-5: Correlation between the measured and simulated Y-axis displacement using GNNMCI model.

### 6.2.2 ANFIS Model

The fast and accurate modelling of thermal errors in machining is an important aspect for the implementation of thermal error compensation. This section presents a novel modelling

approach for thermal error compensation on CNC machine tools. The method combines the adaptive neuro-fuzzy inference system and Grey system theory to predict thermal errors in machining. Instead of following a traditional approach, which utilises original data patterns to construct the ANFIS model, this work proposes to exploit Accumulation Generation Operation (AGO) to simplify the modelling procedures. AGO, a basis of the Grey system theory, is used to uncover a development tendency so that the features and laws of integration hidden in the chaotic raw data can be sufficiently revealed. AGO properties make it easier for the proposed model to design and predict.

To supplement the ANFIS model, the AGO is used to increase the linear characteristics and reduce the randomness from the measuring samples (see section 3.4.1). This simple but effective technique allows the thermal model to be built with a small amount of training data. In short, the proposed model incorporates the AGO method into the ANFIS model to improve its prediction accuracy and robustness with minimal efforts.

To verify the applicability of the proposed model, an example simulating thermal error compensation in previous section is investigated.

Ideally, an ANFIS model would be directly constructed from data patterns that involve all operation conditions. Similar to the previous models, the experimental samples are divided into two separated sets: the training set and the testing set. The training set is used to calibrate/train the model using a FCM and ANFIS algorithm, and the testing set is used to verify the accuracy and the effectiveness of the trained model. The AGO was used to transform these samples to another domain as discussed previously. The five samples were chosen at the beginning of the test, four temperature sensors are used as inputs and the Z-axis displacement as output.

Hence, four temperature sensors were selected as input for the model and the thermal response in Z-direction was chosen as a target variable. After setting the initial parameter values in the ANFIS model, the input membership functions are adjusted using a hybrid learning scheme. In Figure 6-6, an example of MFs for one input before and after learning is presented. Figure 6-6 shows that MFs being initialised with FCM change slightly even after training. It reveals the fact that the initial MFs are quite adaptive to the characteristics of the model and thus speed up the convergence.

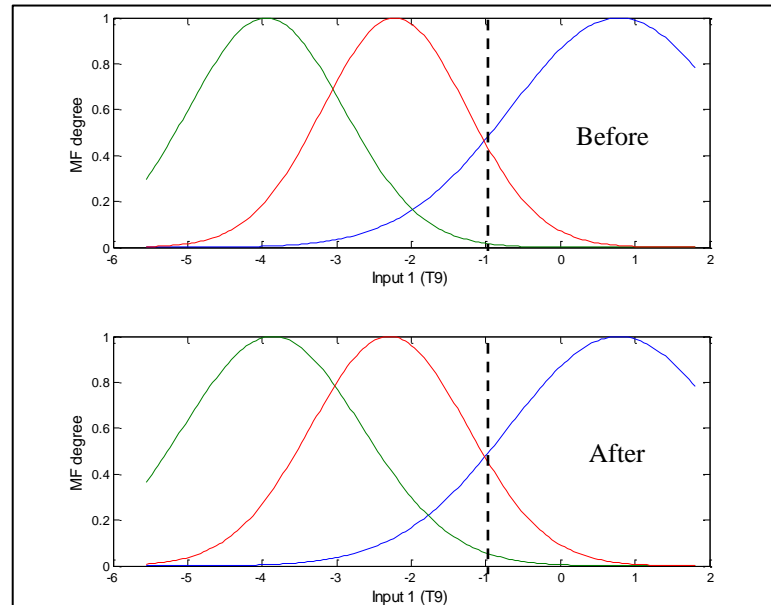


Figure 6-6: Membership functions obtained through ANFIS and FCM clustering.

Next, different ANFIS models were evaluated using Root Mean Square error (RMSE), in order to measure the deviation between the measured and predicted values. It is observed that after 5 epochs were used, the performance does not improve any further. Before generating the final model, it is essential to obtain the optimum number of clusters. It was found that the ANFIS model with 3 clusters exhibited the lowest error RMSE=2.4 for testing dataset.

After finishing the clustering and training process, the proposed ANFIS model can predict the thermal error from a relatively small training sample as GNNMCI model (less than  $\pm 10 \mu\text{m}$  for the Z-axis). The correlation coefficient is 99% and the maximum residual value is approximately  $\pm 6 \mu\text{m}$  (see Figure 6-7).

From these results, it can be observed that the model has promising values during the testing stage. Thus, the proposed model is a powerful and precise predictor of the thermal errors of the machine tool but requiring less training data and converging epochs.

Consequently, this section develops a simple, less computationally intensive and low-cost approach with a high adaptation rate based on ANFIS model and Grey system theory to predict the thermal error compensation on CNC machine tools. The results obtained from the proposed model exhibit slightly better performance than GNNMCI model in the previous section.

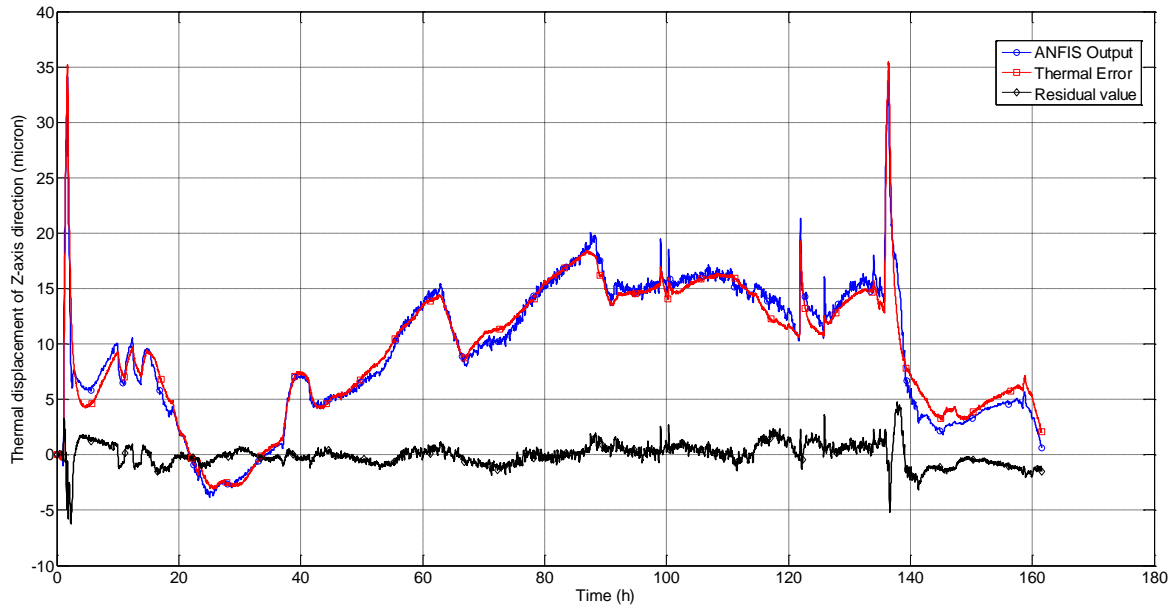


Figure 6-7: Correlation between the measured and simulated Z-axis displacement using the ANFIS model.

### 6.2.2.1 Different Ambient Conditions

In the previous section, the machine was tested as a case-study in winter. Here, the same machine is examined in summer. To further validate the robustness of this modelling methodology, another three-day test was carried out to observe the machine behaviour in the summer season. The overall movement caused by this test is 20  $\mu\text{m}$  in the Z-axis and 15  $\mu\text{m}$  in the Y-axis for an overall temperature swing of approximately 8  $^{\circ}\text{C}$  over the test. Because of different temperature swing values between summer and winter test, the ANFIS model needs to be optimised (see Figure 6-8). One solution to this problem is to recalibrate the model using a new dataset (summer test). This would demonstrate that the thermal model could be built up in a modular form and so is extensible to the remainder of other operation conditions. Figure 6-9 shows simulation results for three-day summer test.

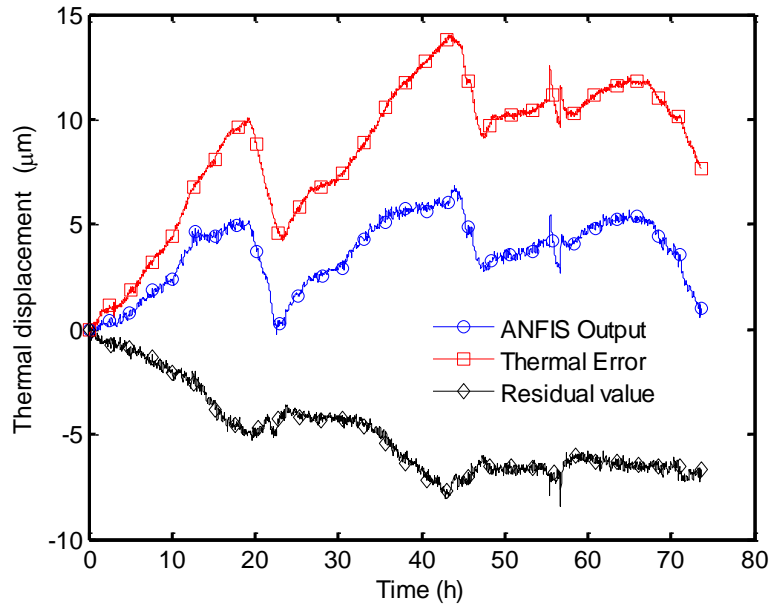


Figure 6-8: Three-day summer test (before optimisation).

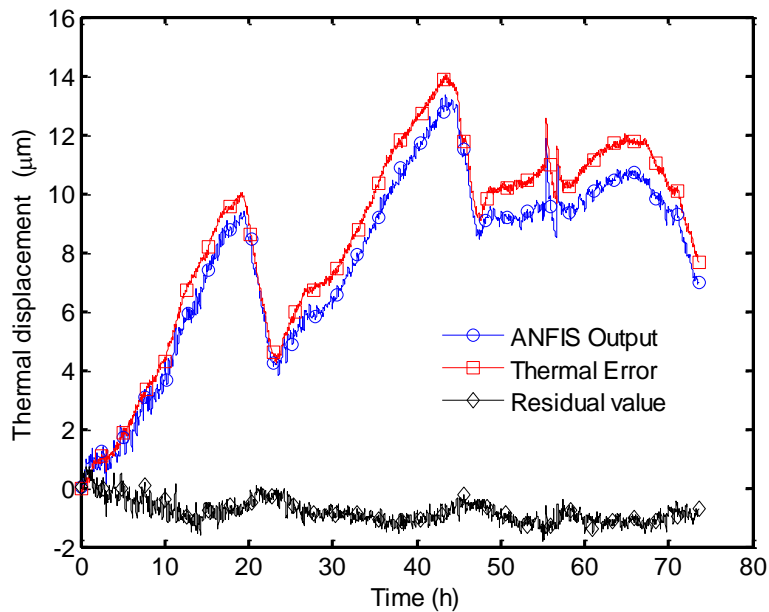


Figure 6-9: Three-day summer test (after optimisation).

As mentioned previously in section 6.2.1, the second method of modelling is to obtain the model at the first stage of the manufacturing process, and then to use this model to predict the machine movement during the rest of the process.

To demonstrate this method, another ETVE test was carried out on the same machine (Machine A) for four days. During the experiment, the room temperature was changing through as wide range as possible. This is achieved by means of using a room heater to warm-up the machine structure and room air conditioning for cooling-down the machine

structure (see Figure 6-10 and Figure 6-11). Figure 6-12 shows machine movement and temperature changes in one plot.

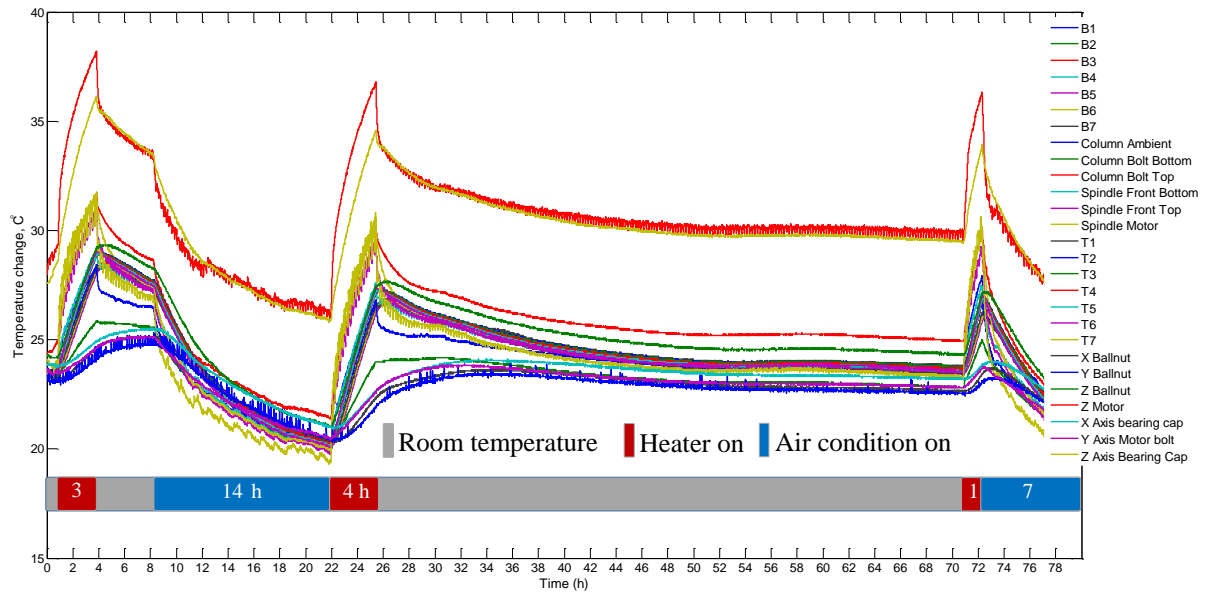


Figure 6-10: Temperature measurements due to environmental changes.

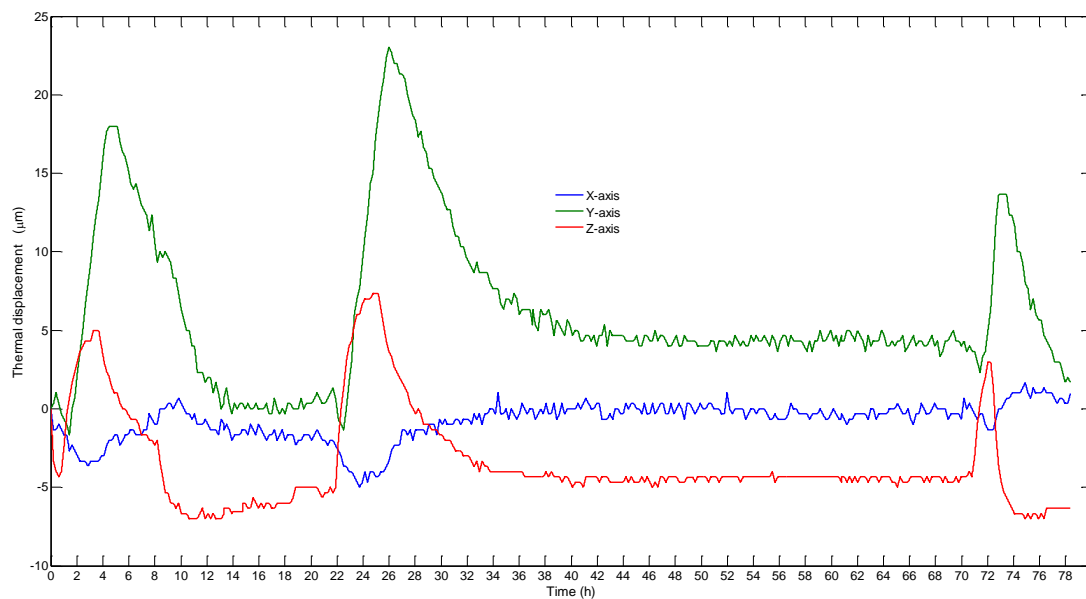


Figure 6-11: Machine movement due to environmental changes.

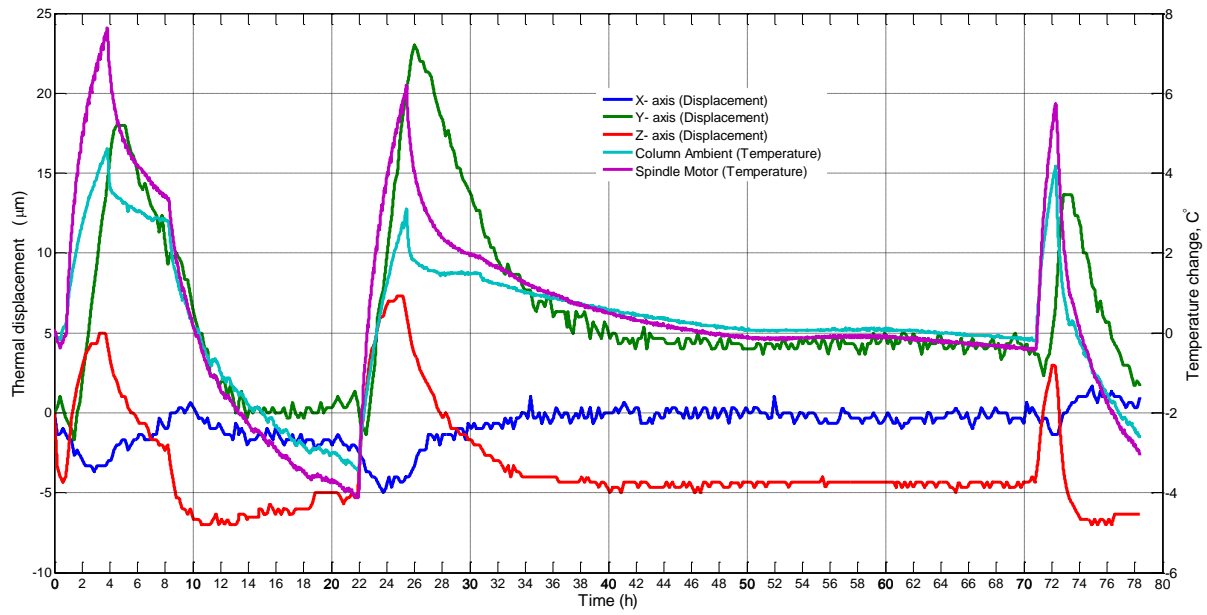


Figure 6-12: Machine movement and temperature changes.

The training samples were obtained from the first stage after the test had been started. After finishing the training of the model, the proposed ANFIS model can predict the normal daily cyclic error accurately and also can track sudden changes of thermal error from a relatively small training sample (Figure 6-13 and Figure 6-14).

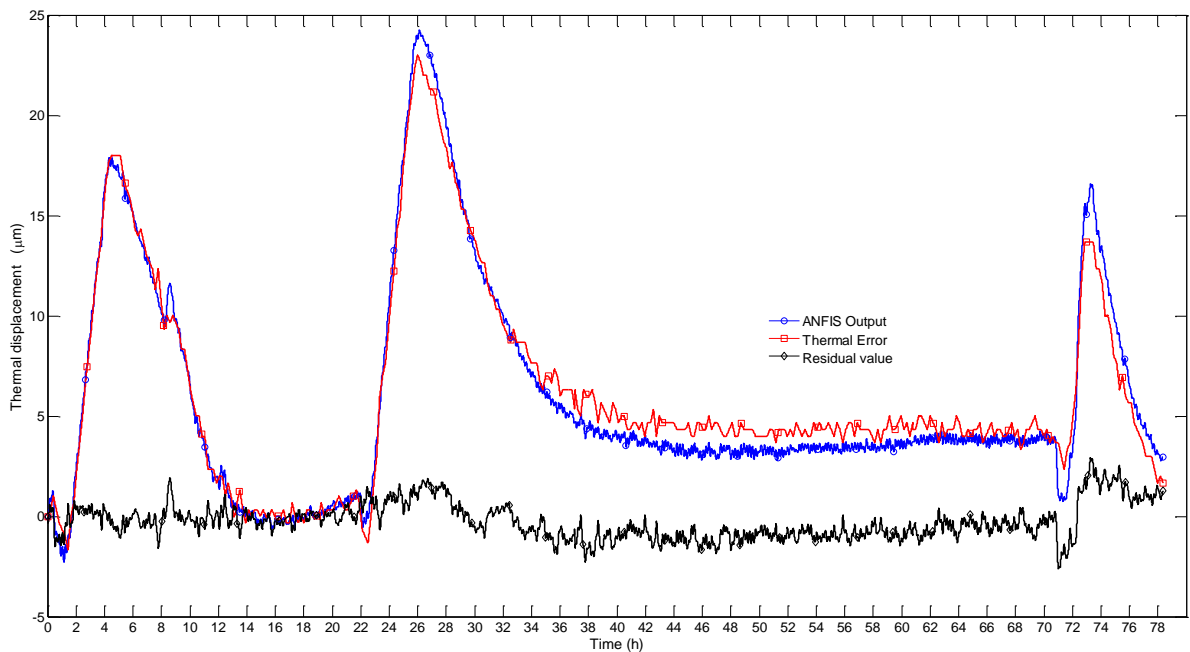


Figure 6-13: Correlation between the measured and simulated Y-axis displacement using ANFIS model.

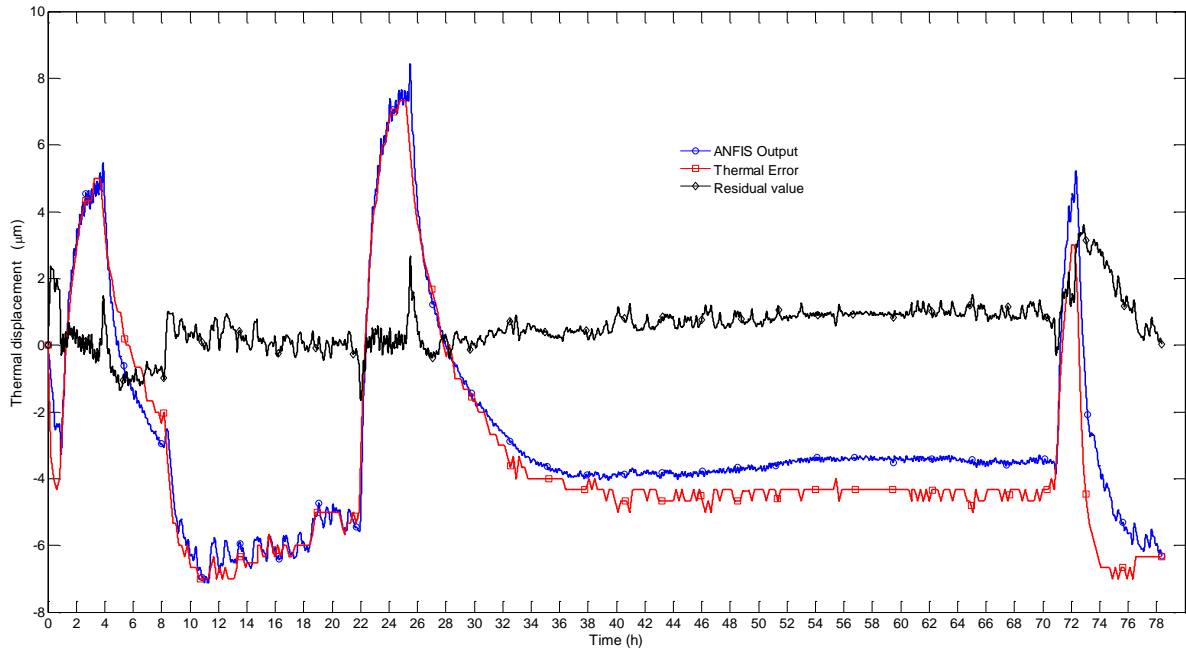


Figure 6-14: Correlation between the measured and simulated Z-axis displacement using ANFIS model.

As a result of the proposed model, the initial ANFIS model can be sufficiently well defined to the point that it might only need a small number of training iterations and a small amount of training data. Thus, the proposed ANFIS model does not require time-consuming iterative learning procedure or prohibitive downtime required to conduct the tests. To further validate the robustness of this modelling methodology, a normal environmental simulation was run using the test presented in section 6.2.2. The proposed model not only preserves a fast learning characteristic but also has an excellent prediction capability. Simulation results show that the thermal error in the Z direction can be significantly reduced to less than  $\pm 6 \mu\text{m}$  using testing dataset (see Figure 6-15).

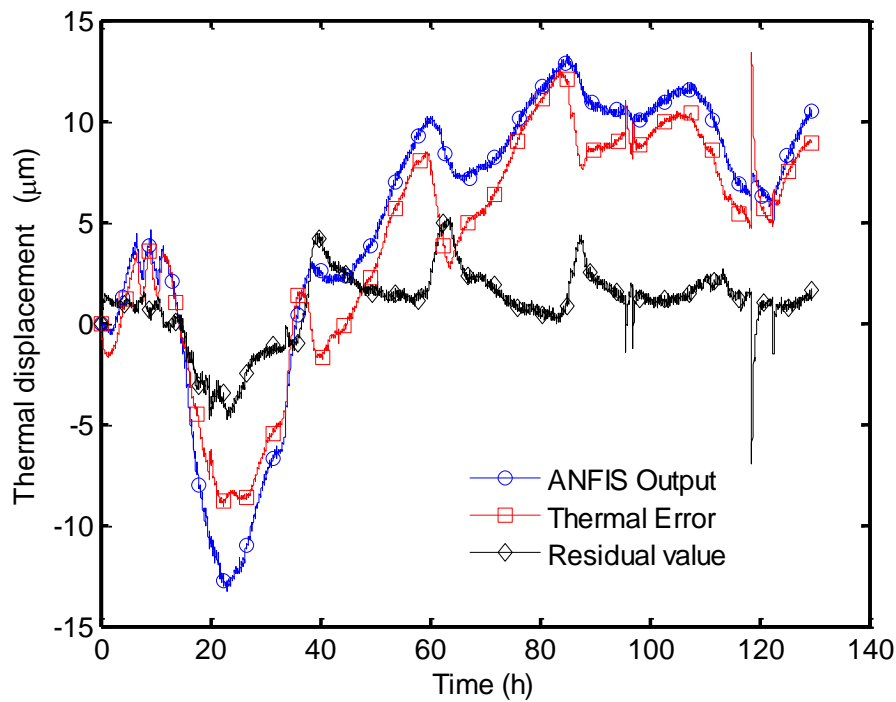


Figure 6-15: Five-day winter test

### 6.3 Robustness of the ANFIS Model

To verify the applicability of the proposed model, an example simulating the machining of a number of parts is investigated. The experiments were performed on a small vertical milling centre (Machine A) and utilised a Renishaw OMP40-2 spindle-mounted probe to monitor distortion. It has a stated unidirectional repeatability of  $1.0\text{ }\mu\text{m}$  at  $480\text{ mm/min}$  with a  $50\text{ mm}$  stylus. The test consists of simulating the machining a number of parts which are machined individually at a datum point on the table. When a part is finished the table moves to the next datum point to start machining the next part. Each part excites the X, Y and Z axes through simulated milling operations. This allows heat to be generated from spindle, motors and axes movement. A probing routine is run before the first machining operation to create a datum baseline for the test on four corners of granite square (see [Figure 6-16](#)). Probing routines are run after the third part and sixth part to measure the response of the tool in the X, Y and Z axes. The thermal data were measured using twenty-six temperature sensors placed in strips at the carrier, spindle boss, axes motors, axes ballscrews, nut, and ambient temperature sensors were placed around the machine to pick up the ambient temperature (see [Table 6-1](#)). A general overview of the experimental setup is shown in [Figure 6-16](#).

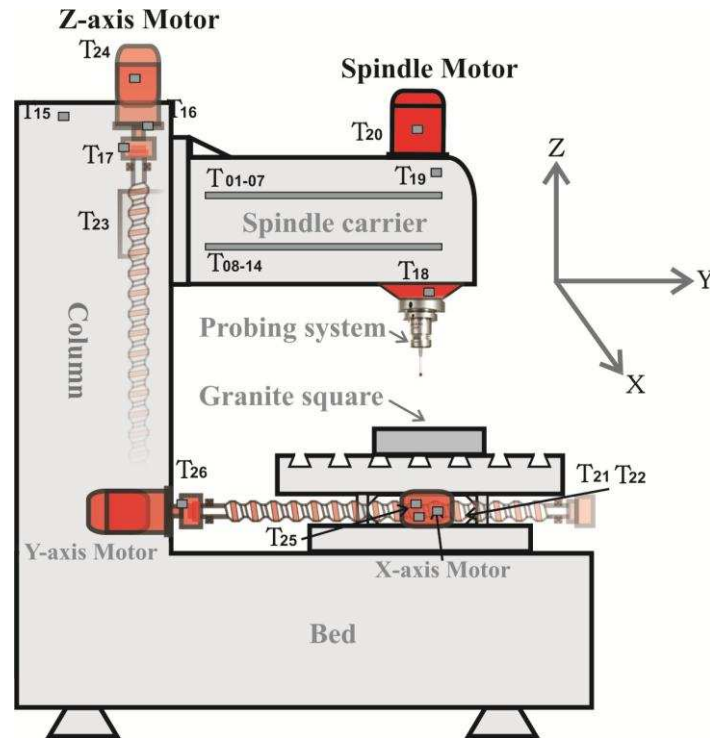


Figure 6-16: A general overview of the experimental setup.

Displacement and temperature data is monitored on a regular basis whilst examining the machine in as wide a variety of ways as possible. The machine was examined by running the spindle at different speeds as illustrated in Figure 6-17 (except for the periods of probing), running the axes from the test position to one extreme with different feedrates, and probably most importantly, changing the ambient condition through as wide range as possible. The latter was achieved by means of placing the machine in temperature-control room, so that the air could be warmed-up and cooled-down uniformly.

The high rotational speed brings a larger thermal displacement to the spindle carrier. Moreover, the higher feedrate generates larger frictional heat at the interface points, and the motor temperature also increases with the higher feedrate (see Figure 6-18, at 350 min). The temperature of measured points rises gradually until the equilibrium state is reached. The temperature sensors were measured simultaneously every 10 seconds. The maximum response of the X-axis is  $27\text{ }\mu\text{m}$ , the Y-axis is  $32\text{ }\mu\text{m}$ , and the Z-axis is  $74\text{ }\mu\text{m}$  (see Figure 6-18, Test-I). In this work, the thermal response of the X-axis was investigated first as an example for the modelling, and potential error compensation.

In this section, the aim is to use the structure of the ANFIS models described in the previous subsections to derive thermal error compensation systems. Moreover, a comparison will be made between the estimates provided by the ANFIS, ANN, and Grey models. With the

purpose of evaluating the prediction performance of the models, the remaining dataset (testing dataset, [Figure 6-19](#)) were used to run the proposed models. The performance of the models used in this study were computed using four performance criteria, including Root Mean Square Error (RMSE), Nash–Sutcliffe Efficiency coefficient (NSE), correlation coefficient (R) and also residual value (see section [3.8](#)).

Table 6-1: The location of the temperature sensors.

Sensors No.	Sensors Name	Locations
T <sub>01-07</sub>	B1-B7	Strip 1 Sensors (placed on the carrier)
T <sub>08-14</sub>	T1-T7	Strip 2 Sensors (placed on the carrier)
T <sub>15</sub>	Column Ambient	Outside the column
T <sub>16</sub>	Column Bolt Bottom	Z Scale
T <sub>17</sub>	Column Bolt Top	Z Scale
T <sub>18</sub>	Spindle Front Bottom	Spindle boss
T <sub>19</sub>	Spindle Front Top	Spindle boss
T <sub>20</sub>	Spindle Motor	Spindle Motor surface
T <sub>21</sub>	X Ballnut	X Scale
T <sub>22</sub>	Y Ballnut	Y Scale
T <sub>23</sub>	Z Ballnut	Z Scale
T <sub>24</sub>	Z Motor	Z axis motor surface
T <sub>25</sub>	X Axis bearing cap	X Scale
T <sub>26</sub>	Y Axis Motor bolt	Y Scale

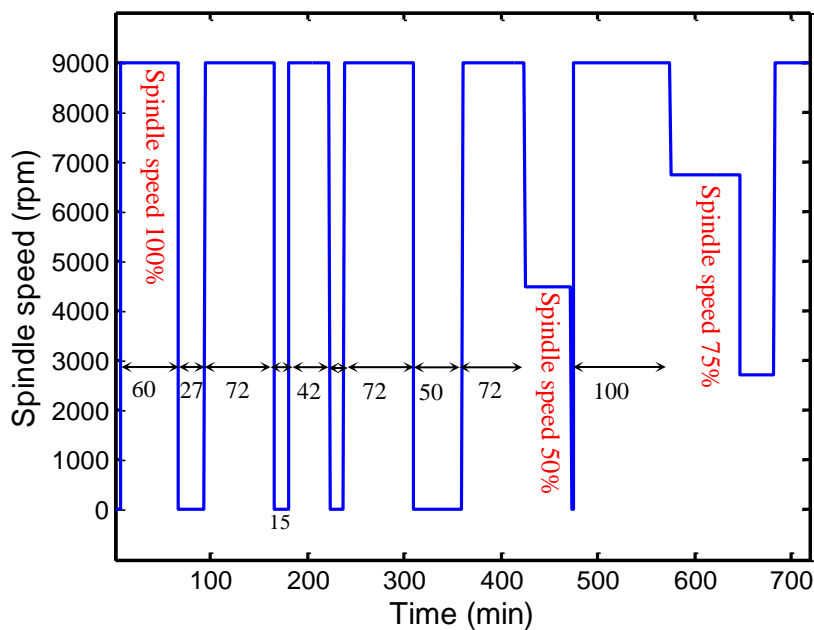


Figure 6-17: Running the spindle at different speeds.

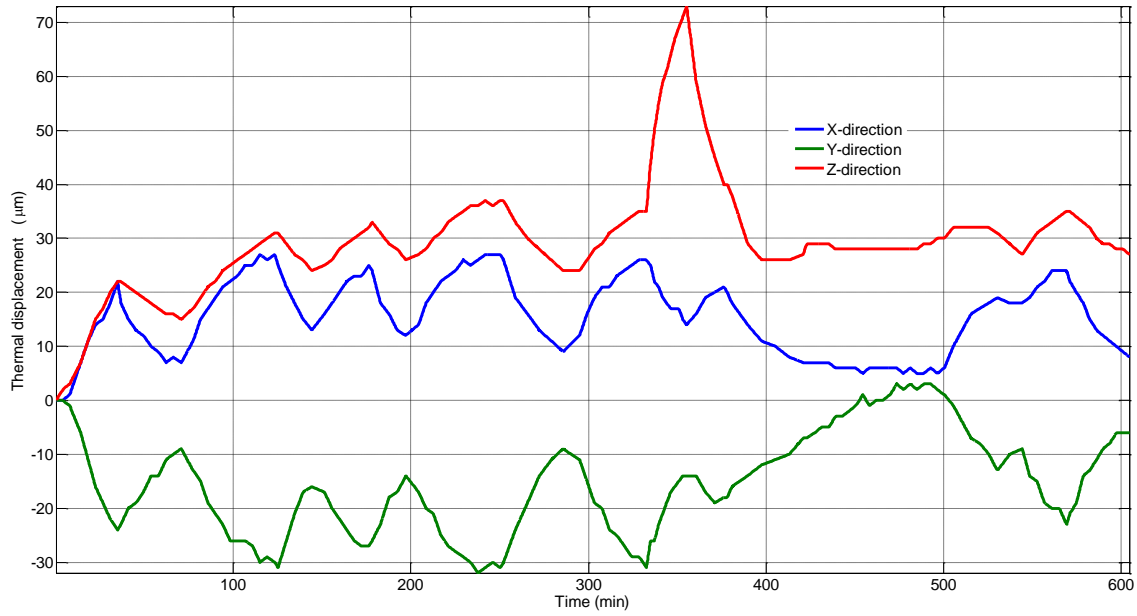


Figure 6-18: The machine movement (Test-I).

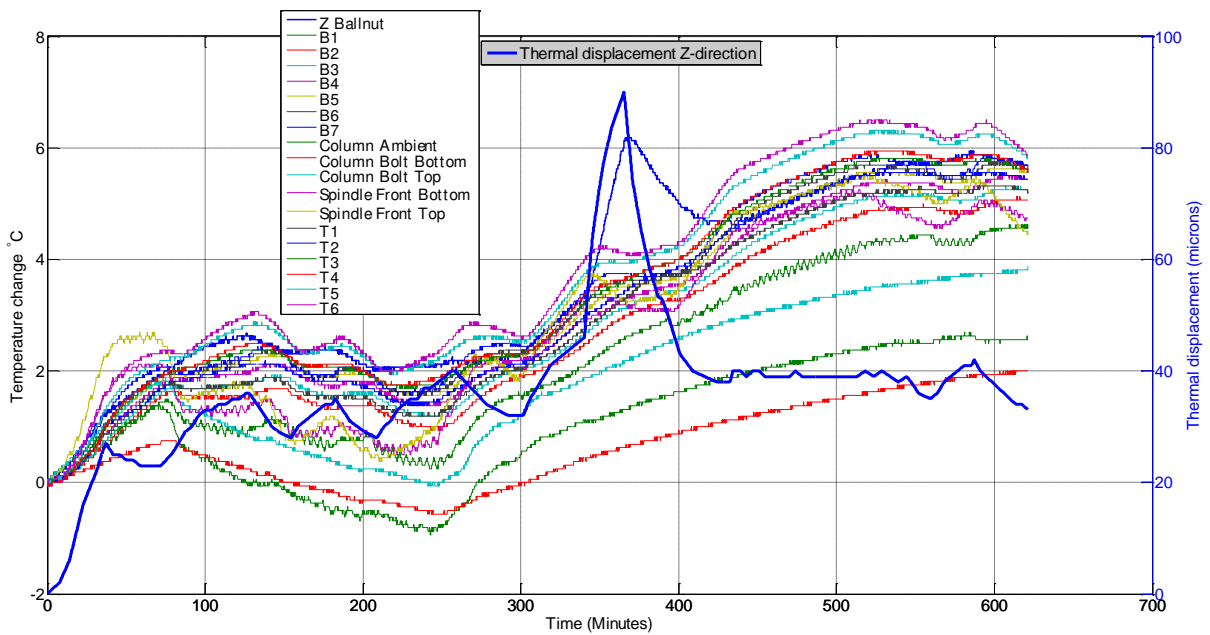


Figure 6-19: Temperature measurements and machine movement in Z-direction (Test-II).

### 6.3.1 ANN Model Development

In order to assess the ability of the ANFIS model relative to that of a neural network model, an ANN model was constructed using the same input variables to the ANFIS with 26 inputs. For the conventional neural network modelling approach, the datasets were also divided into the similar three groups of sets for training, testing and validating. It is worth noting that the

range of the training data must be representative of the entire operating conditions of the machine in order to overcome the problem of extrapolation error.

Usually ANN models have three layers: Input, hidden and output layer. Although, for common engineering problems, one hidden layer is sufficient for model training [120, 121], two or more hidden layers may be needed for other applications [122]. An ANN model with three layers was used in this study: the input layer has 26 input variables and the output layer has one neuron (the thermal response in the X-axis direction).

Selection of the number of neurons in the hidden layer is important for finding a suitable ANN model structure. Although increasing the neuron numbers in the hidden layer, may help to improve the neural network performance, however, the possibility of over-fitting may increase. Furthermore, a large number of hidden neurons can increase model training time. In this work, the minimum RMSE is determined by changing the number of hidden neurons. Therefore, after a series of experiments to find the best architecture, an ANN model with 10 neurons in the hidden layer was constructed to predict the thermal response in the X-axis direction. Figure 6-20 shows the structure of associated network model.

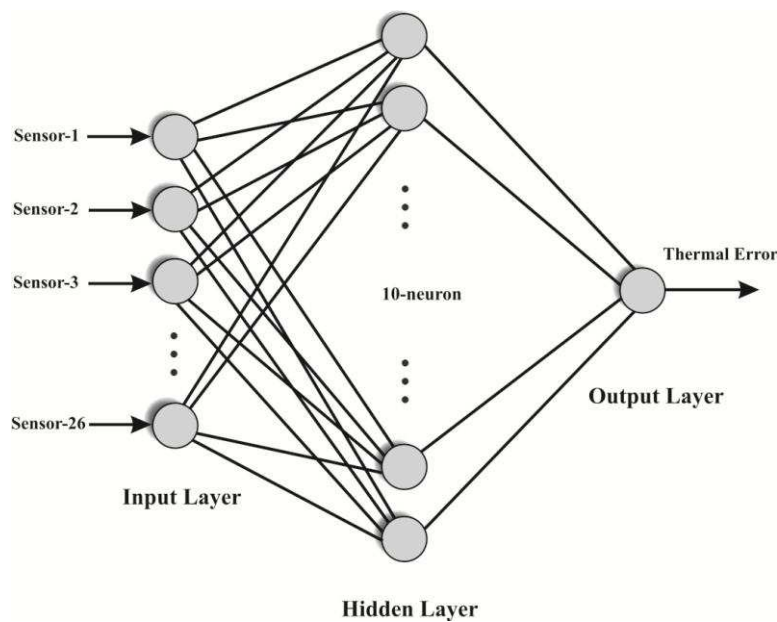


Figure 6-20: The structure of associated network model.

### 6.3.2 Grey Model Development

In order to optimise the Grey model parameters, the same training dataset was used for calibrating the model. Twenty six temperature sensors are used as inputs, and X-axis displacement as output. In the PSO algorithm, the number of the particles is set to be 90

whilst the self-confidence factor and the swarm-confidence factor are  $C_1=2$  and  $C_2=2$ , respectively. The inertia weight  $\omega$  was taken as an adaptive decreasing function in iteration index  $k$  from 0.9 to 0.4. After 100 epochs, the total error was at an acceptable level (RMSE=1.03). Table 6-2 illustrates the final Grey model parameters. The optimisation procedure was presented in section 3.6.

Another Grey model was developed by using the traditional Least Squares (LS) method in order to evaluate the structure parameters. In this section, five steps were involved in developing the model. Step 1, Step 2, Step 5 and Step 6 were the same as those presented in section 3.6. The unknown variables of the equation (3.13) were determined by the traditional least squares method (see Table 6-3).

The final Grey models being optimised and validated in this section has been tested next by a new testing dataset, not used during training and validation stage.

Table 6-2: PSO-based Grey model parameters

b1	b2	b3	b4	b5	b6	b7	b8	b9	b10
6.66	-28.77	22.48	56.62	46.45	-72.21	62.29	-92.32	-18.84	48.78
b11	b12	b13	b14	b15	b16	b17	b18	b19	b20
53.32	-23.20	46.63	81.24	-49.10	-71.93	-53.48	-32.15	-40.09	82.83
b21	b22	b23	b24	b25	b26	b27	u		
-87.03	21.23	-64.47	65.94	-63.69	-1.65	97.68	-26.32		

Table 6-3: LS-based Grey model parameters

b1	b2	b3	b4	b5	b6	b7	b8	b9	b10
1.75	-2.93	-1.04	-26.31	6.97	-19.56	53.75	-2.37	-21.11	-31.16
b11	b12	b13	b14	b15	b16	b17	b18	b19	b20
33.61	-19.86	-13.41	6.43	40.28	-12.23	17.49	-4.63	-28.47	-6.03
b21	b22	b23	b24	b25	b26	b27	u		
9.71	-8.98	-0.31	-9.23	5.09	24.64	-1.35	24.07		

### 6.3.3 Results and Discussion

In this work, the use of ANFIS, ANN and Grey models, for prediction of thermal error of a small VMC machine tool (Machine A), was described and compared. The final models being trained, validated and tested in the previous subsections have been verified further by a new separate dataset, not used during training, validation and testing stages. Predictive results using ANFIS, ANN and Grey models are shown in Figure 6-21, Figure 6-22, Figure 6-23, and Figure 6-24, respectively. The performance of each of the four thermal prediction models is presented and compared in Table 6-4, where the four models are trained using the same

training dataset and validated by the same testing dataset. According to the predictive results and evaluation criteria values in Table 6-4, it is very clear that the ANFIS model has a smaller RMSE, residual value ( $\pm 4 \mu\text{m}$ ), higher efficiency coefficient  $\text{NSE}=0.93$ , and higher correlation coefficient (R) contrasting with the ANN and Grey models. The ANN model performed slightly better than the Grey models for predicting thermal error in X-direction. Nevertheless, the PSO algorithm can act as an alternative training algorithm for the Grey model that can be used for thermal error compensation. It can be also observed from Table 6-4 that the models developed using the artificial intelligence techniques outperformed the statistical model (Grey model with (LS)). However, the ANN model does reduce the residual value to less than  $\pm 6 \mu\text{m}$ , the number of model parameters is high. Furthermore, it is worth noting that these models (i.e., ANN model and both Grey models) need a proper optimisation to predict effectively. For instance, the ANN model needs 10 neurons in the hidden layer, which was difficult to optimise. The Grey model was also time-consuming when trying to find the proper Grey final model. Therefore, the ANFIS model is a good modelling choice for predicting the thermal error of the machine tools with the benefit of fewer rules.

Table 6-4: Performance calculation of the used models.

Models	Performance indices			
	R	RMSE	NSE	Residual
ANFIS model	0.98	1.60	0.93	$\pm 4 \mu\text{m}$
ANN model	0.94	2.42	0.86	$\pm 6 \mu\text{m}$
Grey model with PSO	0.90	3.16	0.67	$\pm 9 \mu\text{m}$
Grey model with LS	0.82	7.26	0.20	$\pm 16 \mu\text{m}$

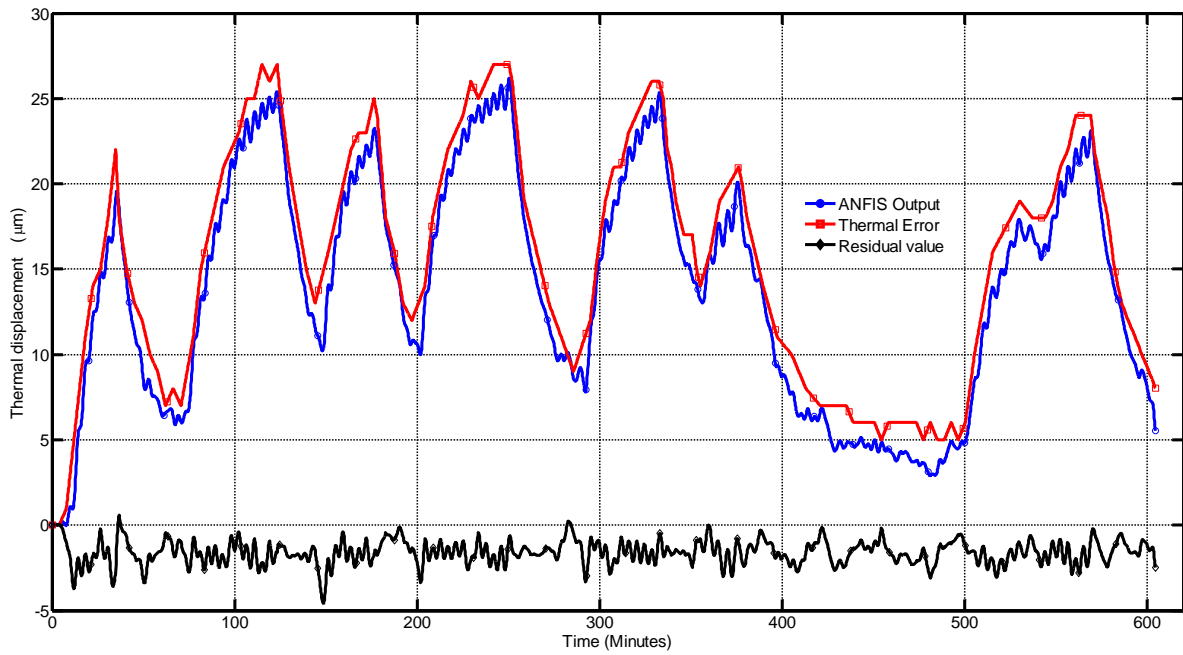


Figure 6-21: ANFIS model output vs the actual thermal response.

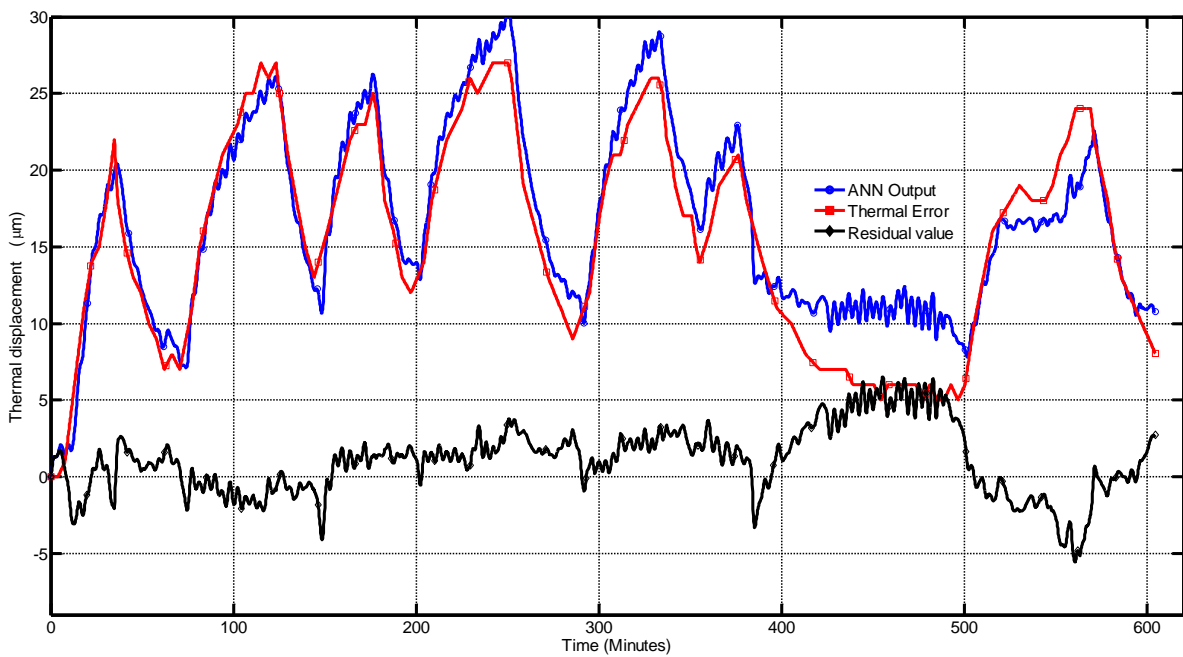


Figure 6-22: ANN model output vs the actual thermal response.

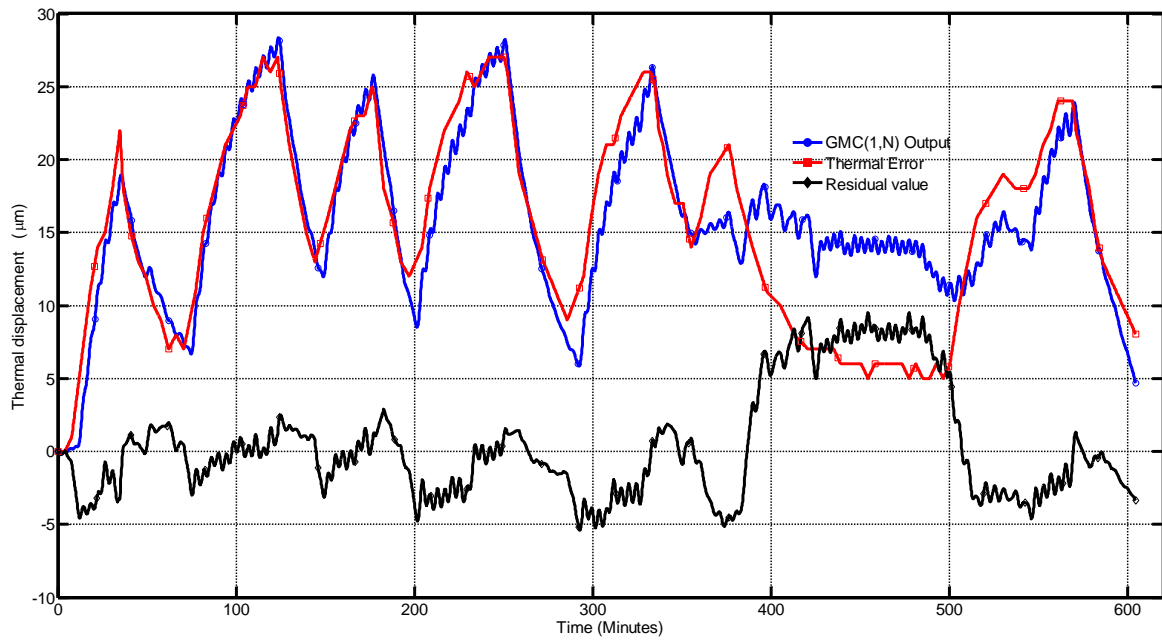


Figure 6-23: Grey model with PSO output vs the actual thermal response.

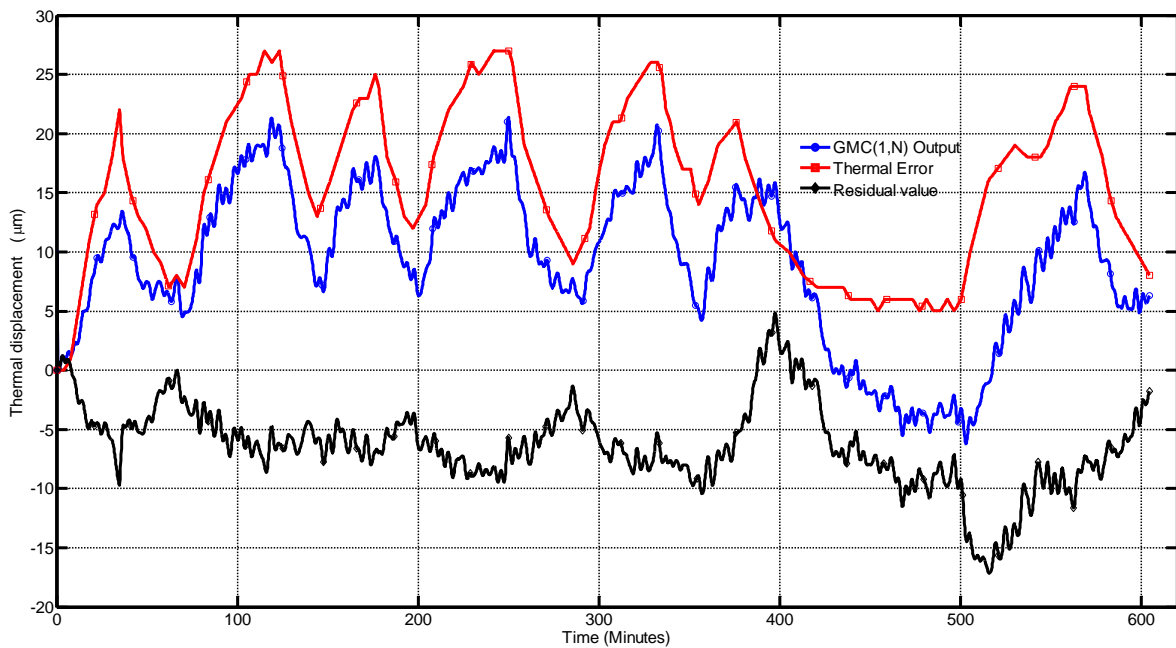


Figure 6-24: Standard Grey model output vs the actual thermal response.

Similar results have been obtained for Y-axis direction using the proposed ANFIS model (see [Figure 6-25](#)).

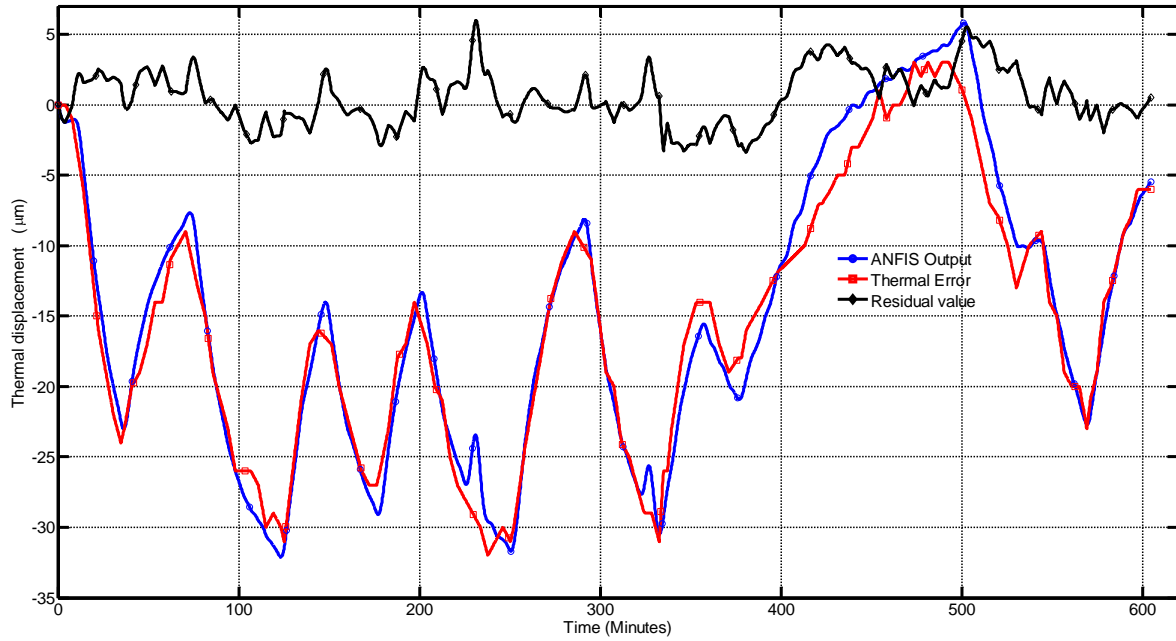


Figure 6-25: ANFIS model output vs the actual thermal response in Y-direction.

Next, the proposed ANFIS model can be applied to predict the thermal error in the Z-direction as shown in Figure 6-26. Although, the correlation coefficient between measured values and predicted values was close to 1 (98%), the result is not as good as demanded in terms of accuracy, especially in the rapid movement of Z-axis (the maximum residual value is approximately  $\pm 11 \mu\text{m}$ ). This phenomenon due to rapid movement of the Z-axis makes the proposed model less robust.

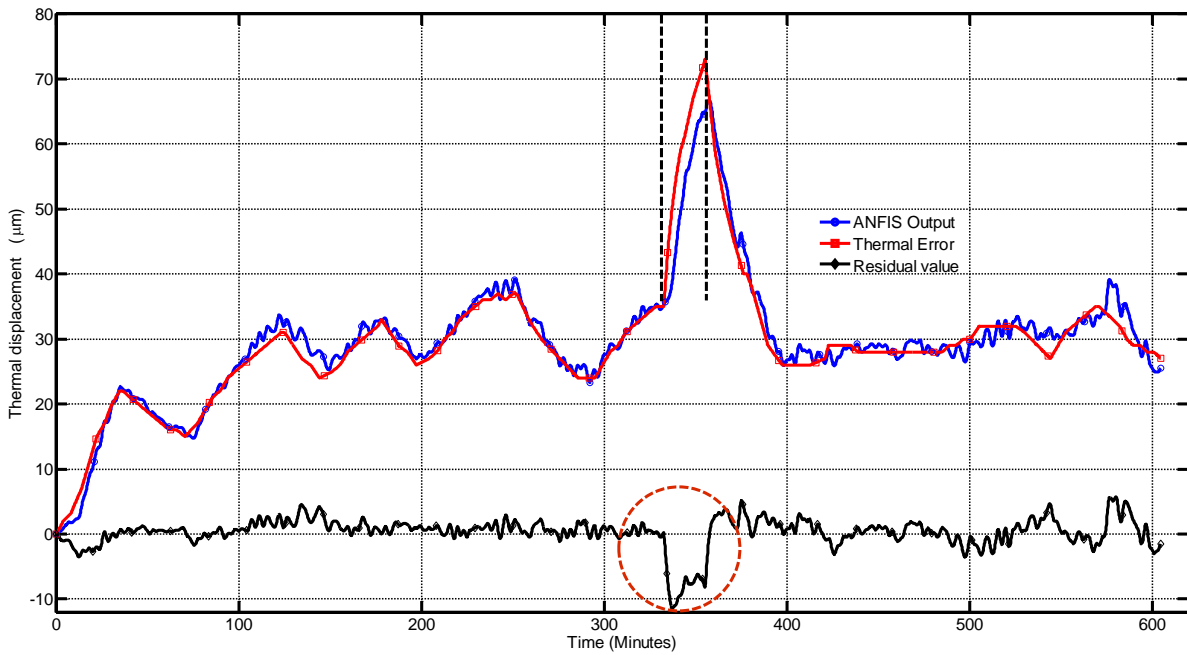


Figure 6-26: ANFIS model output vs the actual thermal response.

Since this effect is a highly non-linear inherent phenomenon, it is necessary to consider it in the modelling process. By taking another number of samples from rapid movement cycle to recalibrate the model, the robustness of the model can be improved further under different operation conditions. However, the Grey models were not able to capture this complexity, thus more advanced nonlinear modelling techniques such as the AI models are justified to capture this phenomena. The result shows that ANFIS model has a high capacity of prediction compared to other models. Figure 6-27 shows the output results of the simulation using ANFIS model. The correlation coefficient is 99% and the maximum residual value is approximately  $\pm 6 \mu\text{m}$ . In practice, the training data could be also obtained by carrying out a short heating and cooling test before the stage of a manufacturing process.

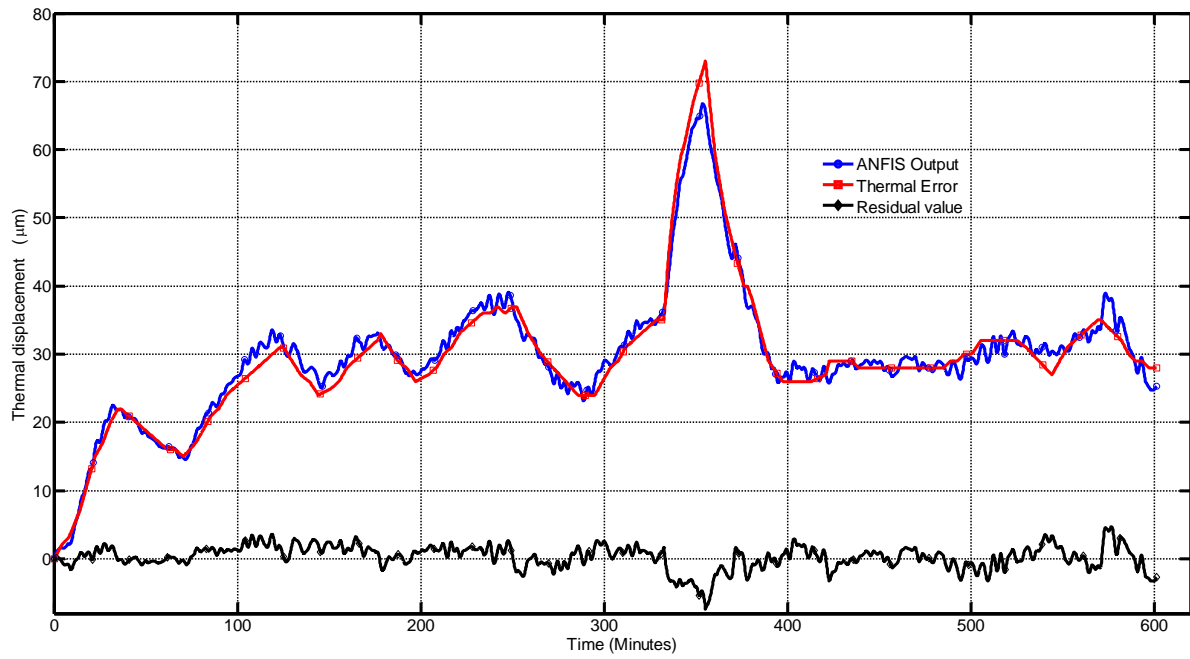


Figure 6-27: Improved ANFIS model output vs the actual thermal response.

## 6.4 Summary

Temperature-induced effects on machine tools are a significant part of the error budget. Changes in ambient conditions are an often overlooked effect that can be difficult to model, especially in unpredictable environments.

In this chapter, a novel thermal error modelling method based on Grey system theory and neural networks was developed to predict the environmental temperature variation error of a machine tool. The proposed model has been found to be flexible, simple to design and rapid to train.

The model is trained using data obtained from a short test of less than ninety minutes, which is desirable for minimising machine downtime. The accuracy of the model has not been compromised by restricting the training data. ETVE results in the Z-axis direction over a 160 hour test showed a reduction in error from over 20  $\mu\text{m}$  to better than  $\pm 3 \mu\text{m}$  considering the normal daily cycles. When also considering unexpected phenomena, such as the rapid change in temperature when a workshop door was opened, the model still performs well, with an improvement from 40  $\mu\text{m}$  to less than  $\pm 10 \mu\text{m}$ .

Similar results were achieved in the Y-axis direction, with this study not considering the X-axis direction due to symmetry of the machine.

To supplement the ANFIS model, the AGO was used to increase the linear characteristics and reduce the randomness from the measuring samples. This simple but effective technique allows the thermal model to be built with a minimum amount of temperature and displacement data in a very short time scale. Thus, a new concept has been added to ANFIS modelling for prediction of thermal errors. In this contribution, an ANFIS model and Grey system theory was successfully used to predict thermal errors of a small vertical milling centre with a limited amount of data for calibrating the model. The proposed method is a significant advantage over other models based on a single technique that have been used by many previous scholars where the data used to build the models is obtained from very long tests. The proposed model has significantly reduced the machine downtime required for a typical environmental testing from hours to only few minutes. According to experimental work, little machine downtime is needed to apply this modelling approach except to re-establish the model if needed.

Three types of data-driven models have been discussed in section 6.3: using ANFIS, ANN, and Grey models, respectively. All models were constructed and tested on a CNC milling machine. The results from the two sets of validation tests show that the ANFIS model has a smaller RMSE, residual value ( $\pm 6 \mu\text{m}$ ) and higher R contrasting with the Grey model and ANN model. Therefore, no single method can satisfy all the requirements for thermal error compensation. One method may complement another to obtain high level of accuracy.

Results also indicate that further improvement in correlation could be achieved by including rapid changes as part of the training data. Thus, the thermal error compensation model using ANFIS introduced in this thesis can be applied to any CNC machine tool because the model does not rely on a parametric model of the thermal error behaviour. In addition, this method is open to extension of other different physical inputs meaning that alternative sensors can be deployed with minimal retraining required.

## Chapter 7: Summary and Conclusions

In this chapter, the summary of the thesis and the major contributions of the research performed are given. Then, the future research that may be conducted in relation to this research area is also given in order of priority.

### 7.1 Thesis Summary and Contributions

The aims of this research were to propose generalised intelligent techniques for robust modelling of thermally induced errors on machine tools, and to validate the applicability of these techniques on different machine tools.

This research work proposes a thermal error modelling method based on the Adaptive Neuro-Fuzzy Inference System (ANFIS) in order to establish the relationship between the thermal errors and the temperature changes. The proposed methodology has the ability to provide a simple, transparent and robust thermal error compensation system. It has the advantages of fuzzy logic theory and the learning ability of the artificial neural network in a single system. Methods of optimising sensor location, using automatic clustering of thermography data, have also been proposed. This allows efficient modelling of new machines.

The proposed approach has been validated on three different machine tools under different operation conditions. Thus the proposed system has been shown to be robust to different internal heat sources (axis and spindle heating), ambient changes and is easily extensible to other CNC machine tools.

The following items are the contributions to knowledge of this work regarding the modelling and testing of the thermal errors of CNC machine tools.

- A comprehensive review of the empirical models for thermal error compensation of CNC machine tools has been conducted. Different types of Artificial Intelligence (AI) models were investigated and throughout the research, comparisons have been made between the new technique and existing proposals from literature.
- The structure of ANFIS model was significantly reduced from the standard methods for thermal error compensation (see [Table 5-7](#) and [Table 6-4](#)). Reduction of the number of rules was one of the mechanisms responsible for achieving good level of interpretability. Therefore, this research focuses on obtaining the best trade-off

between interpretability and accuracy. It should be noted that best reduction of all rules of the ANFIS model was achieved by using a Fuzzy C-Means (FCM) technique. The process of reduction allowed reducing rules of the compensation model which do not affect model accuracy. This was validated by case study. Furthermore, the final model is easily understandable by domain experts for interpretation purposes.

- A thermal imaging camera was used to record temperature distributions across the machine structure during the experiments. The thermal images were saved as a matrix of temperatures with a specific spatial resolution of one pixel, each of which can be considered as a possible temperature measurement point. The optimal locations for the temperature sensors were determined through the Grey model and FCM clustering. After clustering into groups, one sensor from each group is selected according to its influence coefficient value with the thermal response. By this method, the number of temperature sensors required for a robust compensation model was reduced, which significantly minimised the computational time, hardware cost and effect of sensor uncertainty.
- Unlike the existing deterministic models, the proposed method is easily extensible to other physical variables. This means that alternative or additional sensors can be deployed with minimal retraining required. Furthermore, other machine or machining parameters can be acquired directly from the controller to provide some feedforward information. Example is the spindle speed or axis feedrate, although other significant factors can also be considered. It is worth noting that changes to motor behaviour over its lifetime will affect the thermal output at a given speed. For this reason, the inclusion of the primary parameters is non-trivial when looking for long-term accuracy from the model and it can be more robust only to include the derived values that directly affect accuracy.
- The compensation system using Grey model has been found to be flexible, quick, efficient to implement, and has been used to reduce thermal errors from heating of the C and Z axes of a gantry machine by over 85% using a quick heating test for calibrating the model. This dramatically reduces the amount of experimental data, and so reduces the downtime needed for implementing the compensation model. The Particle Swarm Optimisation (PSO) algorithm is an effective technique for identifying the parameters of the proposed model even the training dataset is corrupted by noise. The number of sensors used in this model was minimised by fusion of both

temperature sensors and direct strain measurement from Fibre Bragg Grating (FBG) sensors.

- Hence, it can be concluded that a well-trained and tested ANFIS model can be used as a viable tool to predict the thermal error of the CNC machine tool at different operation conditions.

In conclusion, many novelties have been discovered by investigating different thermal error modelling and compensation techniques. The design, development and testing of these techniques have resulted in presentations at two refereed journal papers [116, 123], five refereed conference papers [50, 53, 117, 124, 125], and other papers in the final stages of preparation.

## 7.2 Future Work

- To extend this proposed modelling approach in future work, several approaches will be needed, including improving the capabilities of inserting more engineering knowledge into the main learning mechanisms of the intelligent system.
- The combination of principle-based models (hard computing) and artificial intelligence tools (soft computing) has not been given sufficient attention in thermal error compensation models. Such attempts have been employed in other areas of manufacturing [126]. FEA models can be combined with artificial intelligence tools to obtain more accuracy and robustness.
- Data-driven models are still believed to be promising in future study of thermal error compensation, due to their characteristics of simplicity, flexibility, robustness and no need for a complex thermal behaviour model.
- Numerous studies in literature proved that direct compensation techniques can be useful for thermal error compensation but further research activity is needed to increase their robustness and reliability for real time applications.

## 7.3 Published Papers

The following list of publications has arisen from this research activity:

### 7.3.1 Refereed Journal Papers

**Ali M Abdulshahed**, Andrew Peter Longstaff, Simon Fletcher: *The application of ANFIS prediction models for thermal error compensation on CNC machine tools*. **Applied Soft Computing** 02/2015. [116].

**Ali M Abdulshahed**, Andrew Peter Longstaff, Simon Fletcher, Alan Myers: *Thermal error modelling of machine tools based on ANFIS with fuzzy c-means clustering using a thermal imaging camera*. **Applied Mathematical Modelling** 04/2015. [123].

### 7.3.2 Refereed Conference Papers

**Ali Abdulshahed**, Andrew P Longstaff, Simon Fletcher: *A particle swarm optimisation-based Grey prediction model for thermal error compensation on CNC machine tools*. Lamdamap 11th International Conference; 03/2015. [117].

**Ali M Abdulshahed**, Andrew P Longstaff, Simon Fletcher: *A novel approach for ANFIS modelling based on Grey system theory for thermal error compensation*. 2014 14th UK Workshop on Computational Intelligence (UKCI), Bradford, UK; 09/2014. [125].

**Ali M Abdulshahed**, Andrew P Longstaff, Simon Fletcher, Alan Myers: *Application of GNNMCI(1, N) to environmental thermal error modelling of CNC machine tools*. The 3rd International Conference on Advanced Manufacturing Engineering and Technologies, Stockholm, Sweden; 10/2013. [53].

**Ali M Abdulshahed**, Andrew P Longstaff, Simon Fletcher, Alan Myers: *Comparative study of ANN and ANFIS prediction models for thermal error compensation on CNC machine tools*. Lamdamap 10th International Conference; 03/2013. [50].

Akshay Potdar, Andrew P Longstaff, Simon Fletcher, **Ali M Abdulshahed**: *Development of modular machine tool structural monitoring system*. The 3rd International Conference on Advanced Manufacturing Engineering and Technologies, Stockholm, Sweden; 10/2013. [124].

### Posters

**Ali M Abdulshahed**, Andrew P Longstaff, Simon Fletcher, Alan Myers: *Optimal temperature variable selection by GRA approach for thermal error modelling*. EPSRC Centre for Innovative Manufacturing in Advanced Metrology (Grant Ref: EP/I033424/1). Mid-Term meeting; 27/03/2014.

### Contribution to projects

HARCO Project (Hierarchical and Adaptive smaRt COmponents for precision production systems application) funded by the European Commission Seventh Framework Programme (FP7), (NMP2-SL-2010-260051), 2013.

- Design of tests, experimental setup and data analysis using MATLAB.

- Develop an intelligent thermal-error compensation model using fusion of both temperature sensors and direct strain measurement from Fibre Bragg Grating (FBG) sensors.

EASE-R3 Project (Integrated framework for a cost-effective and ease of Repair, Renovation and Re-use of machine tools within modern factory).

## References

- [1] R. Ramesh, M. Mannan, and A. Poo, "Error compensation in machine tools—a review: Part II: thermal errors," *International Journal of Machine Tools and Manufacture*, vol. 40, pp. 1257-1284, 2000.
- [2] J. Mayr, et al., "Thermal issues in machine tools," *CIRP Annals - Manufacturing Technology*, vol. 61, pp. 771-791, 2012.
- [3] A. P. Longstaff, S. Fletcher, and D. G. Ford, "Practical experience of thermal testing with reference to ISO 230 Part 3," in *Laser metrology and machine performance VI*, Southampton, 2003, pp. 473-483.
- [4] W. Grzesik, "Experimental investigation of the cutting temperature when turning with coated indexable inserts," *International Journal of Machine Tools and Manufacture*, vol. 39, pp. 355-369, 1999.
- [5] J. Bryan, "International status of thermal error research (1990)," *CIRP annals-manufacturing technology*, vol. 39, pp. 645-656, 1990.
- [6] S. Postlethwaite, J. Allen, and D. Ford, "The use of thermal imaging, temperature and distortion models for machine tool thermal error reduction," *Proceedings of the Institution of Mechanical Engineers, Part B: Journal of Engineering Manufacture*, vol. 212, pp. 671-679, 1998.
- [7] A. White, S. Postlethwaite, and D. G. Ford, "A general purpose thermal error compensation system for CNC machine tools," in *Laser Metrology and Machine Performance V*, Southampton, 2001, pp. 3-13.
- [8] N. S. Mian, S. Fletcher, A. P. Longstaff, and A. Myers, "Efficient thermal error prediction in a machine tool using finite element analysis," *Measurement Science and Technology*, vol. 22, pp. 085107.1-10, 2011.
- [9] L. Filice, F. Micari, S. Rizzuti, and D. Umbrello, "A critical analysis on the friction modelling in orthogonal machining," *International Journal of Machine Tools and Manufacture*, vol. 47, pp. 709-714, 2007.
- [10] V. Norouzifard and M. Hamed, "Experimental determination of the tool–chip thermal contact conductance in machining process," *International Journal of Machine Tools and Manufacture*, vol. 84, pp. 45-57, 2014.
- [11] J. Zhu, J. Ni, and A. J. Shih, "Robust machine tool thermal error modeling through thermal mode concept," *Journal of manufacturing science and engineering*, vol. 130, pp. 061006.1-9, 2008.
- [12] J. Jedrzejewski, Z. Kowal, W. Kwasny, and Z. Winiarski, "In-house system for holistic modelling of machine tool operating properties," in *Systems and Informatics (ICSAI), 2014 2nd International Conference on*, 2014, pp. 411-416.
- [13] M. Weck, P. McKeown, R. Bonse, and U. Herbst, "Reduction and Compensation of Thermal Errors in Machine Tools," *CIRP Annals - Manufacturing Technology*, vol. 44, pp. 589-598, 1995.
- [14] G. Spur, et al., "Thermal Behaviour Optimization of Machine Tools," *CIRP Annals - Manufacturing Technology*, vol. 37, pp. 401-405, 1988.
- [15] J. Ni, "CNC machine accuracy enhancement through real-time error compensation," *Journal of manufacturing science and engineering*, vol. 119, pp. 717-725, 1997.
- [16] J. Mayr, M. Ess, S. Weikert, and K. Wegener, "Comparing different cooling concepts for ball screw systems," in *Proceedings ASPE Annual Meeting*, 2010.
- [17] Y. Ito, *Thermal deformation in machine tools*: McGraw-Hill, 2010.
- [18] H. Haddad and M. Al Kobaisi, "Optimization of the polymer concrete used for manufacturing bases for precision tool machines," *Composites Part B: Engineering*, vol. 43, pp. 3061-3068, 2012.

- [19] H.-C. Möhring, et al., "Materials in machine tool structures," *CIRP Annals - Manufacturing Technology*, vol. 64, pp. 725-748, 2015.
- [20] J. Freeman, A. White, and D. G. Ford, "Ball-screw thermal errors-a finite element simulation for on-line estimation," in *Laser Metrology and Machine Performance V*, Southampton, 2001, pp. 269-278.
- [21] S. Fletcher and D. G. Ford, "Measuring and modelling heat transfer and thermal errors on a ballscrew feed drive system," in *Laser Metrology and Machine Performance VI*, 2003, pp. 349-360.
- [22] E. Abele, Y. Altintas, and C. Brecher, "Machine tool spindle units," *CIRP Annals - Manufacturing Technology*, vol. 59, pp. 781-802, 2010.
- [23] S. Postlethwaite, J. Allen, and D. Ford, "Machine tool thermal error reduction—an appraisal," *Proceedings of the Institution of Mechanical Engineers, Part B: Journal of Engineering Manufacture*, vol. 213, pp. 1-9, 1999.
- [24] Z. Z. Xu, et al., "Thermal error forecast and performance evaluation for an air-cooling ball screw system," *International Journal of Machine Tools and Manufacture*, vol. 51, pp. 605-611, 2011.
- [25] M. A. Donmez, M. H. Hahn, and J. A. Soons, "A Novel Cooling System to Reduce Thermally-Induced Errors of Machine Tools," *CIRP Annals - Manufacturing Technology*, vol. 56, pp. 521-524, 2007.
- [26] S. Jiang and X. Min, "Thermal design of the vertical machining centre headstock by the forced cooling method," *Proceedings of the Institution of Mechanical Engineers, Part C: Journal of Mechanical Engineering Science*, vol. 226, pp. 738-751, 2012.
- [27] W. Feng, Z. Li, Q. Gu, and J. Yang, "Thermally induced positioning error modelling and compensation based on thermal characteristic analysis," *International Journal of Machine Tools and Manufacture*, vol. 93, pp. 26-36, 2015.
- [28] L. Wang, H. Wang, T. Li, and F. Li, "A hybrid thermal error modeling method of heavy machine tools in z-axis," *The International Journal of Advanced Manufacturing Technology*, pp. 1-12, 2015.
- [29] C. Zhang, F. Gao, Y. Che, and Y. Li, "Thermal error modeling of multisource information fusion in machine tools," *The International Journal of Advanced Manufacturing Technology*, pp. 1-9, 2015.
- [30] J. Li, et al., "Thermal-error modeling for complex physical systems: the-state-of-arts review," *The International Journal of Advanced Manufacturing Technology*, vol. 42, pp. 168-179, 2009.
- [31] Y. Li, et al., "A review on spindle thermal error compensation in machine tools," *International Journal of Machine Tools and Manufacture*, vol. 95, pp. 20-38, 2015.
- [32] H. Yang and J. Ni, "Dynamic modeling for machine tool thermal error compensation," *Journal of manufacturing science and engineering*, vol. 125, pp. 245-254, 2003.
- [33] J. Abonyi, *Fuzzy Model Identification*: Springer, 2003.
- [34] J. Dureja, et al., "A review of empirical modeling techniques to optimize machining parameters for hard turning applications," *Proceedings of the Institution of Mechanical Engineers, Part B: Journal of Engineering Manufacture*, pp. 1-16, 2014.
- [35] M. Chandrasekaran, M. Muralidhar, C. M. Krishna, and U. S. Dixit, "Application of soft computing techniques in machining performance prediction and optimization: a literature review," *The International Journal of Advanced Manufacturing Technology*, vol. 46, pp. 445-464, 2010.
- [36] M. Gebhardt, et al., "High precision grey-box model for compensation of thermal errors on five-axis machines," *CIRP annals-manufacturing technology*, vol. 63, pp. 509-512, 2014.

- [37] P. Lindskog, "Fuzzy identification from a grey box modeling point of view," in *Fuzzy model identification*, ed: Springer, 1997, pp. 3-50.
- [38] M. J. Gacto, R. Alcalá, and F. Herrera, "Interpretability of linguistic fuzzy rule-based systems: An overview of interpretability measures," *Information Sciences*, vol. 181, pp. 4340-4360, 2011.
- [39] N. S. Mian, S. Fletcher, A. P. Longstaff, and A. Myers, "Efficient estimation by FEA of machine tool distortion due to environmental temperature perturbations," *Precision engineering*, vol. 37, pp. 372-379, 2013.
- [40] J. Jędrzejewski, W. Kwaśny, Z. Kowal, and Z. Winiarski, "Development of the modelling and numerical simulation of the thermal properties of machine tools," *Journal of Machine Engineering*, vol. 14, pp. 5-20, 2014.
- [41] N. S. Mian, "Efficient machine tool thermal error modelling strategy for accurate offline assessment," Doctoral thesis, Centre for Precision Technologies (CPT), University of Huddersfield, Huddersfield, 2010.
- [42] E. Creighton, A. Honegger, A. Tulsian, and D. Mukhopadhyay, "Analysis of thermal errors in a high-speed micro-milling spindle," *International Journal of Machine Tools and Manufacture*, vol. 50, pp. 386-393, 2010.
- [43] B. Tan, et al., "A thermal error model for large machine tools that considers environmental thermal hysteresis effects," *International Journal of Machine Tools and Manufacture*, vol. 82-83, pp. 11-20, 2014.
- [44] B. R. Hardwick, "Further development of techniques for software compensation of thermally induced errors on CNC machine tools," in *Laser Metrology and Machine Performance (Lamdamap 93)*, 1993, pp. 47-63.
- [45] J. Chen, J. Yuan, and J. Ni, "Thermal error modelling for real-time error compensation," *The International Journal of Advanced Manufacturing Technology*, vol. 12, pp. 266-275, 1996.
- [46] J. Yan and J. Yang, "Application of synthetic grey correlation theory on thermal point optimization for machine tool thermal error compensation," *The International Journal of Advanced Manufacturing Technology*, vol. 43, pp. 1124-1132, 2009.
- [47] Y. Wang, G. Zhang, K. S. Moon, and J. W. Sutherland, "Compensation for the thermal error of a multi-axis machining center," *Journal of materials processing technology*, vol. 75, pp. 45-53, 1998.
- [48] J.-L. Deng, "Control problems of grey systems," *Systems & Control Letters*, vol. 1, pp. 288-294, 1982.
- [49] S. Liu, J. Forrest, and Y. Yingjie, "A brief introduction to grey systems theory," in *Proceeding of IEEE International Conference on Grey Systems and Intelligent Services 2011*, Nanjing, 2011, pp. 1-9.
- [50] A. Abdulshahed, A. P. Longstaff, S. Fletcher, and A. Myers, "Comparative study of ANN and ANFIS prediction models for thermal error compensation on CNC machine tools," in *Laser Metrology and Machine Performance X*, Buckinghamshire, 2013, pp. 79-88.
- [51] Y. Nagata and K. H. Chu, "Optimization of a fermentation medium using neural networks and genetic algorithms," *Biotechnology letters*, vol. 25, pp. 1837-1842, 2003.
- [52] N. Nasr, H. Hafez, M. H. El Naggar, and G. Nakhla, "Application of artificial neural networks for modeling of biohydrogen production," *International Journal of Hydrogen Energy*, vol. 38, pp. 3189-3195, 2013.
- [53] A. Abdulshahed, A. P. Longstaff, S. Fletcher, and A. Myers, "Application of GNNMCI(1, N) to environmental thermal error modelling of CNC machine tools," in

- The 3rd International Conference on Advanced Manufacturing Engineering and Technologies, Stockholm, 2013, pp. 253-262.
- [54] S. Yang, J. Yuan, and J. Ni, "The improvement of thermal error modeling and compensation on machine tools by CMAC neural network," *International Journal of Machine Tools and Manufacture*, vol. 36, pp. 527-537, 1996.
  - [55] Q. Guo, J. Yang, and H. Wu, "Application of ACO-BPN to thermal error modeling of NC machine tool," *The International Journal of Advanced Manufacturing Technology*, vol. 50, pp. 667-675, 2010.
  - [56] J. Chen and G. Chiou, "Quick testing and modeling of thermally-induced errors of CNC machine tools," *International Journal of Machine Tools and Manufacture*, vol. 35, pp. 1063-1074, 1995.
  - [57] K. C. Wang, "Thermal error modeling of a machining center using grey system theory and HGA-trained neural network," in *Cybernetics and Intelligent Systems*, Bangkok, 2006, pp. 1-7.
  - [58] X. Zhu, S. Xiang, and J. Yang, "Novel thermal error modeling method for machining centers," *Proceedings of the Institution of Mechanical Engineers, Part C: Journal of Mechanical Engineering Science*, pp. 1-9, 2014.
  - [59] J.-H. Lee, J.-H. Lee, and S.-H. Yang, "Development of thermal error model with minimum number of variables using fuzzy logic strategy," *KSME international journal*, vol. 15, pp. 1482-1489, 2001.
  - [60] L. Wei, M. Fei, and H. Hu, "Modeling and stability analysis of grey-fuzzy predictive control," *Neurocomputing*, vol. 72, pp. 197-202, 2008.
  - [61] E. Brousseau, S. Dimov, and R. Setchi, "Knowledge acquisition techniques for feature recognition in CAD models," *Journal of Intelligent Manufacturing*, vol. 19, pp. 21-32, 2008.
  - [62] K. C. Wang, "Thermal error modeling of a machining center using grey system theory and adaptive network-based fuzzy inference system," in *Cybernetics and Intelligent Systems*, Bangkok, 2006, pp. 1-6.
  - [63] S. Eskandari, B. Arezoo, and A. Abdullah, "Positional, geometrical, and thermal errors compensation by tool path modification using three methods of regression, neural networks, and fuzzy logic," *The International Journal of Advanced Manufacturing Technology*, vol. 65, pp. 1635-1649, 2013.
  - [64] S. Guillaume, "Designing fuzzy inference systems from data: An interpretability-oriented review," *Fuzzy Systems, IEEE Transactions on*, vol. 9, pp. 426-443, 2001.
  - [65] S. Fletcher, A. P. Longstaff, and A. Myers, "Flexible modelling and compensation of machine tool thermal errors," in *20th Annual Meeting of American Society for Precision Engineering*, Norfolk, VA, Norfolk, 2005.
  - [66] J. Vyroubal, "Compensation of machine tool thermal deformation in spindle axis direction based on decomposition method," *Precision engineering*, vol. 36, pp. 121-127, 2012.
  - [67] J. S. Chen, "Fast calibration and modeling of thermally-induced machine tool errors in real machining," *International Journal of Machine Tools and Manufacture*, vol. 37, pp. 159-169, 1997.
  - [68] J. Han, L. Wang, N. Cheng, and H. Wang, "Thermal error modeling of machine tool based on fuzzy c-means cluster analysis and minimal-resource allocating networks," *The International Journal of Advanced Manufacturing Technology*, vol. 60, pp. 463-472, 2012.
  - [69] J. Han, L. Wang, H. Wang, and N. Cheng, "A new thermal error modeling method for CNC machine tools," *The International Journal of Advanced Manufacturing Technology*, pp. 1-8, 2012.

- [70] S. Liu, Y. Lin, and J. Y. L. Forrest, *Grey systems: theory and applications* vol. 68: Springer-Verlag Berlin Heidelberg, 2010.
- [71] V. Hassani, T. Tjahjowidodo, and T. N. Do, "A survey on hysteresis modeling, identification and control," *Mechanical systems and signal processing*, vol. 49, pp. 209-233, 2014.
- [72] X. Li and R. Du, "Analysis and compensation of workpiece errors in turning," *International journal of production research*, vol. 40, pp. 1647-1667, 2002.
- [73] C. Brecher, P. Hirsch, and M. Weck, "Compensation of Thermo-elastic Machine Tool Deformation Based on Control internal Data," *CIRP Annals - Manufacturing Technology*, vol. 53, pp. 299-304, 2004.
- [74] P. Bosetti and S. Bruschi, "Enhancing positioning accuracy of CNC machine tools by means of direct measurement of deformation," *The International Journal of Advanced Manufacturing Technology*, vol. 58, pp. 651-662, 2012.
- [75] K. T. V. Grattan and T. Sun, "Fiber optic sensor technology: an overview," *Sensors and Actuators A: Physical*, vol. 82, pp. 40-61, 2000.
- [76] M. Kreuzer, "Strain measurement with fiber Bragg grating sensors," HBM, Darmstadt, Germany. 2006.
- [77] J. Huang, et al., "Real-time measurement of temperature field in heavy-duty machine tools using fiber Bragg grating sensors and analysis of thermal shift errors," *Mechatronics*, 2015.
- [78] L. A. Zadeh, "Fuzzy sets," *Information and Control*, vol. 8, pp. 338-353, 1965.
- [79] L. A. Zadeh, *The concept of a linguistic variable and its application to approximate reasoning*: Springer, 1974.
- [80] J. S. R. Jang, "ANFIS: Adaptive-network-based fuzzy inference system," *Systems, Man and Cybernetics, IEEE Transactions on*, vol. 23, pp. 665-685, 1993.
- [81] E. H. Mamdani, "Application of fuzzy logic to approximate reasoning using linguistic synthesis," *Computers, IEEE Transactions on*, vol. 100, pp. 1182-1191, 1977.
- [82] L. A. Zadeh, "Outline of a new approach to the analysis of complex systems and decision processes," *Systems, Man and Cybernetics, IEEE Transactions on*, pp. 28-44, 1973.
- [83] J. Casillas, O. Cordón, F. H. Triguero, and L. Magdalena, *Interpretability issues in fuzzy modeling* vol. 128: Springer, 2003.
- [84] T. Takagi and M. Sugeno, "Fuzzy identification of systems and its applications to modeling and control," *Systems, Man and Cybernetics, IEEE Transactions on*, pp. 116-132, 1985.
- [85] O. Cordón, "A historical review of evolutionary learning methods for Mamdani-type fuzzy rule-based systems: Designing interpretable genetic fuzzy systems," *International journal of approximate reasoning*, vol. 52, pp. 894-913, 2011.
- [86] J.-S. Jang and C.-T. Sun, "Neuro-fuzzy modeling and control," *Proceedings of the IEEE*, vol. 83, pp. 378-406, 1995.
- [87] S. Kar, S. Das, and P. K. Ghosh, "Applications of neuro fuzzy systems: A brief review and future outline," *Applied Soft Computing*, vol. 15, pp. 243-259, 2014.
- [88] J. Soto, P. Melin, and O. Castillo, "Time series prediction using ensembles of ANFIS models with genetic optimization of interval type-2 and type-1 fuzzy integrators," *International Journal of Hybrid Intelligent Systems*, vol. 11, pp. 211-226, 2014.
- [89] A. Karahoca and D. Karahoca, "GSM churn management by using fuzzy c-means clustering and adaptive neuro fuzzy inference system," *Expert Systems with Applications*, vol. 38, pp. 1814-1822, 2011.
- [90] J. Soto, P. Melin, and O. Castillo, "A new approach for time series prediction using ensembles of ANFIS models with interval type-2 and type-1 fuzzy integrators," in

- Computational Intelligence for Financial Engineering & Economics (CIFEr), 2013 IEEE Conference on, 2013, pp. 68-73.
- [91] M. Wei, et al., "Predicting injection profiles using ANFIS," *Information Sciences*, vol. 177, pp. 4445-4461, 2007.
  - [92] J. C. Dunn, "A fuzzy relative of the ISODATA process and its use in detecting compact well-separated clusters," 1973.
  - [93] J. C. Bezdek, *Pattern recognition with fuzzy objective function algorithms*: Kluwer Academic Publishers, 1981.
  - [94] A. K. Jain, "Data clustering: 50 years beyond K-means," *Pattern recognition letters*, vol. 31, pp. 651-666, 2010.
  - [95] V. T, "Performance based analysis between k-Means and Fuzzy C-Means clustering algorithms for connection oriented telecommunication data," *Applied Soft Computing*, vol. 19, pp. 134-146, 2014.
  - [96] S. H. Park, S. J. Kim, K. J. Lim, and S. H. Kang, "Comparison of recognition rates between BP and ANFIS with FCM clustering method on off-line PD diagnosis of defect models of traction motor stator coil," in *Electrical Insulating Materials, 2005.(ISEIM 2005). Proceedings of 2005 International Symposium on*, 2005, pp. 849-852.
  - [97] J.-L. Deng, "Introduction to grey system theory," *The Journal of grey system*, vol. 1, pp. 1-24, 1989.
  - [98] T.-L. Tien, "A research on the grey prediction model GM (1, n)," *Applied Mathematics and Computation*, vol. 218, pp. 4903-4916, 2012.
  - [99] T.-L. Tien, "The indirect measurement of tensile strength of material by the grey prediction model GMC (1, n)," *Measurement Science and Technology*, vol. 16, pp. 1322-1328, 2005.
  - [100] M. Azzeh, D. Neagu, and P. I. Cowling, "Fuzzy grey relational analysis for software effort estimation," *Empirical Software Engineering*, vol. 15, pp. 60-90, 2010.
  - [101] R. C. Eberhart and J. Kennedy, "A new optimizer using particle swarm theory," in *Proceedings of the sixth international symposium on micro machine and human science*, 1995, pp. 39-43.
  - [102] K. Wen, "The grey system analysis and its application in gas breakdown and var compensator finding," *International Journal of Computational Cognition*, vol. 2, pp. 21-44, 2004.
  - [103] S. Liu, Y. Yang, Y. Cao, and N. Xie, "A summary on the research of GRA models," *Grey Systems: Theory and Application*, vol. 3, pp. 7-15, 2013.
  - [104] W.-C. Wang, K.-W. Chau, C.-T. Cheng, and L. Qiu, "A comparison of performance of several artificial intelligence methods for forecasting monthly discharge time series," *Journal of hydrology*, vol. 374, pp. 294-306, 2009.
  - [105] A. Donoso-Bravo, et al., "Model selection, identification and validation in anaerobic digestion: a review," *Water research*, vol. 45, pp. 5347-5364, 2011.
  - [106] M. Matian, A. J. Marquis, and N. P. Brandon, "Application of thermal imaging to validate a heat transfer model for polymer electrolyte fuel cells," *International Journal of Hydrogen Energy*, vol. 35, pp. 12308-12316, 2010.
  - [107] S. Fletcher, A. P. Longstaff, and A. Myers, "Measurement methods for efficient thermal assessment and error compensation," in *Proceedings of the Topical Meeting: Thermal Effects in Precision Engineering*, Maastricht, 2007.
  - [108] S. Fletcher, "Computer aided system for intelligent implementation of machine tool error reduction methodologies," *Doctor of Philosophy*, Centre for Precision Technologies (CPT), University of Huddersfield, Huddersfield 2001.
  - [109] R. Leach, *Fundamental principles of engineering nanometrology*: Elsevier, 2014.

- [110] D. Clough, S. Fletcher, A. Longstaff, and P. Willoughby, "Practical in-situ calibration method for the non-linear output from a low cost eddy current sensor," presented at the Proceedings of the 37th International MATADOR Conference, Manchester, 2012.
- [111] L. Precision, "Differences Between Capacitive and Eddy-Current Sensors," TechNote LT05-0011, 2013.
- [112] L. Yi, L. Mingyao, Y. Chongxiang, and C. Ming, "Measurement of the deformation field for machine tool based on optical fiber Bragg grating sensors," in Innovative Design and Manufacturing (ICIDM), Proceedings of the 2014 International Conference on, 2014, pp. 222-226.
- [113] A. Potdar, A. P. Longstaff, S. Fletcher, and N. S. Mian, "Application of multi sensor data fusion based on Principal Component Analysis and Artificial Neural Network for machine tool thermal monitoring," in Laser Metrology and Machine Performance XI, LAMDAMAP 2015 Huddersfield 2015, pp. 228-237.
- [114] M. Liu, et al., "A new method based on Fiber Bragg grating sensor for the milling force measurement," Mechatronics, 2015.
- [115] Y. Altintas, Manufacturing automation: metal cutting mechanics, machine tool vibrations, and CNC design: Cambridge university press, 2012.
- [116] A. M. Abdulshahed, A. P. Longstaff, and S. Fletcher, "The application of ANFIS prediction models for thermal error compensation on CNC machine tools," Applied Soft Computing, vol. 27, pp. 158-168, 2015.
- [117] A. Abdulshahed, A. P. Longstaff, and S. Fletcher, "A particle swarm optimisation-based Grey prediction model for thermal error compensation on CNC machine tools," in Laser Metrology and Machine Performance XI, LAMDAMAP 2015, Huddersfield, 2015, pp. 369-378.
- [118] S. Naka, T. Genji, T. Yura, and Y. Fukuyama, "A hybrid particle swarm optimization for distribution state estimation," Power Systems, IEEE Transactions on, vol. 18, pp. 60-68, 2003.
- [119] Y. Shi and R. C. Eberhart, "Parameter selection in particle swarm optimization," in Evolutionary programming VII, 1998, pp. 591-600.
- [120] B. Samanta, "Gear fault detection using artificial neural networks and support vector machines with genetic algorithms," Mechanical systems and signal processing, vol. 18, pp. 625-644, 2004.
- [121] L. Wang, N. Zhang, and H. Du, "Real-time identification of vehicle motion-modes using neural networks," Mechanical systems and signal processing, vol. 50-51, pp. 632-645, 2015.
- [122] G. Grassi and P. Vecchio, "Wind energy prediction using a two-hidden layer neural network," Communications in Nonlinear Science and Numerical Simulation, vol. 15, pp. 2262-2266, 2010.
- [123] A. M. Abdulshahed, A. P. Longstaff, S. Fletcher, and A. Myers, "Thermal error modelling of machine tools based on ANFIS with fuzzy c-means clustering using a thermal imaging camera," Applied Mathematical Modelling, vol. 39, pp. 1837-1852, 2015.
- [124] A. Potdar, A. P. Longstaff, S. Fletcher, and A. Abdulshahed, "Development of modular machine tool structural monitoring," in The 3rd International Conference on Advanced Manufacturing Engineering and Technologies, Stockholm, 2013, pp. 263-272.
- [125] A. M. Abdulshahed, A. P. Longstaff, and S. Fletcher, "A novel approach for ANFIS modelling based on Grey system theory for thermal error compensation " in Computational Intelligence (UKCI), 2014 14th UK Workshop on, 2014, pp. 1-7.

- [126] W. M. Geerdes, M. Á. T. Alvarado, M. Cabrera-Ríos, and A. Cavazos, "An Application of Physics-Based and Artificial Neural Networks-Based Hybrid Temperature Prediction Schemes in a Hot Strip Mill," *Journal of manufacturing science and engineering*, vol. 130, pp. 014501.1–5, 2008.
- [127] D. Chen, et al., "An improved PSO algorithm based on particle exploration for function optimization and the modeling of chaotic systems," *Soft Computing*, pp. 1-11, 2014.

## Appendix A: GNNMCI (1, N) Architecture

The fusion model of Grey system and neural network is employed in the modelling of the thermal error of machine tools. The model can reveal the long-term trend of data and, by driving the model by the AGO, rather than raw data, can minimise the effect of some of the random occurrences. Therefore, the first step for building GNNMCI (1, N) is to carry out 1-AGO (first-order Accumulated Generating Operation) to the data, so as to increase the linear characteristics and reduce the randomness from the measuring samples. Particle swarm optimisation algorithm, with capability to optimize complex numerical functions [127], is adopted to train the GNNMCI (1, N) model. Finally, an IAGO (Inverse Accumulated Generating Operation) is performed to predict the thermal error and generate the final compensation values. The model fully takes the advantages of neural networks and Grey models, and overcomes the disadvantages of them, achieving the goal of effective, efficient and accurate modelling. The modelling detail is described as follows:

The Grey prediction Model with Convolution integral GMC (1, N) [98] is:

$$\frac{dX_1^{(1)}}{dt} + b_1 X_1^{(1)} = b_2 X_2^{(1)} + b_3 X_3^{(1)} + \dots + b_N X_N^{(1)} + u, \quad (\text{A.1})$$

where  $b_1$  is the development coefficient,  $b_i (i = 2, 3, \dots, N)$  the driving coefficient, and  $u$  is the Grey control parameter. Therefore, time response sequences can be obtained.

$$\hat{x}_1^{(1)}(k+1) = x_1^{(1)}(1)e^{-b_1 k} + u(t-1) \times \sum_{\tau=1}^k \left\{ e^{-b_1(k-\tau+\frac{1}{2})} \cdot \frac{1}{2} [f(\tau) + f(\tau-1)] \right\}, \quad (\text{A.2})$$

Where  $u(t-1)$  is the unit step function; and  $f(\tau) = \sum_{j=2}^N b_j X_j^{(1)}(\tau) + u \quad k=1, 2, \dots, n$ .

To calculate the coefficients  $b_i$  and  $u$ , the neural network method can be used to map equation (A.2) to a neural network. Then, the neural network model is trained until the performance is satisfactory. Finally, the optimal corresponding weights are used as the Grey neural network weights to predict the thermal error.

Equation (A.2) can be written as;

$$G = u(t-1) \times \sum_{\tau=1}^k \left\{ e^{-b_1(k-\tau+\frac{1}{2})} \cdot \frac{1}{2} [f(\tau) + f(\tau-1)] \right\}. \quad (\text{A.3})$$

Equation (A.2) can be rewritten as:

$$\hat{x}_1^{(1)}(k+1) = \left(x_1^{(1)}(1)\right) e^{-b_1 k} + G. \quad (\text{A.4})$$

Then equation (A.4) can be converted into equation (A.5) as follows:

$$\begin{aligned} \hat{x}_1^{(1)}(k+1) &= \left[ x_1^{(1)}(1) \frac{e^{-b_1 k}}{1 + e^{-b_1 k}} + G \frac{1}{1 + e^{-b_1 k}} \right] (1 + e^{-b_1 k}), \\ \hat{x}_1^{(1)}(k+1) &= \left[ x_1^{(1)}(1) \left( 1 - \frac{1}{1 + e^{-b_1 k}} \right) + G \frac{1}{1 + e^{-b_1 k}} \right] (1 + e^{-b_1 k}), \\ &= \left[ x_1^{(1)}(1) - x_1^{(1)}(1) \frac{1}{1 + e^{-b_1 k}} + G \frac{1}{1 + e^{-b_1 k}} \right] (1 + e^{-b_1 k}). \end{aligned} \quad (\text{A.5})$$

Map equation (A.5) into a neural network, and the mapping structure is shown in Figure A-1

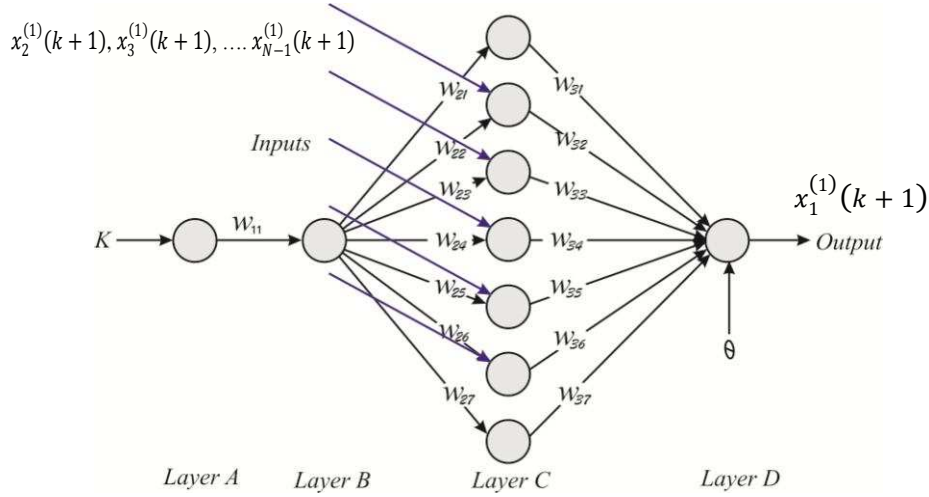


Figure A-1: The mapping structure of GNNMCI (1, 6).

Where  $k$  is the serial number of input parameters;

In this study,  $x_1^{(1)}(k+1)$  is chosen as a dependent variable (network output) and  $x_2^{(1)}(k+1)$ ,  $x_3^{(1)}(k+1)$ , ...,  $x_{N-1}^{(1)}(k+1)$ , as independent variables, ( $N$  is the number of network inputs);

$w_{11}, w_{21}, w_{22}, \dots, w_{2n}; w_{31}, w_{32} \dots w_{3n}$  are the weights of the network;

Layer A, layer B, layer C, and layer D are the four layers of the network, respectively.

Where, the corresponding neural network weights can be assigned as follows:

Let us assume that  $d_1 = f(b_2)$ ,  $d_2 = f(b_3)$ , ...,  $d_{N-2} = f(b_{N-2})$ ,  $d_{N-1} = f(u)$ .

$w_{11} = b_1$ ,  $w_{21} = -x_1^{(1)}(1)$ ,  $w_{22} = d_1$ ,  $w_{23} = d_2$ , ...,  $w_{2N-1} = d_{N-2}$ ,  $w_{2N} = d_{N-1}$

$$w_{31} = w_{32} = w_{33} = \dots = w_{3N} = 1 + e^{-b_1 k}$$

The bias  $\theta$  value of  $x_1^{(1)}(k+1)$  is:

$$\theta = \left(-x_1^{(1)}(k+1)\right)(1 + e^{-b_1 k}) \quad (\text{A.6})$$

The transfer function of Layer B is a sigmoid function  $f(x) = \frac{1}{1+e^{-x}}$ , the transfer functions of other layer's neuron are adopted as a linear function  $f(x) = x$ .

## A.1 GNNMCI (1, N) Learning Algorithm

The learning algorithm of GNNMCI (1, N) can be summarised as follows:

Step 1: For each input series,  $(k, X_j^{(1)}(k))$ ,  $(k = 2, 3, \dots, N)$ , the output of each layer is calculated.

**Layer A:**  $a = w_{11}k$ ;

**Layer B:**  $b = f(w_{11}k) = \frac{1}{1+e^{-w_{11}k}}$ ;

**Layer C:**  $c_1 = bw_{21}$ ,  $c_2 = x_2(k)bw_{22}$ ,  $c_3 = x_3(k)bw_{23}, \dots$ ,  $c_{n-1} = x_n(k)bw_{2n-1}$ ,  $c_n = bw_{2n}$ ; and

**Layer D:**  $d = w_{31}c_1 + w_{32}c_2 + \dots + w_{3n-1}c_{n-1} + w_{3n}c_n - \theta$ .

Step 2: In order to avoid the entrapment in a local minimum, a PSO algorithm is adopted to train the GNNMCI (1, N) model. Here, a particle refers to a weight in the model that changes its position from one move to another based on velocity updates. The flowchart for PSO implementation is given in [Figure A-2](#), and the mathematical description of PSO algorithm is as follows; Suppose that the search space is D-dimensional, then the current position and velocity of the  $i$ th particle can be represented by  $W_i = [w_{i1}, w_{i2}, \dots, w_{iD}]^T$  and  $V_i = [v_{i1}, v_{i2}, \dots, v_{iD}]^T$  respectively, where  $i = 1, 2, \dots, M$  and  $M$  is the number of particles in the swarm.

Particle  $i$  can remember the best position so far, which is known as the local best position  $Pbest_i = [pbest_1, pbest_2, \dots, pbest_{iD}]^T$ . It can also obtain the best position that the whole swarm establish, known as the global best position  $Gbest_i = [gbest_1, gbest_2, \dots, gbest_{iD}]^T$ . The first position and velocity of Particle  $i$  are randomly initialised by the uniformly distributed variables. Afterwards, particle  $i$  adjusts its

velocity of iteration  $k+1$  according to the local and global best positions, as well as the velocity and position of iteration  $k$ , as follows:

$$V_i(k+1) = \omega V_i(k) + C_1 R(Pbest_i(k) - W_i(k)) + C_2 R(Gbest_i(k) - W_i(k)) \quad (A.7)$$

Where  $\omega$  is the inertia factor which is used to manipulate the impact of the previous velocities on the current velocity.  $C_1$  and  $C_2$  are the self-confidence factor and the swarm-confidence factor, respectively.  $R$  is a uniformly distributed random real numbers that can take any value between 0 and 1.

With the updated velocity, the position of particle  $i$  in the iteration  $k+1$  can be obtained as follows:

$$W_i(k+1) = W_i(k) + V_i(k+1) \quad (A.8)$$

The fitness of particle is measured using a fitness function that quantifies the distance between the particle and its optimal solution as follows:

$$f(W_i) = \sum_{k=1}^N [\hat{x}^{(0)}(k) - x^{(0)}(k)]^2 \quad (A.9)$$

Where  $f$  is the fitness value,  $\hat{x}^{(0)}(k)$  is the target output; and,  $x^{(0)}(k)$  is the predicted output based on connection weight (particle) updating.

Step 3: update the velocity and position of each particle based on equations (A.7) and (A.9).

Adjusting the connection weights between layers:

Adjusting the connection weights from LA to LC.

Adjust the bias value  $\Theta$ .

$$\Theta = (-x_1^{(1)}(k+1)) (1 + e^{-w_{11}k})$$

Step 4: If the value of the error meets the requirement of the model, or a pre-determined number of epochs is passed, then the network training will end if not, then return to Step 3.

Step 5: Export the optimal solution  $W_i$ .

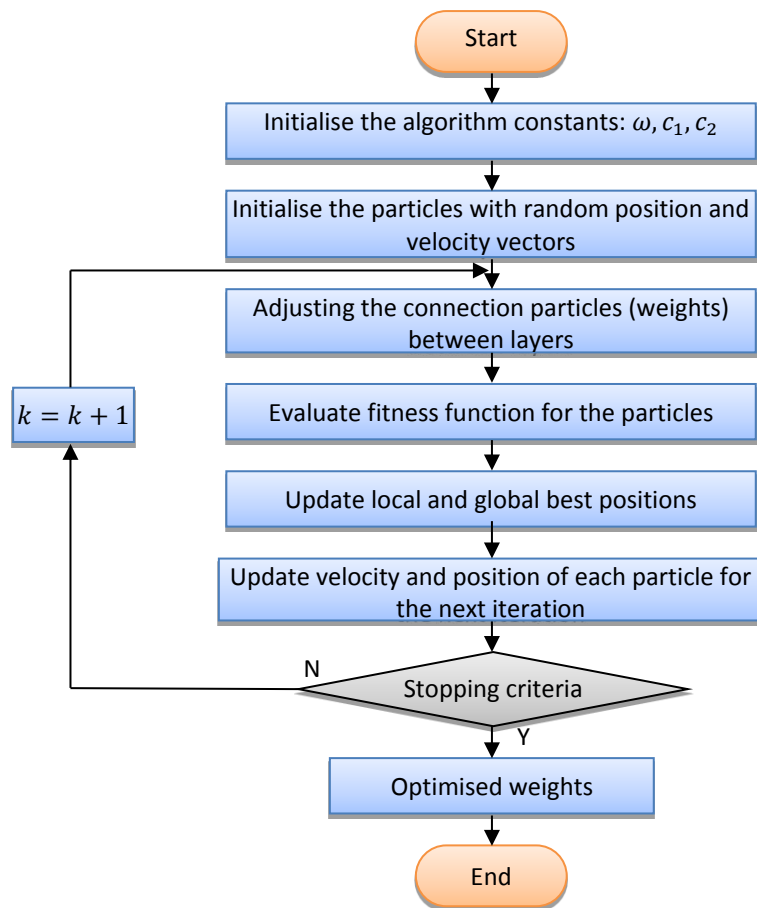


Figure A-2: Flowchart for PSO implementation.